Louisiana State University
LSU Digital Commons

LSU Doctoral Dissertations | Graduate School

2013

Electrophoretic deposition of carbon nanotubes on silicon substrates

Anirban Sarkar
Louisiana State University and Agricultural and Mechanical College

Follow this and additional works at: https://digitalcommons.lsu.edu/gradschool_dissertations

Part of the Electrical and Computer Engineering Commons

Recommended Citation
Sarkar, Anirban, "Electrophoretic deposition of carbon nanotubes on silicon substrates" (2013). *LSU Doctoral Dissertations*. 3518.
https://digitalcommons.lsu.edu/gradschool_dissertations/3518

This Dissertation is brought to you for free and open access by the Graduate School at LSU Digital Commons. It has been accepted for inclusion in LSU Doctoral Dissertations by an authorized graduate school editor of LSU Digital Commons. For more information, please contactgradetd@lsu.edu.

ELECTROPHORETIC DEPOSITION OF CARBON NANOTUBES ON SILICON SUBSTRATES

A Dissertation

Submitted to the Graduate Faculty of the
Louisiana State University and
Agricultural and Mechanical College
in partial fulfillment of the
requirements for the degree of
Doctor of Philosophy

in

Division of Electrical and Computer Engineering
The School of Electrical Engineering and Computer Science

by
Anirban Sarkar
B.Tech, West Bengal University of Technology, 2007
December 2013

Dedicated to Late Shri Dinesh Chandra Sarkar

ACKNOWLEDGEMENTS

I would like to express my profound gratitude to Dr. Theda Daniels-Race, my research advisor, for her unflinching support and guidance over the course of my Doctoral program. Her patience, confidence and faith in me during difficult times have made this dissertation possible.

I am incredibly indebted to Dr. Dooyoung Hah for guiding me during the initial years of my program. I will never forget his caring nature and an extremely understanding attitude towards his students. I feel immensely fortunate to have interacted with such a wonderful person.

I feel truly privileged to have Dr. Martin Feldman, Dr. Isiah Warner and Dr. Georgios Veronis in my graduate committee. I have been associated with Dr. Feldman (Marty) for a very long time. Marty is one of the most intelligent people I have met in my life. His works and ideas of solving research problems through very simple and ingenuous ways continue to amaze me. Dr. Warner's stature in the scientific community is an inspiration for any young researcher. I am thankful to him for making me believe in innovative and original research. The receptive nature of Dr. Veronis made my interactions with him very comfortable.

I would like to convey my sincere gratitude to Dr. Pratul Ajmera for his contributions towards my research endeavors. He has been a true leader.

I am thankful to Mr. Chris O'Laughlin, Mr. Golden Hwaung and Mr. James Breedlove for the years of technical help, discussion and friendship. I will always remember Mr. Roy Oby for his kind words and gestures during my long hours of work at the office and laboratory.

I acknowledge the contributions of all my colleagues, friends and acquaintances in Baton Rouge for keeping me alive during my study. I am grateful to Kalpataru, Agnimitro, Rakesh, Subhajit, Dr. Daniel Herbert, Mr. Sean Hou, Mr. Kalyan Kanakamedala, Mr. and Mrs. Tapan Sarkar, Mr. Unmesh Kirtikar and Mr. Santanu Majumdar for the moments of happiness.

Finally, my family has been the greatest source of my strength in this journey. I am grateful for their infinite love, patience and concern throughout these years. I love you, Ma and Baba.

TABLE OF CONTENTS

ACKNOWLEDGEMENTS iii

LIST OF TABLES viii

LIST OF FIGURES ix

ABSTRACT xiii

CHAPTER 1: BRIEF DESCRIPTION OF CHAPTER CONTENT 1

CHAPTER 2: INTRODUCTION, LITERATURE REVIEW AND PROBLEM STATEMENT . 4
- 2.1: Introduction 4
- 2.2: General growth process of carbon nanotubes 5
- 2.3: Direct growth techniques 8
  - 2.3.1: Arc discharge method 8
  - 2.3.2: Laser ablation method 9
  - 2.3.3: Chemical vapor deposition (CVD) method 10
  - 2.3.4: Summary of problems with direct growth techniques 12
- 2.4: Solution based room temperature deposition of carbon nanotubes 12
  - 2.4.1: Fundamental concepts of colloidal stability 13
  - 2.4.2: Methods for stabilizing colloidal solutions 19
  - 2.4.3: Different techniques for carbon nanotube dispersion 22
  - 2.4.4: Literature review of different coating methods 29
  - 2.4.5: Summary of problems with the coating techniques 33
- 2.5: Electrophoretic deposition (EPD): Fundamentals and concepts 34
  - 2.5.1: Fundamental concepts of electrophoresis 35
  - 2.5.2: Proposed mechanisms of electrophoresis 36
  - 2.5.3: Literature review of electrophoretic deposition of carbon nanotubes 41

CHAPTER 3: MOTIVATION AND RESEARCH GOALS 45
- 3.1: Motivation 45
- 3.2: Research goals 46

CHAPTER 4: ELECTROPHORETIC DEPOSITION OF CARBON NANOTUBES ON SILICON SUBSTRATES 49
- 4.1: Introduction 49
- 4.2: Experimental procedure 49
- 4.3: Results and discussion 52
  - 4.3.1: Dispersion of the CNT solution 52
  - 4.3.2: Characterization of the deposited CNT film 54
  - 4.3.3: Post-EPD agglomeration of the CNT solution 68
- 4.4: Conclusion 69

CHAPTER 5: ELECTROPHORETIC DEPOSITION OF CARBON NANOTUBES ON SILICON SUBSTRATES WITH SURFACE FUNCTIONALIZATION 71
- 5.1: Introduction 71

5.2: Experimental procedure 72
5.2.1: Preparation of CNT solution in IPA and water 72
5.2.2: Preparation of APTES solution with varying concentration 73
5.2.3: Substrate preparation 74
5.2.4: EPD process 74
5.3: Results and discussion 75
5.4: Conclusion and future work 87

CHAPTER 6: SURFACE ENHANCED RAMAN SPECTROSCOPY STUDIES ON SILVER NANOPARTICLE COATED CARBON NANOTUBE NETWORKS FABRICATED BY ELECTROPHORETIC DEPOSITION 89
6.1: Introduction 89
6.2: Experimental procedure 91
6.2.1: Preparation of CNT solution in IPA (CNT-IPA) 91
6.2.2: Synthesis of AgNPs 92
6.2.3: Preparation of 20% APTES solution 92
6.2.4: Substrate preparation by APTES grafting 93
6.2.5: EPD process 93
6.2.6: Silanization of electrophoretically deposited carbon nanotubes 94
6.2.7: Fabrication of SERS substrate 94
6.2.8: Raman Spectroscopy 95
6.3: Results and discussion 95
6.3.1: Characterization of synthesized Ag nanoparticles 95
6.3.2: Silanization of the deposited CNT films 102
6.3.3: Characterization of Ag-CNT-Si SERS substrate 103
6.3.4: Raman spectroscopic results and estimation of SERS enhancement factor 105
6.3.5: Estimation of the overall enhancement factor (E.F.) 115
6.4: Conclusion 120

CHAPTER 7: SUMMARY AND RECOMMENDATION FOR FUTURE WORK 122
7.1: Summary of results in the pursued research 122
7.2: Recommendation for future work 125
7.2.1: Dispersion and electrophoretic deposition of CNTs from ionic liquids 125
7.2.2: EPD from aqueous suspension under modulated electric field 126
7.2.3: EPD of CNTs on insulator surfaces for plastic electronics 126
7.2.4: EPD of silver nanoparticles for better surface coverage and uniform coating 127
7.2.5: SERS study on liquid analyte for bio-medical application 127

REFERENCES 128

APPENDIX A: PERMISSION TO REPRINT FROM JOHN WILEY AND SONS 139

APPENDIX B: PERMISSION TO REPRINT FROM SPRINGER 141

APPENDIX C: PERMISSION TO REPRINT FROM ELSEVIER 142

APPENDIX D: PERMISSION TO REPRINT FROM ACS PUBLICATIONS 148

APPENDIX E: PERMISSION TO REPRINT FROM TAYLOR & FRANCIS 149

VITA 150

LIST OF TABLES

Table 2-1: Overview of EPD of CNTs 44

Table 4-1: Layer Structure of different substrates used in the EPD experiments..... 51

Table 4-2: Electrophoretic deposition results on silicon substrates with different surface coatings under different experimental conditions. 56

Table 6-1: Assignment of the prominent peaks in Raman spectra of R6G. 106

Table 6-2: Raman spectroscopy results on 1 mM, 100 μM and 1 μM R6G concentration on non-SERS Si substrates showing measured intensity values at 1307, 1358 and 1507 cm^{-1}. (Signal intensity is measured in arbitrary units)..... 107

Table 6-3: Surface enhanced Raman spectroscopy (SERS) results on 1 μM, 100 nM and 1 nM R6G concentration on Ag-Si substrates showing measured intensity values at 1305, 1358 and 1505 cm^{-1}. (Signal intensity is measured in arbitrary units). 109

Table 6-4: Surface enhanced Raman spectroscopy (SERS) results on 1 μM, 100 nM, 1 nM and 1 pM R6G concentration on Ag-CNT-Si substrates showing measured intensity values at 1307, 1358 and 1507 cm^{-1}. (Signal intensity is measured in arbitrary units). 112

Table 6-5: Comparison of surface enhanced Raman spectroscopy (SERS) results on Ag-Si and Ag-CNT-Si substrates with 1 μM, 100 nM and 1 nM R6G concentration at 1307, 1358 and 1507 cm^{-1}. (Signal intensity is measured in arbitrary units and E.F. = Enhancement factor). 112

LIST OF FIGURES

Figure 2-1: Schematic diagram of Vapor Liquid Solid (VLS) growth model [Reprinted with permission from Wiley and Sons[4]]. 6

Figure 2-2: Root growth and Tip growth mechanism of carbon nanotubes [Reprinted with permission from Elsevier[7]]. 7

Figure 2-3: Schematic diagram of Yarmulke growth mechanism [Reprinted with permission from Taylor and Francis[5,8]]. 8

Figure 2-4: Schematic diagram of Arc discharge method of synthesis of carbon nanotubes. 9

Figure 2-5: Schematic diagram of Laser ablation method of synthesis of carbon nanotubes. 10

Figure 2-6: Schematic diagram of Chemical vapor deposition (thermal) of carbon nanotubes. .. 11

Figure 2-7: Schematic diagram explaining the concepts of Stern layer, Diffuse Region and Zeta potential [Reprinted with permission from Elsevier[18]]. 16

Figure 2-8: Schematic diagram showing the concept of DLVO theory[17]. 17

Figure 2-9: Schematic diagram showing the energy profiles for different ionic strengths from DLVO concept [Reprinted with permission from Elsevier[18]]. 19

Figure 2-10: Concepts of Steric stabilization (left) and Depletion stabilization (right). 22

Figure 2-11: Different combinations of electro-steric stabilization. 22

Figure 2-12: Surfactant assisted dispersion of carbon nanotubes [Reprinted with permission from Elsevier[25]]. 24

Figure 2-13: Schematic view of the self-assembly of the protein-protected AuNPs on PANHS functionalized CNTs [Reprinted with permission from Elsevier[51]]. 26

Figure 2-14: Covalent functionalization of carbon nanotubes by acid refluxing method. 27

Figure 2-15: Schematic diagram of immobilization of nanoparticles on covalently functionalized carbon nanotube surface [Reprinted with permission from Elsevier[58]]. 29

Figure 2-16: Langmuir Blodgett method of carbon nanotube coating. 30

Figure 2-17: Spray coating method of carbon nanotubes. 32

Figure 2-18: Mayer Rod coating method of carbon nanotubes [Reprinted with permission from ACS publications[75]]. 33

Figure 2-19: Schematic diagram of Electrophoretic Deposition method. 36

Figure 2-20: Schematic diagram of electrical double layer (EDL) distortion and thinning mechanism [Reprinted with permission from Wiley and Sons[82]]. 40

Figure 2-21: Acid refluxing of carbon nanotubes [Reprinted with permission from Elsevier[87]]. 42

Figure 4-1: Dispersed CNT solution obtained after bath sonication of the acid-refluxed CNTs used for EPD experiments. 50

Figure 4-2: Schematic diagram of electrophoretic deposition set-up [Reprinted with permission from Springer[102]]..... 52

Figure 4-3: TEM image of the as-purchased carbon nanotubes. 53

Figure 4-4: TEM image of the acid-treated carbon nanotubes. 54

Figure 4-5: Optical images (top view) of deposited CNT film on patterned aluminium on bare silicon or insulators (SiO_2 or Si_3N_4) with electric field of 10 V/cm for 3 minutes: (a) Sample A, (b) sample B and (c) samle C. (d-f) Schematic cross sectional diagram of (d) sample A, (e) sample B and (f) sample C [Reprinted with permission from Springer[102]]. 57

Figure 4-6: (a) Deposition results on silicon substrates without any metal layer (b) Immersion coating results on aluminum surface..... 60

Figure 4-7: Scanning electron microscopic images of deposited CNT film on the sample A. (a) (Top view) CNT film showing appreciable packing density without voids, (b) (top view) magnified image of the CNT film [Reprinted with permission from Springer[102]]. 61

Figure 4-8: Scanning electron microscopic images of deposited CNT film on the sample A. (c) (cross-section) CNT film deposited on Al/Si and (d) (cross-section) magnified image of the CNT film [Reprinted with permission from Springer[102]]. 62

Figure 4-9: Raman spectrum of the carbon nanotube film deposited on sample A for 2 minutes of EPD at an applied electric field: 10 V/cm [Reprinted with permission from Springer[102]]..... 63

Figure 4-10: Thickness of CNT films on different samples as a function of applied electric field at constant deposition time of 3 minutes..... 65

Figure 4-11: Thickness of CNT films on different samples as a function of deposition time at a constant applied electric field of 15 V/cm. 65

Figure 4-12: Average surface roughness of the CNT films deposited on different samples as a function of applied electric field at constant deposition time of 3 minutes. 67

Figure 4-13: Average surface roughness of CNT films deposited on different samples as a function of deposition time at a constant applied electric field of 15 V/cm. 67

Figure 4-14: Degraded CNT solution with precipitated carbon nanotubes after a failed EPD attempt with bare silicon substrates [Reprinted with permission from Springer[102]]. 69

Figure 5-1: Dispersed CNT solution used for EPD experiments (a) stable suspension in isopropyl alcohol (CNT-IPA) and (b) stable suspension in water (CNT-Water). 73

Figure 5-2: Schematic diagram of 3-Aminopropyl-triethoxysilane (APTES)..... 74

Figure 5-3: Schematic diagram of the electrophoretic deposition set-up. 75

Figure 5-4: Schematic diagram displaying the process of hydroxylation after piranha treatment and silanization by APTES treatment on silicon surface prior to the electrophoretic deposition (EPD) step. 76

Figure 5-5: Optical images of CNT film deposited on silicon samples by EPD with different APTES concentration at an applied E-field of 15 V/cm for 3 min (a) 10% APTES, (b) 20% APTES, (c) 50% APTES and (d) 100% APTES. All the samples exhibit remarkable film quality. 78

Figure 5-6: Optical images of CNT films deposited by electrophoretic deposition at an applied E-field of 15V/cm for 3 min on (a) 20% APTES treated silicon sample showing superior coating quality in contrast to (b) HMDS treated silicon surfaces..... 80

Figure 5-7: Deposition results comparing electrophoretic deposition (EPD) and dip coating on surface functionalized silicon substrates (a) CNT film deposited by EPD at an applied E-field of 15V/cm for 3 min with 20% APTES treatment (b) Dip coated silicon samples in CNT-IPA solution for 6 min with 20% APTES treatment showing agglomerated deposit and (c) Dip coated silicon samples results in CNT-water solution for 6 min with 50% APTES treatment showing poor CNT surface coverage. 81

Figure 5-8: Optical images comparing the electrophoretic deposition results at an applied E-field of 15V/cm on 20% APTES treated silicon substrates (a) from CNT-IPA suspension for 3 min, (b) from CNT-water suspension for 3 min and (c) from CNT-water suspension for 6 min..... 83

Figure 5-9: Scanning electron microscopic images of CNT film on 20% APTES treated silicon sample deposited at an applied electric field of 15V/cm for 3 min showing appreciable surface coverage and packing density without voids (a) at ×10k magnification and (b) at ×20k magnification. 84

Figure 5-10: Raman spectra of CNT films deposited on silicon samples with varying APTES concentration (5%, 10%, 20%, 50% and 100%). Inset shows Raman spectrum of raw CNT powder used in the work. 85

Figure 5-11: Thickness of CNT films deposited on silicon samples with varying APTES concentration at different applied electric field (E-field: 5V/cm, 10V/cm and 15V/cm) for constant deposition duration of 3 min..... 86

Figure 6-1: Schematic diagram of electrophoretic deposition set-up[102]. 94

Figure 6-2: Optical images of the synthesized silver nanoparticle solution designated as Solution A, B and C from left to right..... 97

Figure 6-3: TEM image of silver nanoparticles in solution A showing severe aggregation. 97

Figure 6-4: TEM image of silver nanoparticles in solution B (Average particle diameter: 70-80 nm). 98

Figure 6-5: TEM image of silver nanoparticles in solution C showing minimum aggregation (Average particle diameter: 30-40 nm). 98

Figure 6-6: Schematic diagram of the surface functionalization of silicon surface by APTES treatment. 100

Figure 6-7: Scanning electron microscopic images of CNT film on 20% APTES treated silicon sample deposited at an applied electric field of 15V/cm for 3 mins showing appreciable surface coverage and packing density without voids (a) at ×10k magnification and (b) at ×20k magnification. 101

Figure 6-8: Schematic diagram of the surface functionalization of carbon nanotubes by APTES treatment. 103

Figure 6-9: Scanning electron microscopic images of silver nanoparticles coated on silanized CNT film deposited on 20% APTES treated silicon sample (a) at ×10k magnification and (b) at ×20k magnification. 104

Figure 6-10: Raman spectra of 1 mM, 100 μM and 1 μM R6G concentration on silicon substrates. 106

Figure 6-11: Surface enhanced Raman spectra of 1 μM, 100 nM and 1 nM R6G concentration on Ag-Si substrates 108

Figure 6-12: Surface enhanced Raman spectra of 1 pM, 1 nM, 100 nM and 1 μM R6G concentration on Ag-CNT-Si substrates. 111

Figure 6-13: Comparison of Raman spectra for 1 μM R6G concentration on silicon, Ag-Si SERS and Ag-CNT-Si SERS substrates. 113

Figure 6-14: Comparison of Raman spectra for 1 nM R6G concentration on Ag-Si SERS and Ag-CNT-Si SERS substrates. 114

Figure 6-15: Surface enhanced Raman spectra of 1×10^{-12} M R6G concentration on Ag-CNT-Si substrate and 1×10^{-9} M R6G concentration on Ag-Si substrate with respect to reference Raman spectra of 1×10^{-3} M R6G concentration on non-SERS Si substrates. The calculated E.F at 1358 cm^{-1} is 2.78×10^{9} and 5.6×10^{6} respectively. 119

ABSTRACT

This dissertation research describes the feasibility study and investigation of Electrophoretic Deposition (EPD) of carbon nanotubes (CNTs) for applications in semiconductor research. In recent years, the EPD technique has been considered as an economical, room temperature, solution based wet coating technique for thin and thick CNT films on arbitrary substrates. In this study, fabrication of uniform coatings of acid-treated CNTs has been pursued on bare silicon substrates by EPD from aqueous and organic suspensions. Research endeavors are extended to examine EPD of CNTs on silicon substrates with various surface coatings such as metal (aluminum), insulator layers (silicon dioxide and silicon nitride) and self-assembled polar organosilane (APTES) molecules. Microstructural imaging, spectroscopic analysis and characterization of the morphology of the CNT films have also been reviewed in relation to the deposition parameters such as inter-electrode electric field, deposition duration and APTES concentration.

For research and development involving advanced spectroscopic analysis, Surface Enhanced Raman Spectroscopy (SERS) studies have been conducted on horizontally aligned EPD fabricated porous CNT networks coated with silver nanoparticles (AgNPs). The acquired Raman spectra of AgNP-CNT hybrid nanostructures display significant enhancement in the Raman intensity values of Rhodamine6G (R6G) analyte by several orders of magnitude with respect to the reference sample. Improvement in the Raman signals has pushed the detection limit to as low as 1×10^{-12} M. The experimental results, reported in this dissertation, thus establish the novelty of EPD in the fabrication of the AgNP coated porous CNT substrate for routine SERS analysis of different target analytes.

CHAPTER 1: BRIEF DESCRIPTION OF CHAPTER CONTENT

This chapter presents a brief description of chapters 2 through 7 in this dissertation.

Chapter 2 ("Introduction, Literature review and Problem Statement") introduces basic background on the general definition and properties of carbon nanotubes (CNTs) and their direct growth techniques such as electric arc discharge, laser ablation and chemical vapor deposition. Also discussed are the limitations of these techniques which have led to the solution based, room temperature coating approach compatible with a variety of substrates and low temperature technologies. A comprehensive literature review has been presented to reveal the following:

i. Fundamental concepts of colloidal stability, DLVO theory and different non-covalent and non-covalent functionalization techniques pursued for CNT dispersion
ii. Detailed account of the state-of-the-art solution based CNT coating methods (such as Langmuir Blodgett coating, spray deposition, ink jet printing) and limitations in regard to control of deposition parameters, packing density and homogeneity of film quality
iii. Fundamental concepts and proposed mechanisms of electrophoretic deposition (EPD) technique pursued in this dissertation
iv. Review of the reported EPD of CNTs to-date on predominantly metal or metal coated substrates and the limitations of these methods which define the underlying motivation of our research endeavor outlined in the subsequent chapters

Based on the present state-of-the-art and innovations needed to address the existing status of electrophoretic deposition (EPD) of carbon nanotubes, Chapter 3 ("Motivation and Research Goals") outlines the motivation and enlists the research objectives pursued in the research for this dissertation. These research goals are listed under three major topics, namely (1) electrophoretic deposition of carbon nanotubes on silicon substrates; (2) electrophoretic deposition of carbon nanotubes on surface functionalized silicon substrates; and (3) surface

enhanced Raman spectroscopy (SERS) studies on silver nanoparticle coated carbon nanotube networks fabricated by electrophoretic deposition as a potential application

Chapter 4 ("Electrophoretic Deposition of carbon nanotubes on silicon substrates") presents a comprehensive account of the electrophoretic deposition experiments of acid refluxed CNTs on silicon substrates with various insulator (silicon dioxide-SiO_2 and silicon nitride-Si_3N_4) and metal coatings (aluminum, copper). Deposition results with regard to preferential CNT coating and adhesion on bare, piranha treated/ acid etched and metal patterned silicon samples have been reported in detail as well. The effects of electric field, deposition time, and underlying films on the thickness and surface roughness of the CNT film are studied. An interesting observation pertaining to the degradation of the CNT solution following unsuccessful EPD attempts on bare silicon substrates and a probable explanation to that end has also been conveyed in the chapter.

Chapter 5 ("Electrophoretic Deposition of carbon nanotubes on silicon substrates with surface functionalization") introduces the concept of surface functionalization by self-assembling organosilane molecule (3-amino-propyl-triethoxysilane or APTES) on piranha treated hydroxylated silicon surfaces. Different comparative studies between aqueous (CNT-water) and non-aqueous (CNT dispersed in isopropyl alcohol or IPA referred to as CNT-IPA) suspension in regard to fabricated film quality and the benefits of EPD as a fast, reliable and reproducible coating technique over the dip coating method have also been reported extensively throughout the chapter. The effect of varying APTES concentration (5%-100%) on the Raman spectroscopy and thickness of the deposited CNT film has been revealed in detail as well.

Chapter 6 ("Surface enhanced Raman spectroscopy studies on silver nanoparticle coated carbon nanotube networks fabricated by Electrophoretic Deposition") of this dissertation

introduces the concept of Raman Spectroscopy and Surface Enhanced Raman Spectroscopy (SERS) as a versatile analytical tool for the spectroscopic analysis of various compounds in different scientific applications. In this study, the ingenuity of electrophoretic deposition technique as a fast, reproducible and single-step coating process in conjunction with the self-assembling organosilane surface treatment has been communicated in the fabrication of horizontally aligned CNT based porous SERS substrates. The subsequent sections of this chapter also reveal pertinent details involving the synthesis of silver nanoparticles (AgNPs), with average diameter ranging from 30 nm-80 nm, the stabilization effect mediated by the surfactant (e.g. poly-vinyl-pyrrolidone or, PVP) molecules in the prevention of AgNP aggregation and solution degradation, and immersion coating of the AgNPs on the silanized CNT networks. The Rhodamine6G (R6G) molecule has been selected as the target analyte. The surface enhanced Raman spectra of R6G molecules with varying concentrations (from 1 milli-molar- (mM) - i.e. 1×10^{-3} M to 1 pico-molar-(pM) - i.e. 1×10^{-12} M) on the Ag-CNT-Si SERS substrates has been disclosed in conjunction with comparative SERS results on AgNP coated planar Si substrates (Ag-Si). The concluding section of this chapter has been composed in the discussion on superior detection limits in our SERS study and estimation on enhancement factor (E.F.) from the acquired Raman spectra.

Chapter 7 ("Summary and Recommendation for future work") outlines a comprehensive summary of the results of the present research. It lists the conclusions drawn from different aspects of this dissertation and offers recommendation for further research in potential application paradigm.

CHAPTER 2: INTRODUCTION, LITERATURE REVIEW AND PROBLEM STATEMENT

2.1: Introduction

Since the discovery of carbon nanotubes (CNTs) by Iijima[1,2], substantial research has been pursued in analyzing their physical and chemical properties. A single strand of carbon nanotube can be envisioned as sheets of graphene rolled into a hollow cylindrical shape. Depending on the number of graphene sheets wrapped into the cylinder, the carbon nanotubes can be classified as: (a) single walled carbon nanotubes (SWCNTs), (b) double walled nanotubes (DWCNTs), and (c) multi-walled carbon nanotubes (MWCNTs). The typical diameter and length of these nanotubes range from 5 nm to 50 nm and 10 μm to 100 μm, respectively.

Single-walled nanotubes (SWNTs) consist of a single rolled up sheet of graphene whereas multi-walled nanotubes (MWNTs) are composed of a collection of multiple concentric sheets bound by Van der Waals forces. The fundamental structure of the tubes is defined by the diameter, length, number of concentric shells and chirality of the tubes. The electronic nature exhibits metallic or semiconducting properties depending on the helicity of the tubes. The nanotube helicity can be explained by the variation by which the graphene sheets can be rolled up to form a cylinder. The helicity and diameter of the nanotubes can be obtained from a pair of integers (n, m) which is expressed in the form of a vector, known as the "chiral vector", $C_h = na_1+ma_2$ where a_1 and a_2 are the unit vectors. Depending on the arrangement of carbon atoms around the nanotube diameter, the nanotubes can be classified as the armchair ($n = m$), zigzag ($n = 0$ or $m = 0$), or chiral (any arbitrary values of n and m) variety. All armchair SWNTs show metallic behavior; those with $n - m = 3k$, where k is a nonzero integer, are semiconductors with a small band gap; and the rest display semiconducting with a band gap that inversely depends on the nanotube diameter.

Over the last decade of nanoscience research, significant attention has been paid in the optimization of nanotube synthesis by direct growth techniques such as arc discharge, laser ablation, and chemical vapor deposition (CVD). The nanotube growth conditions and controlling parameters such as temperature, time, feedstock hydrocarbon precursors, and nano-metallic growth catalysts have been studied extensively. The purification methods such as post-synthesis treatment and characterization of the synthesized nanotubes have been investigated comprehensively as well. The relevant sections of this chapter outline the details of the direct growth techniques, the drawbacks of these methods and a comprehensive review of the solution-phase wet deposition techniques for CNT thin film research.

2.2: General growth process of carbon nanotubes

The exact growth mechanism of carbon nanotubes is still a subject of intense study and research. It has been proposed that depending on the precise growth parameters such as the temperature, the nature of the nucleation catalysts and carbon-catalyst interaction, more than one mechanism might be operative during the formation of CNTs. Most of these growth models, put forth to understand the exact mechanism, can be explained under the purview of the vapor-liquid-solid (VLS) mechanism[3,4] as illustrated in **Figure 2-1**. In the VLS process, metal clusters, acting as growth precursors, are heated above their metal-carbon eutectic temperature in the presence of a hydrocarbon vapor source (shown as *i* in the figure). The carbon atoms adsorb on the catalyst particles, forming a liquid metal-carbide (indicated as *ii* in the figure) and eventually consume the whole catalyst particle through bulk and surface diffusion. Finally, super-saturation is reached as carbon starts to precipitate into a crystalline tubular form (shown as *iii*). The figure also outlines the role of the metal catalyst in offering enough nucleation sites to initiate and orient the nanotube growth and controlling the diameter of the tubes.

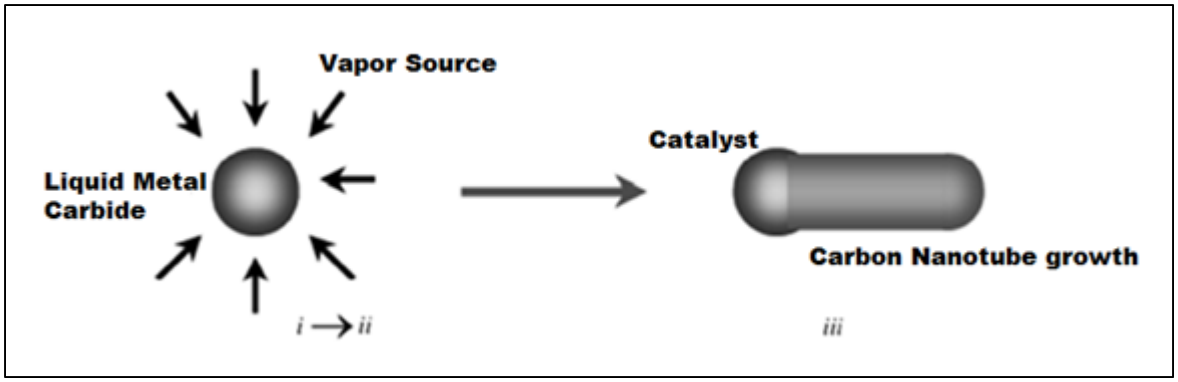

Figure 2-1: Schematic diagram of Vapor Liquid Solid (VLS) growth model [Reprinted with permission from Wiley and Sons[4]].

Two models are generally accepted pertaining to the VLS growth method of the carbon nanotubes: (a) tip-growth, and (b) root growth[5–7]. When the catalyst-substrate interaction is weak, hydrocarbon from the feedstock source decomposes on the top surface of the metal, the carbon diffuses down through the metal, and CNT precipitates out across the metal bottom, pushing the whole metal particle off the substrate. Once the metal is fully covered with excess carbon, its catalytic activity ceases and the CNT growth is stopped. This is known as the "tip-growth" model.

"Root or base growth" can be observed when the catalyst-substrate interaction is strong and the CNT precipitation fails to push the metal particle up from the growth surface; so the eventual precipitation emerges out from the metal's apex (farthest from the substrate, having minimum interaction with the substrate). As shown in **Figure 2-2**, the metal nanoparticle remains adhered to the substrate as the nanotubes continue to grow in the upward direction.

The "tip-growth" has been observed to be dominant with MWCNTs while the "root or base growth" has been mostly associated with SWCNTs. As can be understood, the direction of the growth strongly depends on the stiction of the catalyst particle to the substrate.

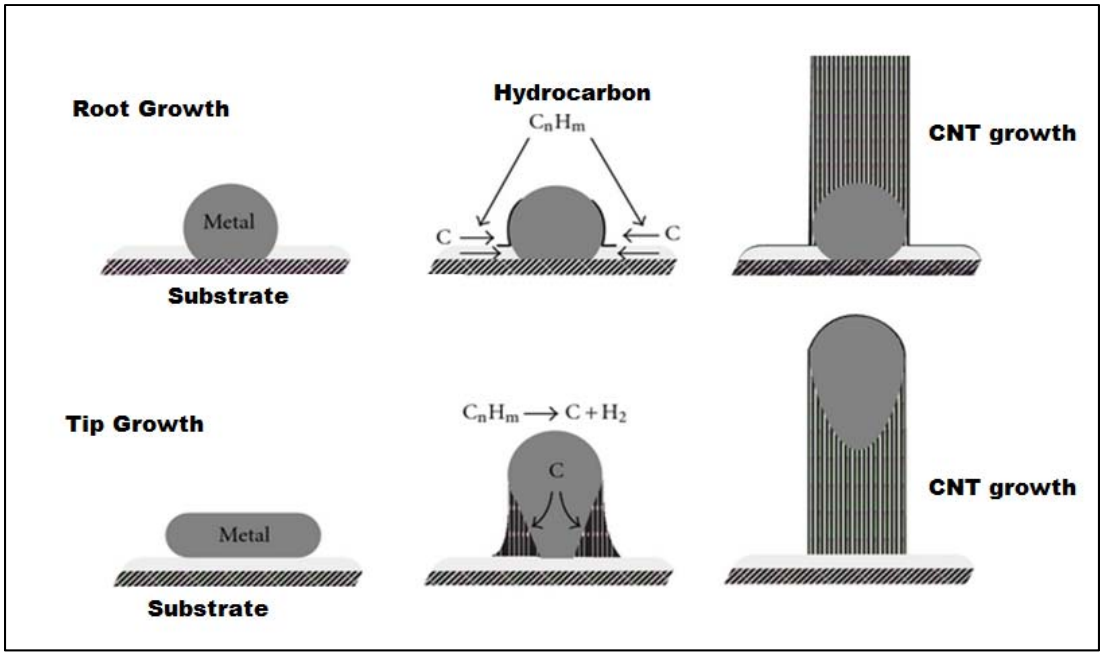

Figure 2-2: Root growth and Tip growth mechanism of carbon nanotubes [Reprinted with permission from Elsevier[7]].

Depending on the size of the catalyst particle, Dai *et al.*[5,8] proposed a mechanism wherein carbon forms a hemispherical graphene cap (known as Yarmulke growth) on the catalyst particle as shown in **Figure 2-3**. When the particle size is too small, insufficient carbon adsorption fails to form the desired cap and if the particle size exceeds a certain threshold, an excess quantity of carbon forms a hemispherical cage that would eventually encapsulate the particle, preventing the growth process. Once the hemispherical cap forms with the right volume of the catalyst particle, the surface energy is reduced which benefits the growth process. Further addition of carbon around the circumference of the catalyst particle in a cylindrical fashion constitutes the emergence of a tubular structure referred to as carbon nanotube (CNT).

The growth process slows down due to the gradual accumulation of amorphous carbon or soot on the exposed surface of the catalyst particles. This process has been referred to as "catalyst poisoning" which eventually stops the growth of the nanotubes.

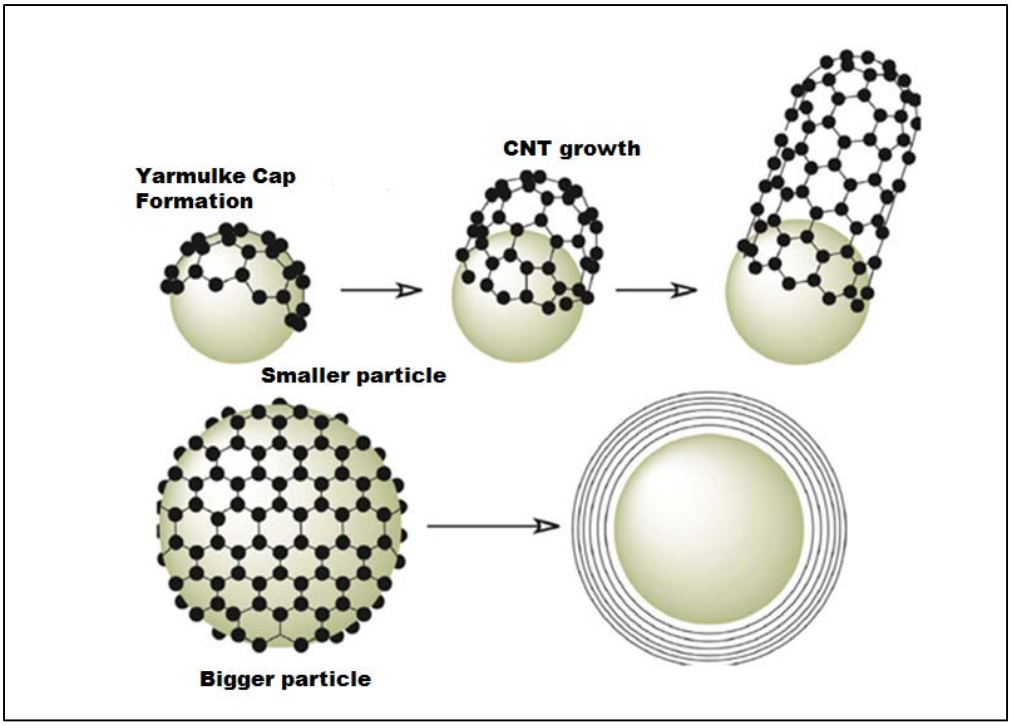

Figure 2-3: Schematic diagram of Yarmulke growth mechanism [Reprinted with permission from Taylor and Francis[5,8]].

2.3: Direct growth techniques

In this section, different direct growth techniques for the carbon nanotube synthesis are briefly reviewed. Carbon nanotubes are generally synthesized by three main techniques[9–12]: (a) arc discharge, (b) laser ablation, and (c) chemical vapor deposition (CVD).

2.3.1: Arc discharge method

This is the simplest and most common method for the synthesis of carbon nanotubes. The nanotubes are synthesized through arc-vaporization of two carbon electrodes (doped with or without metal catalyst) separated by approximately 1mm in an inert gas filled chamber. A direct current of 50 to 100 Amperes creates a high temperature plasma discharge between the two electrodes. The intense arc-discharge results into vaporization of the carbon anode and carbon nanotube deposits are subsequently obtained at the cathode. The deposit contains a mixture of

reaction byproducts in the form of nanotubes, graphite and fullerenes and therefore, needs further purification steps. This technique can be pursued to produce both SWCNTs and MWCNTs. Numerous studies on the growth mechanism in this synthesis technique reveal that the quality and the quantity of the nanotube yield are extremely sensitive to the type and concentration of the catalyst metals, inert gas pressure, plasma control, current and the temperature of the arc-discharge. **Figure 2-4** shows the experimental set up for the synthesis of carbon nanotubes by the arc-discharge method.

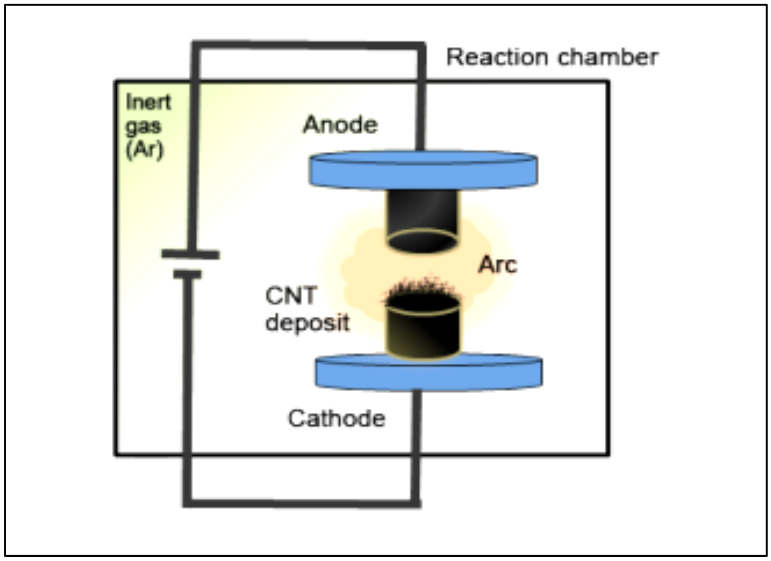

Figure 2-4: Schematic diagram of Arc discharge method of synthesis of carbon nanotubes.

2.3.2: Laser ablation method

In this method, pioneered by Smalley *et al.*[13], (as shown in Figure **2-5**) a high power laser beam is focused on a graphite target in an inert gas filled enclosure. Both continuous and pulsed laser beams of adequate power can be used for the purpose. The carbon at the graphite vaporizes and condenses at a water cooled collector as carbon nanotube deposits. MWCNTs are synthesized if a pure graphite target is used whereas a graphite electrode doped with catalyst

metals produces SWCNTs. It has been reported that laser vaporization produces a higher yield of CNTs with improved purity and narrower size distribution than the ones produced by arc discharge.

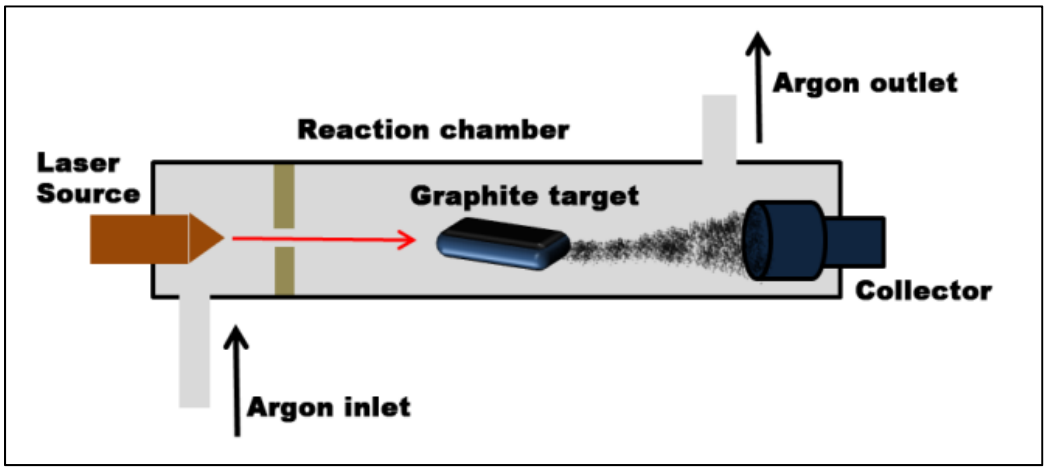

Figure 2-5: Schematic diagram of Laser ablation method of synthesis of carbon nanotubes.

2.3.3: Chemical vapor deposition (CVD) method

Chemical vapor deposition techniques[14–16] involve decomposition of carbon feedstock gas or hydrocarbons in presence of a catalyst. The synthesis method consists of a two- step process:

i. Deposition of catalyst metal onto a substrate, followed by chemical etching or thermal annealing.
ii. Nanotube growth at the catalyst sites thorough VLS growth mechanism.

Chemical etching or thermal annealing is performed to pattern the metal catalyst on the target substrate. Recently, e-beam lithography and evaporation, and physical vapor deposition processes e.g. sputtering, thermal evaporation have been widely utilized to pattern and deposit catalyst nanoparticles for the purpose.

Resistively heated coils, filaments or plasma are mostly used to decompose the carbon feedstock source and the metal coated substrates during this technique. The heating process decomposes the carbon molecules into reactive atomic carbon species and induces catalyst nucleation on the substrates. These reactive carbon species then diffuse towards the heated substrate and start to grow as hollow tubes at the nucleation sites as described by the VLS growth model. **Figure 2-6** exhibits a schematic diagram of the thermal CVD for the synthesis of the CNTs.

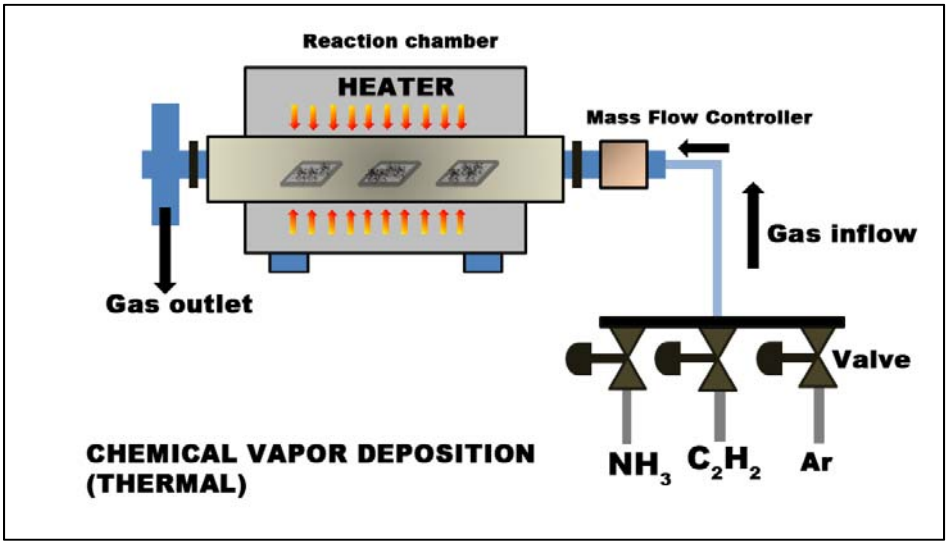

Figure 2-6: Schematic diagram of Chemical vapor deposition (thermal) of carbon nanotubes.

Given the aforementioned principle, different techniques for the synthesis of carbon nanotubes, based on the CVD method, have been developed over the last decade, such as plasma enhanced CVD, thermal chemical CVD, alcohol catalytic CVD, vapor phase growth, laser assisted CVD, CoMoCat process and the high pressure CO disproportionation process. A detailed explanation of these techniques can be obtained from the reports of Szabo *et al.*[11] and Daener *et al.*[14].

2.3.4: Summary of problems with direct growth techniques

The direct growth techniques for CNTs have achieved significant success in optimizing growth parameters such as the effect of temperature, pressure and the type of feedstock gas, and the nature of the metallic catalysts. Nevertheless, these synthesis techniques suffer from incompatibility issues which are addressed below:

i. The high growth temperature (typically around ~900°C) show incompatibility in the direct integration of the CNTs in a wide range of low temperature application such as organic/plastic and flexible electronics, MEMS based thin film sensors and actuators.

ii. The complex thermodynamics and temperature of the synthesis process also impose limitation on the choice of compatible substrates e.g. polyethylene terephthalate (PET) polymer and polycarbonate (PC) based flexible/bendable substrates

iii. All currently known synthesis techniques for CNTs result in major concentrations of unwanted impurities in the form of metallic growth catalysts and soot like carbonaceous skeins. The presence of these unwanted byproducts in the synthesis yield leads to unpredictable behavior of the CNTs in device performance.

iv. An indispensable need of state-of-the-art sophisticated vacuum systems in almost all these techniques contributes to high processing time and cost of instrumentation and maintenance.

2.4: Solution based room temperature deposition of carbon nanotubes

To mitigate the challenges imposed by direct growth techniques, various room temperature, solution based wet coating methods have been actively pursued in both academic and industrial research. When compared to the direct growth methods, a solution based process offers numerous benefits, e.g. an economical fabrication strategy, simple and cost-effective experimental set up, conventional silicon and plastic/polymer substrate compatibility and faster

deposition rate with the prospects of mass production pertaining to roll-to-roll deposition techniques.

The solution based deposition techniques are greatly influenced by several factors such as degree of CNT dispersion, solution stability, surface activation of the substrate, application and removal of dispersion aids (surfactants) during and after coating and use of additional binder materials to improve adhesion of the deposit to the substrate. The following section focuses on the general attributes of colloidal stability, dispersion of the CNT solution/suspension, discussion of the mentioned factors and various deposition methods.

2.4.1: Fundamental concepts of colloidal stability

Preparation of a stable dispersion of the particles to be deposited on a target surface from suitable solvent is an essential prerequisite for successful EPD. In colloid chemistry, the stability of a solution is adjudicated by an important parameter known as the "Zeta potential".

The development of a net charge at the particle surface in a solution affects the distribution of ions in the surrounding solid-liquid inter-facial region. The charged particle in the suspension remains surrounded by ions with an opposite charge (known as counter ions) in a concentration higher than the bulk concentration of these ions. An Electrical Double-layer[17,18] (in **Figure 2-7**) is thus created and can be distinguished into two regions:

i. an inner region (Stern layer) where the counter ions are strongly bound to the particle, and
ii. an outer (diffuse layer) region where these are less firmly attached and co-exist with the co-ions (ions of similar charge as the particle)

Under the application of a suitable electric field, the counter ions and the particle are expected move in opposite directions. However, the counter ions are also attracted by the

particle, and as a result, a fraction of the counter ions surrounding the particle will not migrate towards the opposite electrode but move along with the particle. The boundary, thus created, at the diffuse layer is called the surface of hydrodynamic shear or slipping plane. The potential that exists at this boundary is known as *zeta potential* (ξ) or electro-kinetic potential.

The potential (ψ) at a distance x from the Stern plane is represented by the following form of the Poisson–Boltzmann expression[18]:

$$\psi = \psi_{\delta} \exp(-\kappa x) \quad \text{.....(1)}$$

where κ is the Debye–Huckle parameter, $1/\kappa$ is the distance at which the potential ψ drops to $1/e$ of its value at the Stern plane, ψ_{δ}, and this distance is called the *double layer thickness* or *Debye length*. The thickness is controlled by the concentration and valence nature of the ions in solution. A high concentration of ions (high ionic strength) in the medium generally results in a decrease of the double layer thickness and consequent decrease in the potential. The thickness is commonly represented in the following form[18]:

$$\frac{1}{\kappa} = \left(\frac{\varepsilon \varepsilon_0 kT}{e^2 \sum_i n_i z_i^2} \right)^{\frac{1}{2}} \quad \text{.....(2)}$$

where e is the electronic charge, n_i is the concentration of ions with charge z_i, ε is the dielectric constant of the liquid, and ε_0 is the permittivity of a vacuum. For aqueous solutions at 25 °C, the value of κ (m^{-1}) is given by[7]:

$$\kappa = 2.3 \times 10^9 (\sum_i n_i z_i^2)^{\frac{1}{2}} \quad \text{.....(3)}$$

where n_i is the molar concentration and z_i is the valence nature of ion i.

The ξ potential determines the velocity (v) with which the particles move under the influence of an applied electric field (E) and the *electrophoretic mobility* (μ) which is defined by[18]:

$$\mu = \frac{v}{E} \quad \text{.....(4)}$$

The *mobility* of the particle depends linearly on the dielectric constant (or permittivity) of the fluid, the potential gradient, and the zeta potential and is inversely proportional to the fluid viscosity. This mobility given by the following Henry equation[18]:

$$\mu = \frac{2}{3}\frac{\varepsilon_0 \varepsilon_r \xi}{\eta} f(\kappa r) \quad \text{.....(5)}$$

where ε_0 is the permittivity of vacuum, ε_r is the relative permittivity of the solvent, η is the solvent viscosity, $f(\kappa r)$ is the Henry coefficient, which depends on the relation between the thickness of the double layer ($1/\kappa$) and the core radius (r) of the particle. For a point charge ($\kappa r \ll 1$, Huekel–Onsager case) or a flat surface ($\kappa r \gg 1$, Helmholtz –Smoluchowski case), this coefficient is 3/2 and 1, respectively.

In simple terms, the zeta potential can be defined as the potential difference between the dispersion medium of interest and the stationary or static layer of fluid attached to the dispersed particle in the medium. The magnitude of the zeta potential offers an estimate of the potential stability of the colloidal system. If all of the particles in the colloidal suspension possess a large zeta potential (negative or positive), sufficient electrostatic repulsion exists between the particles. The mutual repulsive forces prevent agglomeration or flocculation of the particles resulting in a stable dispersed suspension. Particles with low zeta potential values tend to “clog” and form aggregates with each other, therefore resulting in the precipitation and eventual degradation of the suspension medium.

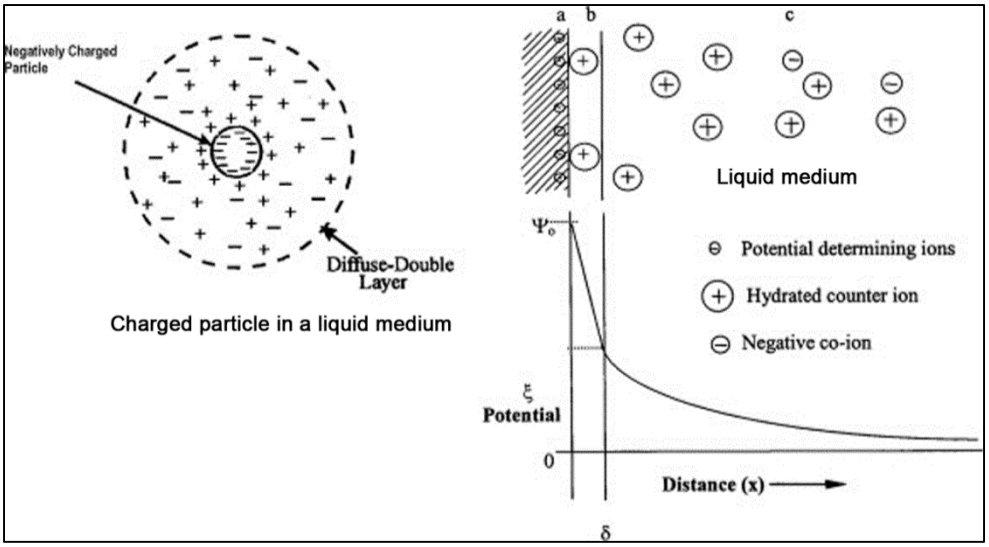

Figure 2-7: Schematic diagram explaining the concepts of Stern layer, Diffuse Region and Zeta potential [Reprinted with permission from Elsevier[18]].

One of the most significant factors in the interpretation of the efficiency of solution based particle coating techniques e.g. electrophoresis is the state of dispersion and colloidal stability of the suspension throughout the process. Particle aggregation occurs when the attractive van der Waals force exceeds the repulsive electrostatic ones. A quantitative estimate of the relationship between stability of suspension in terms of interparticle forces and energies of interactions that exist between colloidal particles in a liquid has been described by the classical DLVO theory[17,19–21] pioneered by Derjaguin and Landau, and Verwey and Overbeek. The DLVO theory explains the variation in energy profile between two approaching particles by mathematically estimating the energies of attraction (London Van der Waals attraction, V_A) or repulsion (V_R) versus the interparticle distance. These forces are added together to yield the total interaction energy, V_T which gives us the following equation[7]:

$V_T = V_A + V_R$ ……..(6)

Figure 2-8 shows the variation of potential energy as a function of inter-particle distance. As can be seen from the graph, V_R decreases exponentially while V_A decreases inversely with

separation distance. The maximum value in the energy profile (primary maximum) represents a potential energy barrier which prevents close approach of the two particles. The significant points in the graph are: (i) the height of the energy barrier, and (ii) the depth of the potential well (primary minimum) at very small distances. When the maximum potential energy barrier is quite large enough compared to the thermal energy (k_BT) of the particles, the system reaches "stability" as the particles fail to surmount the barrier. Under such circumstances, a substantial repulsive potential energy barrier will inhibit the close approach of the particles thereby stabilizing them against aggregation. Once the potential barrier has been surmounted, the particles are held in a deep primary minimum from where particles could not escape.

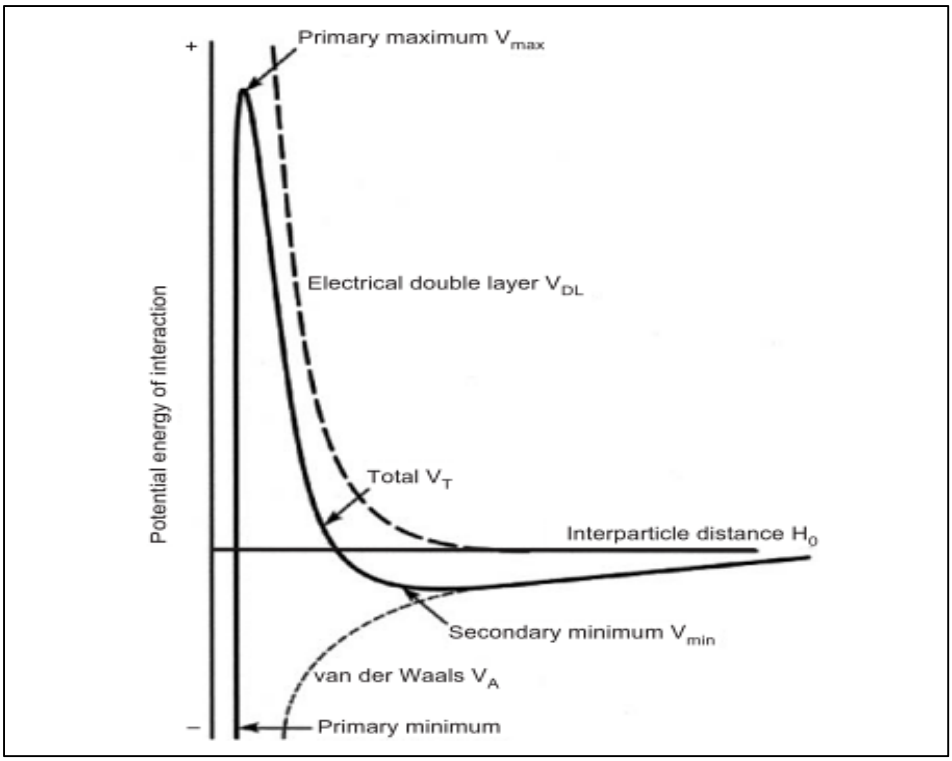

Figure 2-8: Schematic diagram showing the concept of DLVO theory[17].

Theoretically Van der Waals forces of attraction are infinitely strong in the primary minimum. This results in severe aggregation of the particles in the solution.

Depending on the ionic strengths[18], the total potential energy of interaction versus interparticle distance shows four classes of shapes with large variations in stability (as shown in **Figure 2-9**). At very low ionic strengths, the potential energy curve (Curve A) represents only strong and long range repulsive forces producing a totally dispersed system. At a slightly higher but still low enough ionic strength, a primary minimum and a maximum can be seen in the total interaction energy profile (curve B). But the energy is still repulsive in nature. The graph explains that even if it is energetically favorable for the interacting particles to come into close contact, these particles need to possess sufficient energy to overcome the energy barrier for the formation of an aggregate. However, in the intermediate ionic strength, the graph indicates the presence of a primary minimum, a primary maximum and a secondary minimum (curves C and D). The secondary minimum in the potential energy curves is a characteristic feature at relatively large interparticle distance in a reasonably more concentrated electrolyte solution. When the minimum is moderately deep, compared with the thermal energy (k_BT), reversible flocculation may occur. The flocculation is sufficiently stable not to be disrupted by Brownian motion but may dissociate under an externally applied force such as vigorous agitation. The colloid particles experience no repulsive force in a medium of high ionic strength and fall directly into the deep primary minimum (curve E). Under such circumstances, fast coagulation occurs and the system is completely unstable.

Stabilization of colloidal dispersions may be influenced by steric stabilization and structural forces. These mechanisms become substantial due to the physical presence of hydrophilic surfactant macromolecules adsorbed on the particle surface. The surfactant-mediated

stabilization is achieved due to the mutual force of repulsion between the adsorbed macromolecules. Presence of these forces can also change the shape of the energy barrier or primary minimum that controls the particle–substrate interaction. Caution must be exercised in using a controlled amount of sterically stabilized suspension for the wet coating methods since the surface properties of the deposited particles may be altered due to the presence of residual surfactant molecules in the final deposit.

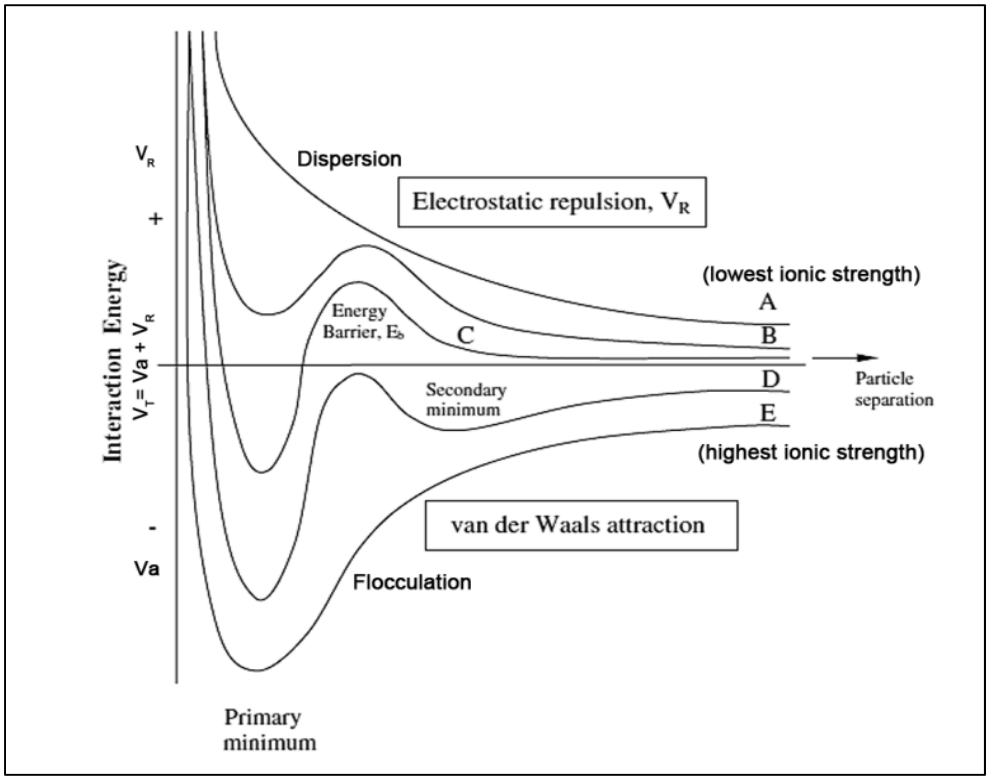

Figure 2-9: Schematic diagram showing the energy profiles for different ionic strengths from DLVO concept [Reprinted with permission from Elsevier[18]].

2.4.2: Methods for stabilizing colloidal solutions

Due to the presence of dominant and prevailing Van der Waals attractive forces between similar colloidal particles, it is necessary to introduce repulsive forces of comparable magnitude

between the particles to prevent aggregation and impart dispersion stability. Stability can be obtained by wrapping the colloidal particles with an electrical double layer (electrostatic or charge stabilization) or adsorbed polymeric molecules (steric and depletion stabilization) or the combination of both. The combination of both electrostatic and steric stabilization results into electro-steric stabilization. A brief account of the fundamental concepts of stabilization is discussed below:

i. Electrostatic stabilization

Electrostatic stabilization[20] can be achieved by imparting Coulombic force of repulsion to the particles in polar liquids. In liquid dispersion media, ionic groups can adsorb on the surface of a colloidal particle through different mechanisms to form a charged layer. The interaction between this charged particle and the surrounding counter-ions in the solution leads to the formation of electrical double layers. The intended charge stabilization can be obtained due to the mutual repulsion between these double layers surrounding the particles.

The thickness of the double layer depends on the ionic strength of the dispersion medium. The ionic strength can be expressed as:

$$I = \frac{1}{2} \times \sum_i z_i^2 c_i \quad \text{.....(7)}$$

where c_i is a molar concentration of ith ion present in the solution and z_i is its charge.

It has been reported that the degree of electrostatic stabilization in colloidal chemistry is extremely sensitive to the ionic strength of the dispersion medium. At low ionic strengths the thickness of the double layer is about 5-10 nm, which is of the same order of the range of Van der Waals attraction. This explains the reason behind obtaining charge stabilization due to mutual repulsion of same magnitude in dispersed suspension of low ionic strength. The thickness of the double layer is reduced significantly with increasing the ionic strength. At high ionic

strengths, the thickness of the double layer is less than 1 nm. Under this circumstance, the range of double layer electrostatic repulsion is usually insufficient to counterbalance the Van der Waals attraction. Coagulation of the most charge-stabilized dispersion medium has been frequently observed with the increasing ionic strength.

ii. Polymeric stabilization

With regard to DLVO theory, the role of the surfactant molecules, introduced in a dispersion medium, is to lower the potential energy barrier to promote coagulation, or to impart some form of electrostatic or physical hindrance against the inter-particle interaction, thereby promoting mutual repulsion to establish colloidal stability in the suspension. The stabilization achieved due to the grafting of the polymeric surfactant molecules between the interacting particles is referred to as "polymeric stabilization".

There are two different mechanisms accepted for polymeric stabilization of colloidal dispersion[22]: (a) Steric stabilization, and (b) Depletion stabilization.

a) Steric stabilization

Steric stabilization of colloidal particles is achieved by physical adsorption or grafting of macromolecules on the surfaces of the particles as depicted in the **Figure 2-10**. The mutual repulsion between the grafted polymers leads to stabilization.

b) Depletion stabilization

Depletion stabilization of colloidal particles is imparted by macromolecules that are freely moving in the solution and acting as physical barriers against particle coagulation.

Electrostatic and steric stabilization can be combined together as *electro-steric* stabilization. The electrostatic component may result due to a net charge on the particle surface and/or charges associated with the polymer attached to the surface (i.e. through an attached

polyelectrolyte) as shown in **Figure 2-11**. Combinations of depletion stabilization with both steric and/or electrostatic stabilization are also observed. The combination of depletion and steric stabilization is very common when high concentrations of free polymer molecules exist in the dispersion medium.

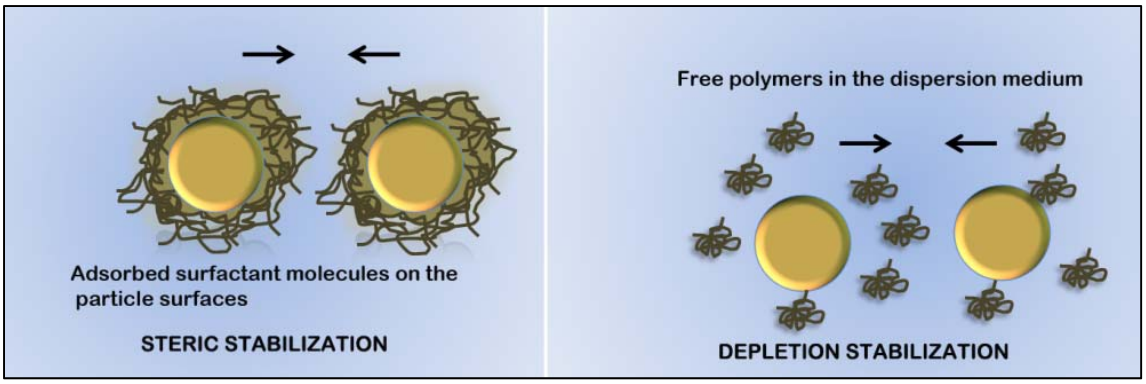

Figure 2-10: Concepts of Steric stabilization (left) and Depletion stabilization (right).

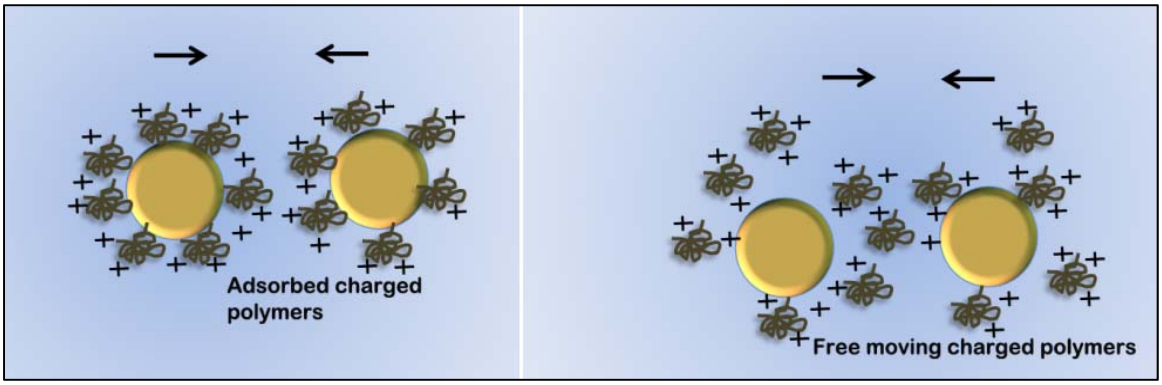

Figure 2-11: Different combinations of electro-steric stabilization.

2.4.3: <u>Different techniques for carbon nanotube dispersion</u>

The carbon nanotube yields produced by direct growth techniques are generally agglomerated in nature and exhibit strong hydrophobic properties. This results in frequent CNT precipitation in the suspension medium during the dispersion and deposition steps. Therefore,

one of the major challenges in fabricating carbon nanotube thin films on arbitrary substrates is to disentangle and separate the bundled skeins into individual nanotubes to obtain stable dispersion for the coating process. Various surface modification techniques have been developed to improve stability and prevent deterioration of the suspension medium. This process, known as the surface functionalization of the carbon nanotubes, involves introduction of charged chemical moieties on the nanotube surfaces using various covalent and non-covalent processes23–25. The interacting forces between these chemical moieties restrict significant agglomeration and entanglement of the dispersed nanotubes, leading to remarkable stability, re-usability and extended lifetime of the suspension medium. Different surface functionalization methods have been pursued to-date and the choice of these methods, by virtue of their benefits and limitations, is dictated by the nature of application involving these functionalized nanotubes. The following paragraphs highlight some of the non-covalent and covalent functionalization methods pursued in this direction.

The non-covalent route of surface modification[26] is one of the most common methods in this direction. In this technique, polymer chains or various surfactant molecules are made to physically adsorb on the surface of nanotubes without any chemical bonding. This type of nanotube functionalization has received a lot of academic interest owing to the non-invasive and non-destructive mode of interaction with minimum defects which preserves the original properties of the nanotubes.

The non-covalent functionalization process can be broadly divided into the following categories:

i. Surfactant and polymer assisted dispersion
ii. Direct dispersion of the pristine or functionalized nanotubes in organic solvents

iii. Use of protein, DNA and starch as dispersion aids.

The functionalization processes are described briefly below:

i. Surfactant and polymer assisted dispersion:

Surfactant and polymer assisted dispersion[27] is the most widely followed route for stable dispersion of the CNT solution. Surfactants are usually classified as: (a) anionic (negatively charged in water), (b) cationic (positively charged in water) and (c) non-ionic (neutrally charged in water). A wide variety of surfactants have been investigated to obtain stable dispersion of carbon nanotubes, e.g. sodium dodecyl benzene sulfonate (SDBS)[28], dodecyltrimethylammonium bromide (DTAB)[29], hexadecyltrimethylammonium bromide (CTAB)[30], octyl phenol ethoxylate (Triton X-100)[31] and sodium dodecyl sulfate (SDS)[32]. Surfactants aid in the dispersion of carbon nanotubes in aqueous solutions mainly through hydrophobic/hydrophilic interactions. It has been proposed that the hydrophobic tail of the surfactant molecule adsorbs on the surface of nanotubes while the hydrophilic head associates with water for dispersion[25]. The following Figure **2-12** illustrates the orientation of the surfactant molecules in this technique.

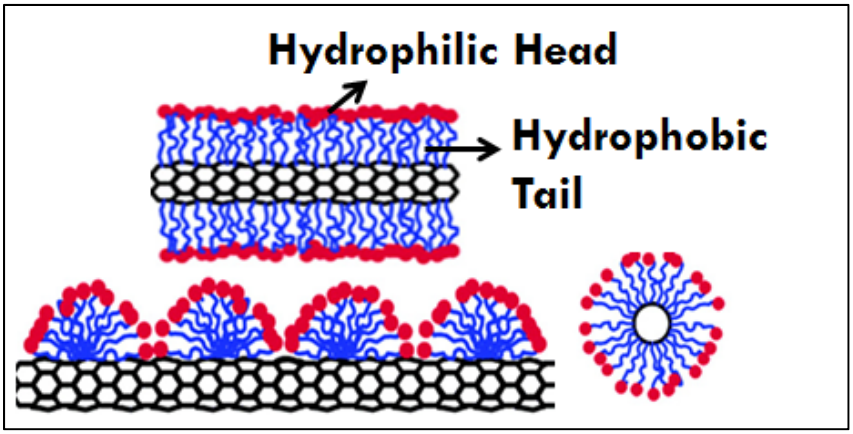

Figure 2-12: Surfactant assisted dispersion of carbon nanotubes [Reprinted with permission from Elsevier[25]].

Polymer wrapping[33,34] of the pristine or functionalized nanotubes is a common method for dispersion especially for CNT-polymer composite film deposition. Polyaniline, polypyrrole[35], polythiophene, polyethylene glycol (PEG) and block co-polymers (BCPs) have been frequently investigated towards this direction. Non-covalent functionalization using different aromatic moieties such as organic dyes has also been successfully pursued[36,37]. However for CNT thin film applications, polymer assisted dispersion is generally not recommended. This is because of the bulky nature of the long polymer chains and challenges to remove the embedded polymer from the deposits after thin film fabrication.

ii. Direct dispersion of the pristine or functionalized nanotubes in organic solvents:

CNT dispersions can also be achieved by direct introduction of the nanotubes in different organic solvents[38] as the suspension medium. The advantage of dispersing the nanotubes without using surfactants is to avoid undesired surfactant or polymer residue in the fabricated film. Several types of solvents have been examined to prepare CNT suspensions for different coating methods including distilled water[39], mixtures of acetone and ethanol[40], and pure organic solvents such as ethanol[41], isopropyl alcohol (IPA)[42,43], n-pentanol[44], toluene, chloroform, tetrahydrofuran (THF)[45] and dimethlyformamide (DMF)[46]. A prior functionalization step of the pristine nanotubes, e.g. covalent functionalization often aids the dispersion process in organic solvents. For example, acid refluxed CNTs with -COOH groups can be dispersed in butanol/toluene and xylene/ethanol mixtures, which are otherwise known to be poor solvents for pristine CNTs. In a separate study by Tour *et al.*[34], the best solvents reported for dispersing CNTs were 1,2-dichorobenzene (95 mg/L), chloroform (31 mg/L), and *N*-methylpyrrolidinone (10 mg/L)[47].

iii. Use of protein, DNA and starch as dispersion aids

Both non-covalent (physio-absorption) and covalent (chemical bond formation) methods have been explored to engineer the interfacial interaction between the as-grown CNTs and biological molecules. Biological macromolecules such as proteins (e.g. Streptavin)[48], oligosaccharides and DNA assisted non-covalent functionalization[49,50] render an environmental friendly and biocompatible method for biological applications. Wei *et al.*[51] demonstrated the self- assembly of protein-protected gold nanoparticles (AuNPs) on functionalized MWCNTs by the use of hydrophobic PANHS protein through controlled non-covalent treatment. The schematic diagram of the work is shown below (**Figure 2-13**). Sidewall non-covalent functionalization of CNTs has also been carried out by the adsorption of pyrene moieties of bifunctional molecules such as 1-pyrenebutanoic acid, succinimidyl ester for the immobilization or grafting of ferritin, streptavidin[52] and monoclonal IgG C_{60} specific monoclonal antibody on the SWCNTs[53].

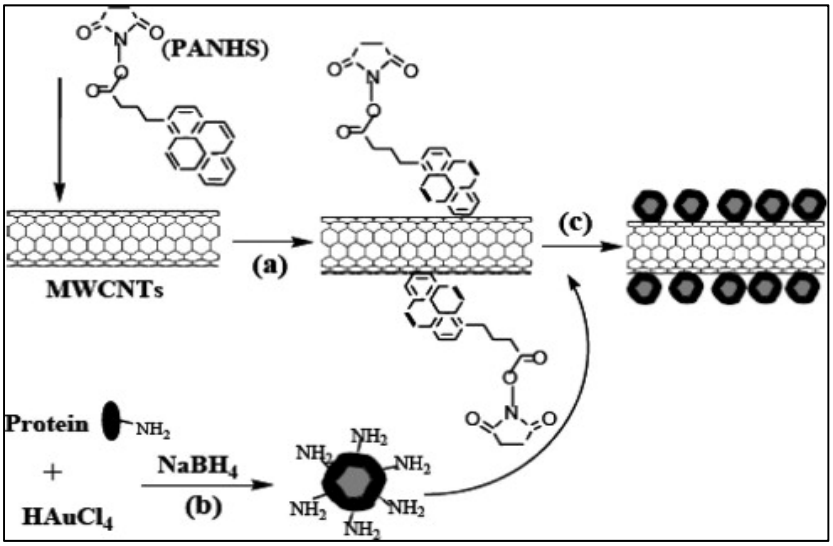

Figure 2-13: Schematic view of the self-assembly of the protein-protected AuNPs on PANHS functionalized CNTs [Reprinted with permission from Elsevier[51]].

In the covalent route of CNT surface modification, polymer chains or reactive species can be chemically attached to the surface of the nanotubes[54]. The process is generally accomplished by aggressive chemical reactions with different chemical agents, strong acids[55,56] being the most common ones.

Acid refluxing of the pristine carbon nanotubes, using a mixture of strong oxidizing acids such as concentrated nitric acid and sulphuric acid, under ambient or elevated temperature is the most common method of covalent modification (**Figure 2-14**). The acid treatment of the carbon nanotubes offers the following benefits:

i. It helps in the purification of the pristine nanotubes by dissolving the unwanted metal catalyst impurities and residual reaction byproducts from the growth process.

ii. Shortening of the tube lengths is achieved since the acid solution attacks various defective sites of the synthesized nanotubes.

iii. The acid-heat treatment on the pristine carbon nanotubes attaches negative carboxylic groups (-COOH) on the surface of the tubes, thereby imparting negative surface charges. The resultant electrostatic repulsion prevents inter-tubular agglomeration and ensures appreciable stability of the CNT suspension during the dispersion process.

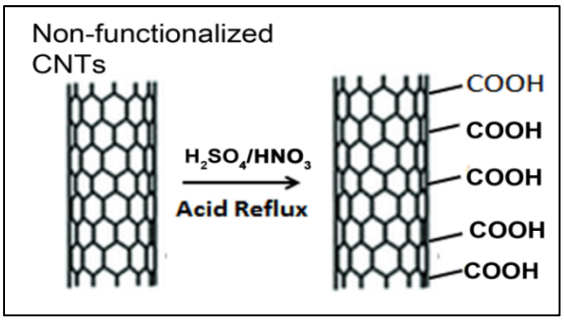

Figure 2-14: Covalent functionalization of carbon nanotubes by acid refluxing method.

Velasco-Santos *et al.*.[57] reported the advantages of chemical functionalization of nanotubes in improving the composite properties. In the study, *in situ* polymerization of methyl methacrylate (MMA) was achieved both in the presence of un-functionalized and acid - functionalized nanotubes. It was concluded that the covalent functionalization provides an efficient and attractive route for producing synergetic composite materials with carbon nanotubes since the generated reactive groups in the surface modification step assisted in binding polymer chains to the nanotubes during the course of polymerization.

Synthesis of nano-hybrid materials from CNTs and nanoparticles is also reported in which the nanoparticles are covalently immobilized on the nanotubes surface[58]. To achieve the required functionalization, the nanotubes were treated with nitric acid followed by thionyl chloride ($SOCl_2$) to generate COCl groups on the surface. Magnetite colloid solution was reacted with COCl- treated nanotubes at room temperature using ultrasonication as explained in **Figure 2-15**. The process demonstrated the effectiveness of the chemical pretreatment of nanotubes in generating active sites for the magnetite particles to anchor on the carbon nanotube surfaces. The resulting nano-hybrids were also easily dispersible in aqueous solvents and exhibited appreciable stability over a considerable time period.

Covalent attachment of proteins with the CNTs through direct covalent methods or with linking molecules has been demonstrated as well. Huang *et al.*[59] and Jiang *et al.*[60] have shown successful immobilization of protein molecules (e.g. Bovin Serum Albumin or BSA) on the carbon nanotube surfaces by diimide activated amidation covalent reaction.

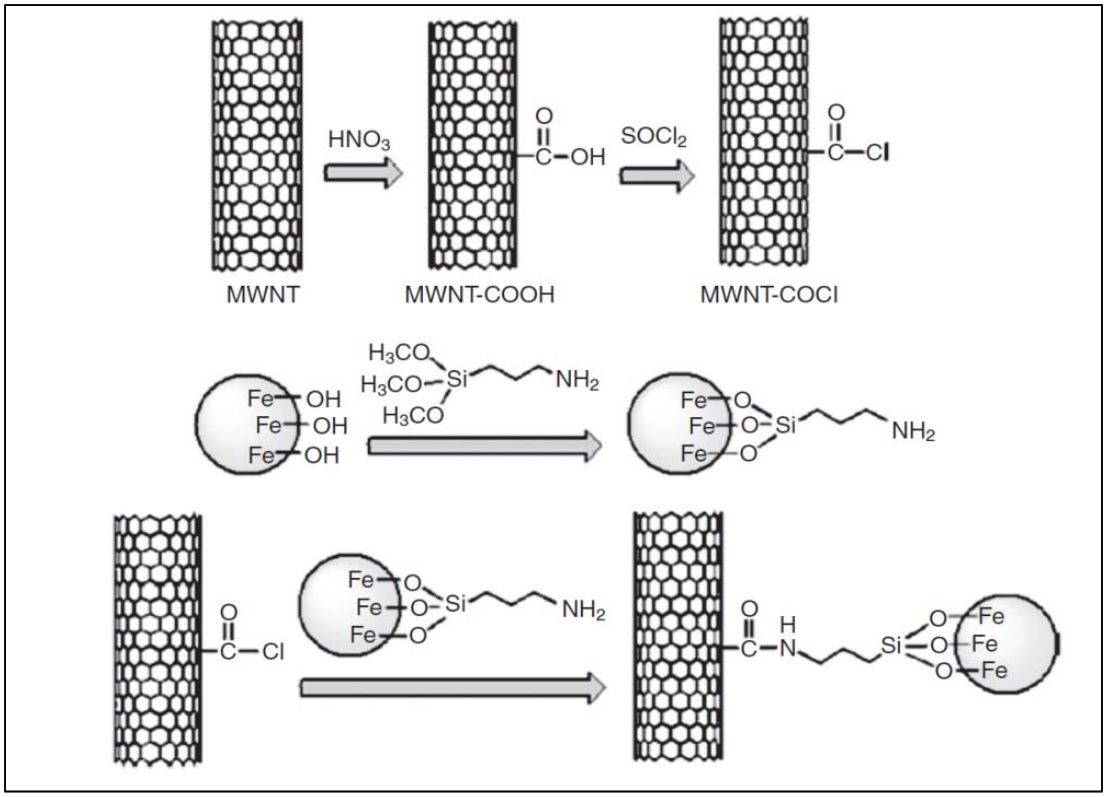

Figure 2-15: Schematic diagram of immobilization of nanoparticles on covalently functionalized carbon nanotube surface [Reprinted with permission from Elsevier[58]].

2.4.4: Literature review of different coating methods

The basic principle of room temperature deposition method is to coat an arbitrary substrate from a dispersed solution of the intended material followed by controlled drying without introducing agglomeration in the deposit. In surfactant or polymer assisted deposition, an additional step of washing and removing the dispersion aid from the deposit is necessary.

Following the stable dispersion of the carbon nanotubes in aqueous medium or organic solvents, numerous innovative solution-based CNT coating techniques have been developed for the purpose. Some of the prominent methods include ‘’logs-on-a-river” approach, also known as Langmuir-Blodgett (LB) method, self-assembly of functionalized CNTs on chemically modified substrates, linker-free directed assembly of CNTS by using SAM molecules, local surface

charging, dip coating, drop casting, spray coating, spin coating, inkjet printing and Mayer Rod coating.

In the "logs-on-a-river" concept[61], known as the "Langmuir- Blodgett (LB)" method[62,63], a monolayer thick layer (known as Langmuir monolayer) spread at the air/water interface is transferred onto a solid substrate by repeated subsequent dipping and lifting the substrate from the solution. Precise control of the surface spreading of CNTs on water is necessary for the process. The multilayer deposition can be achieved through layer-by-layer coating method by repeated horizontal or vertical dipping, and lifting method. The LB method offers a simple and convenient approach for fabricating monolayer or sub-monolayer films but is generally very slow with unreliable results in fabricating CNT multilayer films.

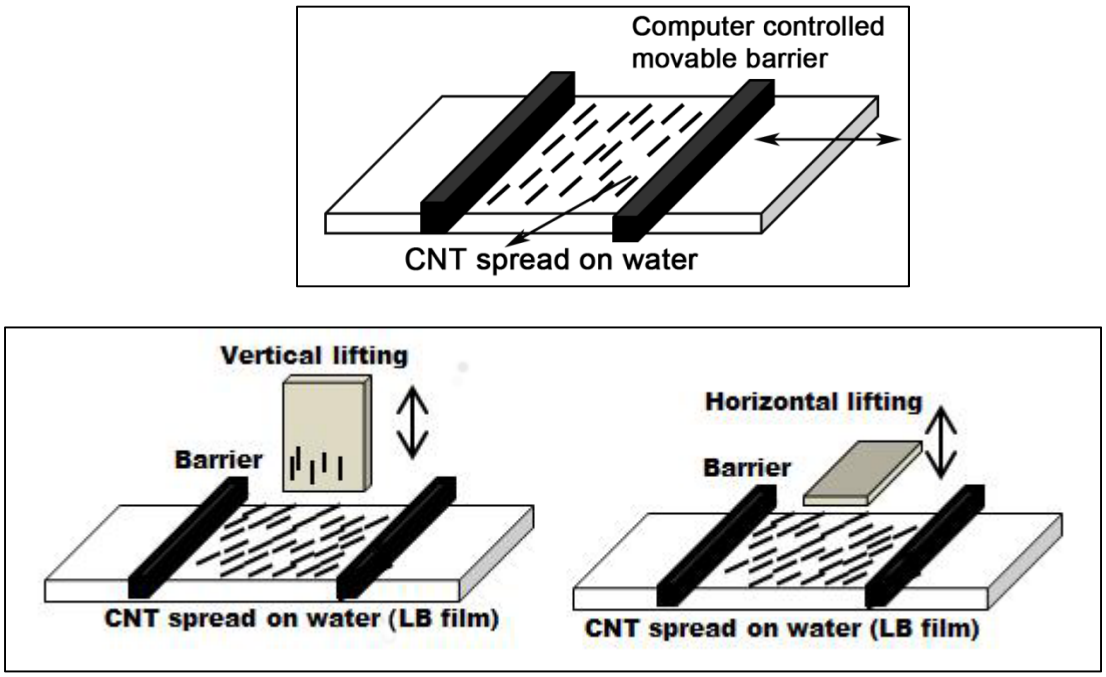

Figure 2-16: Langmuir Blodgett method of carbon nanotube coating.

Dip coating[64] method is a variation of the LB method and has been frequently used also to fabricate transparent and conductive films on various substrates. One major disadvantage of these kinds of coating methods is that both sides of the substrates are coated during the deposition step which may not be desired for certain applications.

Self-assembly (SA)[65–67] is a relatively fast and cheap method to fabricate thin films on a surface. SA relies on the interfacial surface interaction and attractive forces between the interacting CNTs and the functionalized surface. In the surface functionalization step, either polar chemical groups (such as amino ($-NH_2$) or carboxyl (-COOH)), octadecyltricholosilane (OTS), octadecathiol (ODT) or nonpolar groups (such as methyl ($-CH_3$)) can be grafted to activate the surface. Functionalization of the CNTs may also be required as a pre-processing step prior to self-assembly. As the substrate is immersed in the dispersed solution, CNTs are attracted toward the polar groups and self-assemble to form multilayer films. Another SA approach is to locally charge the target substrate[68] and allow Coulombic forces to guide the assembly of the CNTs on it. The self-assembly coating method can be made compatible with the existing, high throughput patterning processes e.g. photolithography, stamping and dip-pen nanolithography and therefore has attracted enough research attention recently.

Substantial research attempts have been pursued to utilize spray coating technique[69,70] for depositing CNT thin films for different applications such as CNT-based transistors, transparent electrodes and field emission devices. In this method, a controlled amount of CNT solution or ink is sprayed onto a target substrate. The substrate is heated to facilitate drying the liquid. The temperature for the substrate is adjusted by the choice and rate of evaporation of the solvent or CNT ink to avoid any significant agglomeration.

Some of the other competing coating methods include spin coating[71] and drop casting. A small amount of dispersed CNT solution is dropped onto a substrate followed by high-speed spinning of the substrate (spin coating) or simply air drying (drop casting). Spin coating is useful for generating monolayer or sub-monolayer films although multiple attempts are required for thick films. Drop casting is the most popular method in coating a substrate in academic research. This technique, however, results into agglomerated or, stacked nature of the CNTs on the depositing surfaces.

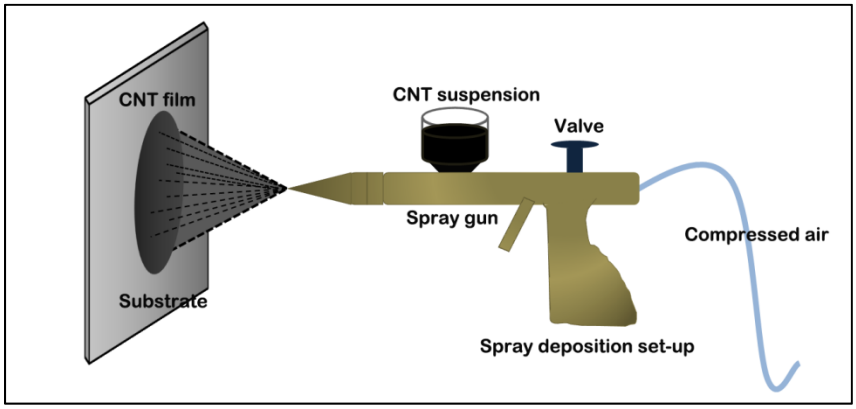

Figure 2-17: Spray coating method of carbon nanotubes.

Inkjet printing of the CNT solution[72–74] has also been reviewed comprehensively. The high repeatability, scalability and the ability to print fine patterns and noncontact injection with high deposition rate makes the process highly promising for a commercial coating technique in future.

The most widespread deposition method in industry involves coating CNT ink solution on a substrate by Mayer Rod followed by controlled drying[75]. A controlled amount of dispersed CNT ink is coated on a substrate by a stainless steel rod wound tightly with stainless steel wire (Mayer rod). A heating bar is used to control the post deposition drying process. Owing to its

simplicity, this coating method can be scaled up to "roll-to-roll" techniques for CNT thin film deposition on extremely large area substrates.

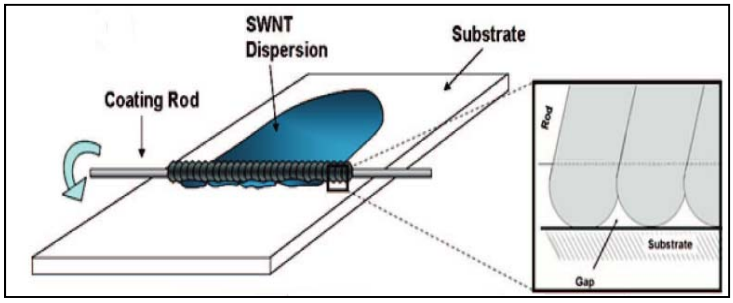

Figure 2-18: Mayer Rod coating method of carbon nanotubes [Reprinted with permission from ACS publications[75]].

2.4.5: Summary of problems with the coating techniques

Although the coating techniques discussed in the previous section, offer an economical and versatile deposition approach in the fabrication of CNT thin films, these methods show limitations with regard to the processing logistics. The limitations are outlined below:

i. Most of these coating methods e.g. Langmuir- Blodgett (LB) are efficient in fabricating monolayer or sub-monolayer CNT films but remain incompetent for fabricating multilayer films. Multiple attempts are required to fabricate thick films, which inevitably leads to longer processing time and unpredictable behavior in the reproducibility of the deposition process.

ii. Reliability of these methods e.g. drop casting, dip coating pertaining to film quality, packing density and the homogeneity of the deposits over large surface area still remain as unresolved fabrication challenge.

iii. The frequent occurrence of discontinuity in the film structure or sparse deposits complicates the deposition model.

iv. Deposited films show inconsistency in film thickness, morphology or precise control over thickness and lack of reproducibility in the deposition results add to the bottlenecks of these existing methods.

v. Although these coating methods are known for their economical and simple deposition approach, advanced controlling units such as flow rate controllers (e.g. spray coating, ink-jet printing), inefficient material usage due to loss of EPD suspension (e.g. in spin coating) and re-usability issues contribute to the operational cost.

2.5: Electrophoretic deposition (EPD): Fundamentals and concepts

With the prevailing interest in the search and implementation of a simpler deposition model, one promising technique that has been investigated for room temperature deposition of carbon nanotubes in recent days is *electrophoretic deposition (EPD)*[76,77]. EPD has been traditionally employed in the processing of ceramics, coatings and composite materials. Presently, EPD has been employed for the processing of fiber reinforced composite ceramics, textile structures, infiltration of porous substrates and deposition of nanoparticles, biomaterials and thin films[78]. It has been developed as an extremely efficient and fast process for production of multilayer films or coatings from colloidal suspensions in a single processing step. EPD offers several benefits including an economical approach towards thin film fabrication due to its cost-effectiveness, the need for a relatively simple apparatus, long range consistency in deposit thickness and morphology, high deposition rate, appreciable packing density leading to continuity of the film, high material usage efficiency, re-usability of the solution, a wide range of substrate compatibility for versatile applications and, the ability to be scaled up to large product volumes and sizes. The potentials to apply thin and thick deposits with precise control on the deposition parameters in a single processing step even on substrates with complex chemistry make the process attractive in MEMS, printable electronic devices and nano-electronics

applications. Conventionally, one of the requisites for EPD is that the substrate should be electrically conductive. However the possibility of forming deposits on semi-conducting and non-conducting substrates by EPD has presented enormous potentials of integration of this deposition technique in a wider spectrum of materials research and technology. The next section illustrates a comprehensive account of the fundamental concepts of EPD, the proposed mechanisms and review of the state-of-the-art EPD of carbon nanotubes on conducting substrates.

2.5.1: Fundamental concepts of electrophoresis

EPD can be described by two essential processes[17,18]. In the first step, charged particles, dispersed in a solvent or an aqueous medium, migrate towards the desired electrode by the application of a suitable electric field to the suspension. This step is known as "electrophoresis". In the second step, the particles collect and adhere to the electrode surface to form a coherent deposit (deposition). **Figure 2-19** depicts the fundamental ideas governing the deposition process.

Depending on the polarity of the electrodes on which deposition is accomplished, EPD can be classified into: (a) cathodic EPD, and (b) anodic EPD. When the particles in the suspension acquire positive charges, the deposition occurs on the cathode and the process is called cathodic electrophoretic deposition. The deposition of negatively charged particles on positive electrode (anode) is termed as anodic electrophoretic deposition. Therefore, by suitable modification of the surface charge on the particles, any of the two modes of deposition is possible.

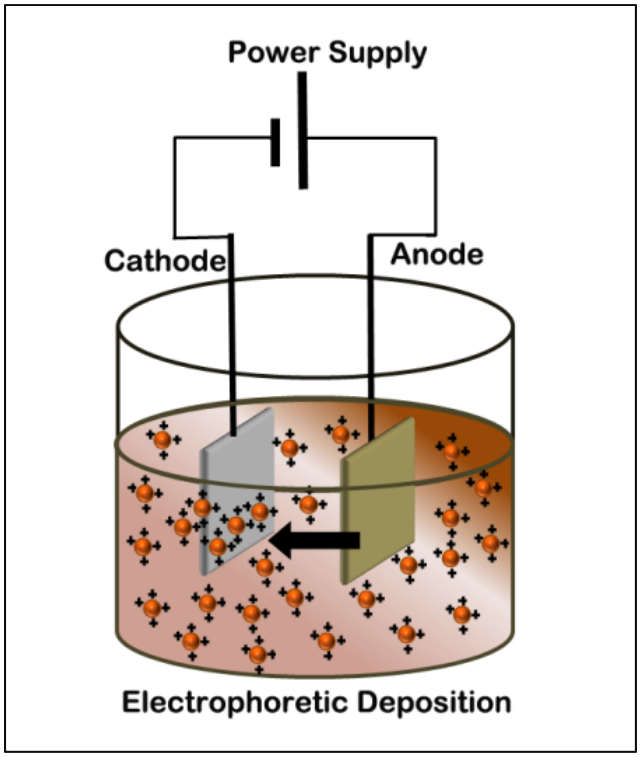

Figure 2-19: Schematic diagram of Electrophoretic Deposition method.

2.5.2: Proposed mechanisms of electrophoresis

Substantial research efforts have been extended to explain the kinetics and mechanism of deposition during EPD. Several theoretical and mathematical modeling studies are being carried out to clarify the influence of the electrochemical parameters on the complex interactions between solvent, particles and the applied electric field. Electrophoretic deposition is reported to be distinct from electrochemical deposition since binding of the obtained deposit on the target electrode is not necessarily due to electron transfer, and the particles being deposited are larger than ions - i.e. micro and nanoparticles. However, a general agreement pertaining to particle aggregation/destabilization near the electrode (the deposition step) has not been reached yet. Tassel and Randall[79] recognizes some electrochemical changes near the electrode which would disrupt the equilibrium in the EPD suspension, so that particles that are dispersed in the bulk due

to electrostatic/steric stabilization can be forced to flocculate at the electrode. The authors have also summarized the mechanisms on the basis of densification, direct electrostatic force, electro-sedimentation ion depletion enhanced electrophoretic interaction, salting out, charge reduction/neutralization, squeezing out, bridging flocculation and desorption of neutral/charge polymer and polyelectrolyte neutralization. Zhitomirsky[80] has divided the EPD mechanisms into three categories: (1) charge neutralization or electrocoagulation, (2) zeta potential lowering and (3) particle accumulation. Particle coagulation on the depositing electrode is a complex phenomenon since each charged particle in suspension has an associated EDL and it is thus possible that the first layer of deposited particles might repel and prevent deposition of incoming particles. The conundrum that remains unresolved pertains to the mechanism by which the mutual repulsion existing between the deposited particle and the incoming particle in the EPD solution is overcome which eventually leads to particle coagulation at the electrode during EPD[81]. The migration step depends on the bulk properties of the colloidal dispersion (bath conductivity, viscosity, particle concentration, size distribution and surface charge density)[18]. It has been suggested that the primary function of the applied electric field is to provide acceleration of the particles towards the opposite electrode with the electrostatic Coulombic force as the driving force. Several theories explaining the deposition mechanism have been proposed in this regard without any universal consensus[18,79,81–83]. Those are: (1) decrease in inter-particle repulsion of the particles close to the electrodes due to the pressure of the incoming particles (flocculation by particle accumulation), (2) neutralization of the particle upon contact with the deposition electrode or deposit (particle charge neutralization mechanism), (3) decrease in the interparticle repulsion and collapse of the particles to form a deposit due to increase in

electrolyte concentration (electrochemical particle coagulation), and (4) thinning of the double layer phenomenon (electrical double layer (EDL) distortion and thinning mechanism).

The following pointers highlight some of the competing mechanisms proposed to describe the deposit formation process.

i. Flocculation by particle accumulation

The first attempt to explain the phenomenon of EPD was made by Hamaker and Verwey[84,85]. They suggested that the formation of deposit by electrophoresis is akin to the formation of sediment due to gravitation. The primary function of the applied electric field in EPD process is to force the particles towards the target electrode and to accumulate near it. The pressure exerted by the incoming particles enables particles next to the deposit to overcome the inter-particle repulsion and form deposits.

ii. Particle charge neutralization mechanism

Grillon *et al.*.[86] suggested that particles undergo charge neutralization upon contact with the deposition electrode or the deposit and then become static. It explains deposition of powders, that are charged due to salt addition to the suspension. This mechanism explains the deposition process for monolayer deposits but is invalid under the following conditions: (a) EPD for longer times (thick deposits), (b) when particle–electrode processes are prevented, e.g. semi-permeable non-conducting membrane induces deposition between the electrodes, and (c) pH altering electrochemical reactions near or at the electrode

iii. Electrochemical particle coagulation mechanism

This mechanism implies reduction of the repulsive forces between particles which eventually leads to coagulation. The proposed reduction in repulsion and eventual coagulation occurs due to increase of electrolyte concentration as discussed by Koelmans[81]. The proposed

increase in ionic strength near an electrode was found of the same order as required to flocculate a suspension. Koelmans proposed the increase in electrolyte concentration near the depositing electrode lowers the zeta potential and induces flocculation. This mechanism is plausible when electrode reactions generate OH^-, e.g., suspensions containing water. This mechanism is however invalid when there is no increase of electrolyte concentration near the electrode.

iv. Electrical double layer (EDL) distortion and thinning mechanism

The explanation for particle deposition mechanism when there is no increase of electrolyte concentration near the electrode was offered by Sarkar and Nicholson[82]. By considering the movement of a positively charged oxide particle towards the cathode in an EPD cell, they have proposed the following model as shown in **Figure 2-20**.

The proposed mechanism can be described in three main steps:

a. When a charged particle, along with the counter ion populated diffuse double layer is subjected to an electric field, the double layer envelope undergoes a distortion in a way such that it tends to become thinner ahead and wider behind the particle (i.e. at the tail)
b. During the migration of the charged particle towards the intended electrode, ions of similar charge will move in same direction as the particle and react with the counter ions accompanying the charged particle. The reaction induces a “thinning” process of the double layer of the particle.
c. As this neutralization reaction continues, the double layer around the ‘tail’ of the particle starts to grow even “thinner” so that the next incoming particle (which has a thin leading double layer at the head) approaches close enough for London Van der Waals attractive force to dominate and induce coagulation/deposition to form the deposit.

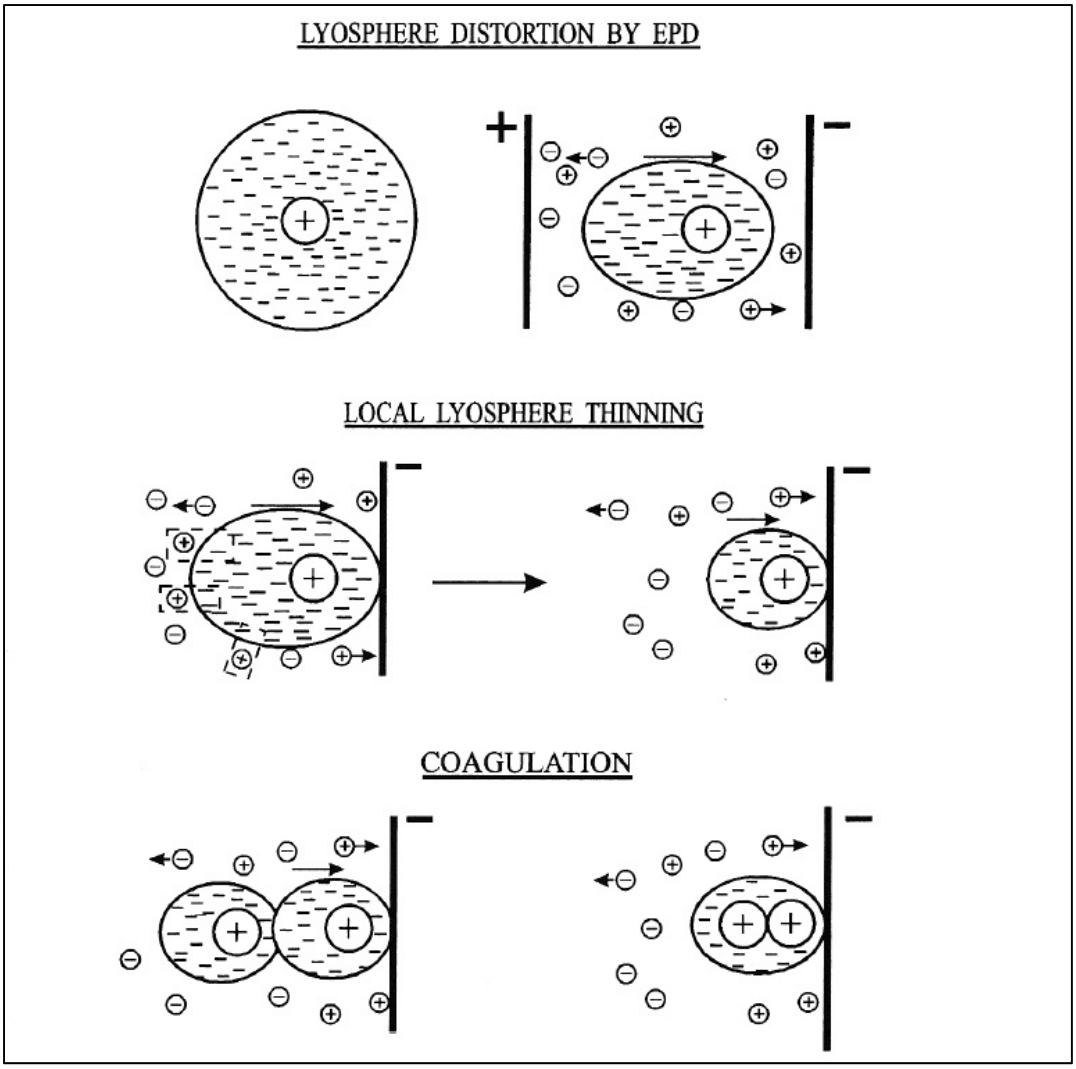

Figure 2-20: Schematic diagram of electrical double layer (EDL) distortion and thinning mechanism [Reprinted with permission from Wiley and Sons[82]].

The thinning of the double layer leading to coagulation is acceptable considering the high concentration of particles near the electrode which leads to high collision efficiency. Also, this mechanism works for incoming particles with thin double layer heads, coagulating with particles already in the deposit and leading to thick deposits. Until recently, the electrical double layer distortion and thinning mechanism is the most widely accepted theory for electrophoretic deposition on conducting substrates.

2.5.3: Literature review of electrophoretic deposition of carbon nanotubes

Electrophoretic deposition (EPD) has been gaining increasing interest as an economical and versatile wet processing technique for the production of novel thin coatings of CNTs, mostly on conductive substrates. The deposition technique has been pursued for a wide range of applications such as CNT reinforced composite films and structures, field emission devices, fuel cells and supercapacitors. The following paragraphs present a detailed literature review with regard to preparation of suspension medium and EPD of CNTs pursued till date.

As reported by Van der Biest and Vandeperre[17], the desired approach in preparing ideal suspension for electrophoretic deposition is to essentially create high zeta potential on the particles, while maintaining low ionic conductivity of the suspension. As produced carbon nanotubes are chemically inert and often are procured in agglomerated and entangled masses with various metallic and carbon impurities. A post synthesis treatment is therefore necessary to purify and disperse the CNTs in a suitable solvent. The common strategies involve thermal oxidation, acid reflux in strong acid solution e.g. concentrated nitric acid (HNO_3) and sulphuric acid (H_2SO_4) at ambient or elevated temperature and annealing to purify the raw product. As has been pointed out, the acid-heat treatment renders purification of the pristine nanotubes and shortening of the tube length in a single processing step. The treatment also introduces enough carboxylic groups (-COOH) on the surface of the nanotubes which imparts negative surface charges. This establishes sufficient inter-tubular repulsion, thereby ensuring remarkable stability of the CNT suspension all through the EPD experiments. The following diagram (Figure **2-21**) depicts the functionalization process of the CNTs after acid refluxing.

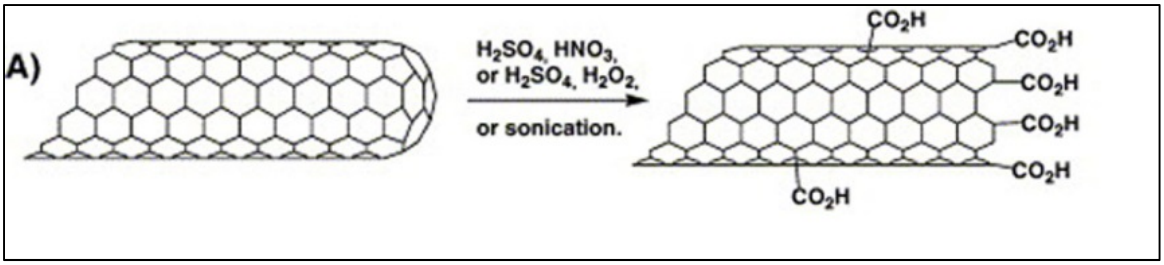

Figure 2-21: Acid refluxing of carbon nanotubes [Reprinted with permission from Elsevier[87]].

Polymer based surfactants are frequently used to impart steric stabilization in the dispersion of CNTs in suitable solvents. Both unpurified and acid refluxed/surfactant treated nanotubes have been dispersed to obtain stable EPD suspension in a variety of solvents such as distilled water[39] and pure organic solvents such as ethanol[41], acetone/ethanol mixtures[40], isopropyl alcohol (IPA)[42,43], n-pentanol[44], tetrahydrofuran (THF)[45], dimethlyformamide (DMF)[46]. However, surfactant assisted dispersion is generally not desirable in EPD due to the decomposition of the polymers in aqueous media under the applied electric field and the presence of residual surfactants in the final deposit which may be detrimental to the performance of the thin CNT film in device applications.

The earliest reference of EPD of CNT appears in the work performed by Du *et al.*[40] who explored the possibility of using EPD to deposit multi-walled CNTs from ethanol/acetone suspension. They observed deposition of a porous CNT film due to evolution of hydrogen gas at the cathode when acetone was used as the solvent and the effect of composition of the solvent mixture (ratio of acetone-to-ethanol) in the microstructure of the films. Thomas *et al.*.[88] successfully deposited and characterized homogeneous MWCNT films onto stainless steel substrates using EPD from aqueous suspensions of acid-oxidized nanotubes, without employing additional surfactant, polymer, or stabilizing agents. The work reviews the CNT deposition kinetics and the influence of applied electric field and deposition time with the deposition yield

and thickness. A mathematical model for the kinetic of EPD of CNTs based on Hamaker's law was also reported which indicates good agreement with experimental results. Jung *et al.*[89] deposited a thin film of horizontally aligned SWCNTs from an aqueous mixture of CNT and detergent for field emission device applications. EPD of uniformly CNT coatings on glass plates with silver or ITO film layer was also studied by Wang *et al.*[90] to study the emission properties of CNT films for display applications. Roth *et al.*[91] fabricated thin, conductive, carbon nanotube networks on borosilicate glass and poly-ethylene terephthalate or PET substrate with 10 nm layer of evaporated aluminum or titanium. During the deposition process, the metal coating was oxidized to their respective oxides which turned the deposition surface transparent. Wei Li *et al.*[92] reported fabrication of CNT-polyvinyl alcohol composite hydrogel on copper substrates for bio-sensing applications. There has also been recent development in the fabrication by electrophoretically coated CNT reinforced hydroxyapatite (HA)[93] and Bioglass based 3D scaffold coatings[94] for biomedical applications. Moreover, composites consisting of ceramic nanoparticles and MWCNT have also been produced recently by sequential EPD and by electrophoretic co-deposition[95,96]. A comprehensive study on electrophoretic deposition of carbon nanotubes on different substrates is reported by Boccaccini *et al.*[77]. The following table outlines a brief summary of the substrate/electrode properties, CNT suspension and the intended applications of the EPD of CNTs performed till date.

Table 2-1: Overview of EPD of CNTs.

References	**Substrate or electrode properties**	**CNT suspension**	**Target application**
Cho *et al.*[88], Thomas *et al.*[76]	Stainless steel	Acid refluxed CNTs in aqueous solution	Porous electrodes, heat extraction devices, active coating for tissue engineering scaffolds
Pan *et al.*[97]	Aluminum	CNT with EPI REZ resin and curing agent in ethanol	Fabrication of CNT based composite sheets
Wang *et al.*[90]	Glass plates with silver or ITO coating	Different volume ratio of acetone and ethanol	Cold cathode fabrication for field emission devices
Wei Li *et al.*[92]	Copper	Hydrogen peroxide and acid refluxed CNTs in water	CNT-Polyvinyl alcohol (PVA) hydrogel composites for biological applications, biosensors
Pei *et al.*[98]	Stainless steel	SDS treated CNTs in aqueous suspension	Optoelectronic applications
Bae *et al.*[42]	Titanium (Ti)	Acid refluxed CNTs in isopropyl alcohol (IPA)	Investigation of field emission properties
Du *et al.*[40]	Metal electrodes	Acetone and ethanol with different volume ration	Electrochemical studies, electrodes for rechargeable battery and actuators
Du and Pan[99]	Nickel foils	Acid refluxed in ethanol	Fabrication of CNT based supercapacitors
Oh *et al.*[41]	Indium Tin Oxide (ITO) and Chromium (Cr) coated glass	Acid refluxed CNTs in ethanol	Fabrication of field emission cathodes
Roth *et al.*[91]	Borosilicate glass and PET substrates with aluminum(Al) and titanium (Ti) coating	Acid refluxed and sodium dodecyl sulphate (SDS) treated CNTs	Photovoltaic applications, electronic device application on rigid and flexible substrates

CHAPTER 3: MOTIVATION AND RESEARCH GOALS

3.1: Motivation

In recent years, *electrophoretic deposition (EPD*) has been pursued as room-temperature, solution-based deposition approach of nanomaterials and has been enjoying extensive research investigations due to its versatility, cost-effectiveness and precise control of deposit thickness in a single processing step. Considered to be a well-established ceramic processing technique only until the early 1990's, the applications of EPD have been expanded to explore a broad range of advanced materials including novel ceramics, composite metals and polymers in the last 20 years of materials science. Contrary to the general assumption that electrophoretic deposition is only limited to conductive substrates, there are recent literature reports where attempts have been pursued to perform electrophoretic deposition on non-conducting substrates[19,100,101]. One of the crucial applications fields of the EPD technique would be in the fabrication of homogenous and continuous thin and thick films of CNTs for semiconductor research and development - e.g. in nano-electronics for thin film transistors (CNT-TFT), nanoporous electrodes and device integration in MEMS based sensor platform, supercapacitors and emissive display (CNT-FED) technologies. Fabrication of CNT reinforced metallic nanocomposites and new synergetic structural materials for MEMS micro-actuators and micro-resonators through sequential or co-deposition EPD on silicon based substrates from a multicomponent suspension would be an attractive subject worth investigating. Interestingly, as has been reported by **Table 2-1** in the previous chapter, the research trend of EPD of carbon nanotubes has been, so far, concentrated mostly on metal substrates such as stainless steel, aluminum, nickel, titanium, and glass plates with conductive coating. Research endeavors exploring the feasibility study of EPD of CNTs on semiconducting surfaces such as silicon and allied dielectric substrates such as silicon dioxide (SiO_2) and silicon nitride (Si_3N_4) are relatively scarce. Therefore, a significant research focus

should be directed in the explorative studies of the deposition kinetics and results of EPD of CNT thin and thick films on bare, metal coated and organosilane treated silicon and silicon based dielectric substrates.

3.2: Research goals

Considering the research endeavors pertaining to the state-of-the-art EPD of CNTs only on conductive substrates, the present dissertation describes explorative studies, for the first time, in the deposition attempts of CNTs on semiconductor substrates by specifically addressing the following aspects:

i. EPD of CNTs on Si substrates without surface treatment
   a. Feasibility study and investigation of EPD of CNT films on bare silicon substrates without any pre-deposition functionalization of the substrate surface.
   b. Investigation of EPD of CNTs on patterned silicon dioxide, silicon nitride and thin metal films (such as aluminum) patterned on silicon surfaces using aqueous suspension and low voltage deposition (< 30-40V).
   c. Characterization of the deposited CNT film thickness in relation to the deposition parameters such as duration of deposition and inter-electrode electric field.
   d. Examination of the stability and re-usability of the EPD suspension in the post-deposition period.

ii. EPD of CNTs on Si substrates with organosilane surface treatment
   a. Surface functionalization of silicon substrates with organosilane based compounds with polar and non-polar functional groups e.g. hexamethyldisilazane (HMDS) and 3-amino-propyl-triethoxysilane (APTES) respectively.

b. Investigation of EPD of CNTs on surface treated Si substrates with regard to CNT film adhesion and coating, and deposition parameters (duration of deposition and inter-electrode electric field).

c. Comparative studies between organic solvent based EPD suspension (such as isopropyl alcohol or IPA) and aqueous suspension.

d. Comparative studies to establish the benefits of EPD over dip or immersion coating for the deposition of CNT thin films with respect to control of thickness, uniformity and packing density of the deposit.

e. The effect of surface treatment with varying concentration of organosilane on the thickness and spectroscopic behavior of the deposited films.

iii. Fabrication of surface enhanced Raman spectroscopy (SERS) substrate as an application based on EPD-fabricated porous CNT networks

a. The applicability of EPD as a fast and single-step processing technique for the fabrication of horizontally aligned porous CNT networks.

b. Synthesis of surfactant stabilized silver nanoparticles (AgNPs) with controlled diameter and fabrication of SERS substrates by immersion coating of the nanoparticles on silanized CNT networks (Ag-CNT-Si substrates).

c. Examination of the detection limit by analyzing the Raman spectra of Rhodamine6G (R6G) analyte with varying concentration and estimation of the enhancement factor (E.F.) of the SERS study.

d. Comparative studies demonstrating the efficiency of AgNP coated porous CNT networks fabricated by EPD over AgNP coated planar Si substrates as active SERS substrates.

With the prevailing interest in the inclusion of EPD technique in the semiconductor industry, it is essential to design a reliable and feasible deposition model that must address the limitations of the present state-of-the-art. To this extent, the research objectives, outlined in this section, should contribute to the development of the EPD technology for next generation electronic applications.

CHAPTER 4: ELECTROPHORETIC DEPOSITION OF CARBON NANOTUBES ON SILICON SUBSTRATES

4.1: Introduction

The importance in extending the present state-of-the-art EPD of CNTs on semiconducting substrates to broaden its application scope in semiconductor research and development-e.g. fabrication of thin film transistors (TFTs) with CNTs as the active materials, nanoporous electrodes, supercapacitors with device integration in MEMS based sensor platform, and field emissive display (CNT-FED) technologies has been outlined in the previous chapters. In this chapter, EPD experiments of acid refluxed CNTs on bare, piranha treated/acid etched and metal patterned silicon substrates has been examined in detail. The experiments primarily reveal the nature of CNT deposition and adhesion on the Si samples without a polar or non-polar organosilane functionalization treatment. The subsequent sections of this chapter reveal pertinent details in regard to preparation of a CNT suspension for the intended EPD process, the deposition process, spectroscopic and microstructural imaging and characterization of the CNT films in relation to the deposition parameters such as interelectrode electric field and duration of deposition.

4.2: Experimental procedure

The experimental procedure is divided into three sections: (i) preparation of stable CNT solution for EPD, (ii) substrate preparation and (iii) EPD process.

i. Preparation of CNT solution

100 mg of as-obtained multi-walled CNTs (purity: >95%, average wall thickness: 3-19 graphene layers, dimension: 7-15 nm (O.D.) × 0.5-200 μm (length), CVD, Sigma Aldrich, USA) were refluxed in 40 ml concentrated sulfuric (H_2SO_4) and nitric (HNO_3) acid (3:1 volume ratio). The solution was heated at 120°C for 45 minutes on a hot plate. The acid-heat treatment of the

CNT solution resulted into a black slurry that was subsequently cooled for 1 hour. The acid-refluxed tubes were then mixed with deionized (DI) water, and the solution was washed and filtered in medium retentive filter papers (pore size: ~11 μm) repeatedly until the resulting solution indicated pH 7 (neutral). The solution was then placed inside a bath ultrasonicator for 2 hours to obtain a stable CNT solution. The concentration of the carbon nanotubes in the final solution was slightly less than 1 mg/ml. The dispersed CNT solution as shown in **Figure 4-1** was kept inside the chemical hood undisturbed for 72 hours to examine the stability of the solution. The CNT suspension did not indicate any visual signs of agglomeration and thus, indicated stability for further processing.

Figure 4-1: Dispersed CNT solution obtained after bath sonication of the acid-refluxed CNTs used for EPD experiments.

ii. Substrate preparation

Silicon wafers (resistivity: 0-100 Ω-cm) were used in all EPD experiments. Three different types of test samples were fabricated as described in **Table 4-1** using the standard silicon processing techniques. For the samples B and C, 280-nm-thick silicon dioxide was grown

by thermal oxidation at 900°C, patterned by UV photolithographic process/shadow masking and wet etched by 48% HF solution to expose the silicon layer underneath. For sample C, silicon nitride of film thickness 150 nm was deposited by low pressure chemical vapor deposition (LPCVD, Nano Fabrication Center, University of Minnesota, USA), patterned by the photolithographic process/shadow masking and etched by CF_4 plasma reactive ion etch (RIE) to expose the silicon dioxide layer underneath. A thin film of aluminum (300 nm) was finally deposited on all of the samples by thermal evaporation and patterned by the lift-off technique.

Table 4-1: Layer Structure of different substrates used in the EPD experiments.

Sample	**Layer Structure**
A	Al(300 nm)/Si
B	Al(300 nm)/SiO_2(280nm)/Si
C	Al(300 nm)/Si_3N_4(150 nm)/SiO_2(280nm)/Si

iii. Electrophoretic deposition process

The electrophoretic deposition of CNTs was carried out in a custom built set-up, as illustrated in **Figure 4-2**, using a silicon sample as the anode and stainless steel (1.5 × 1 × 0.2 cm^3) as the cathode which was degreased with acetone before use. The distance between the electrodes was fixed at 2 cm. An electrical connection was provided to the exposed silicon surface in all of the anode samples during the deposition process. To investigate the effect of electric field and deposition time on the film thickness and quality, two sets of EPD conditions were tried: (i) varying voltage from 5 V to 30 V (or electric field from 2.5 V/cm to 15 V/cm) for constant deposition time of 3 minutes and (ii) varying deposition time ranging from 0.5 minutes to 3 minutes for a constant voltage of 30 V (or electric field of 15 V/cm). Before each set of

experiments, the CNT solution was bath sonicated for about 25 minutes to minimize bundled CNTs in the deposition process. After the deposition process, the samples were air dried for 24 hours.

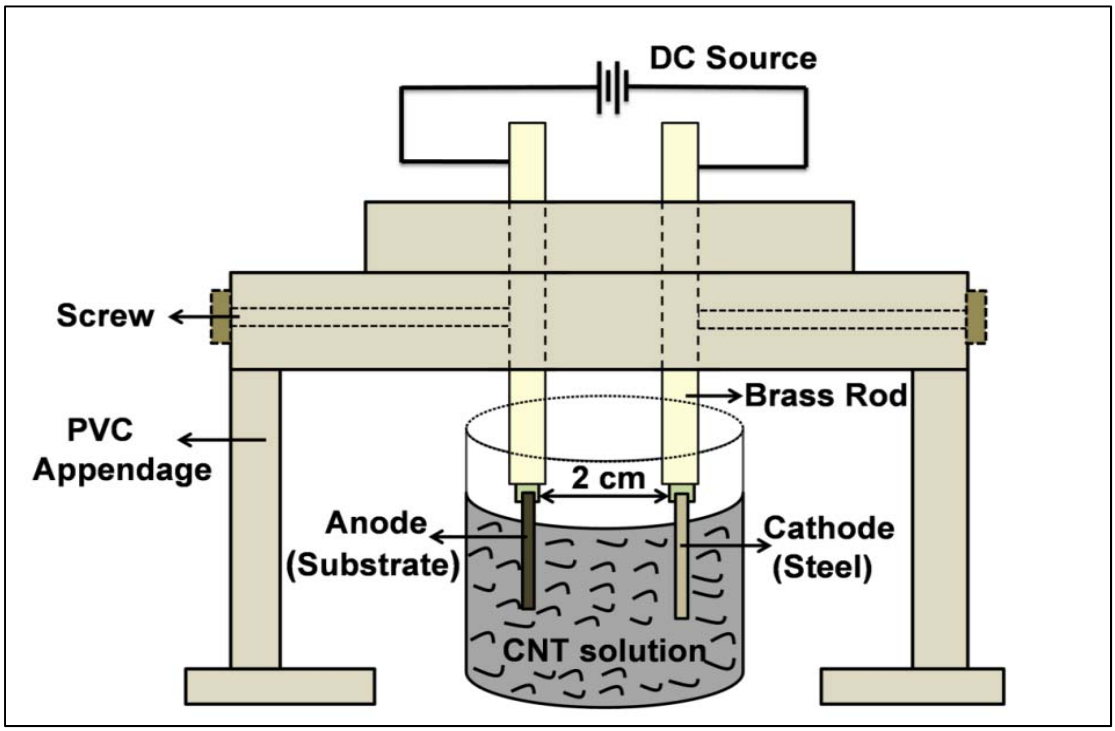

Figure 4-2: Schematic diagram of electrophoretic deposition set-up [Reprinted with permission from Springer[102]].

4.3: Results and discussion

4.3.1: Dispersion of the CNT solution

The acid-heat treatment on the as-purchased carbon nanotubes attaches negative carboxylic groups (-COOH) on the surface of the tubes, thereby imparting negative surface charges. The resultant electrostatic repulsion prevents inter-tubular agglomeration and ensures appreciable stability of the CNT suspension during the dispersion process. Additionally, such aggressive treatment on the nanotubes aids in dismantling the CNT agglomerates, and dissolves

the residual metal catalysts leading to simultaneous purification and shortening of the tube lengths in one processing step.

Transmission Electron Microscopy (TEM) imaging has been performed to ascertain the effects of oxidative acid treatment on the carbon nanotubes. **Figure 4-3** exhibits the agglomerated nature of the as-purchased pristine nanotubes before the acid treatment. As can be seen, the nanotubes remain in an entangled mass in the form of dense agglomerated skeins. Also the presence of metal catalysts (black dots) from the growth process can be noted. **Figure 4-4** reveals the dispersed nature of the CNTs with less agglomeration after acid treatment. The images also reflect the dissolution of unwanted residual metal catalysts in the nanotube solution and shortening of the tubes after the acid-heat treatment.

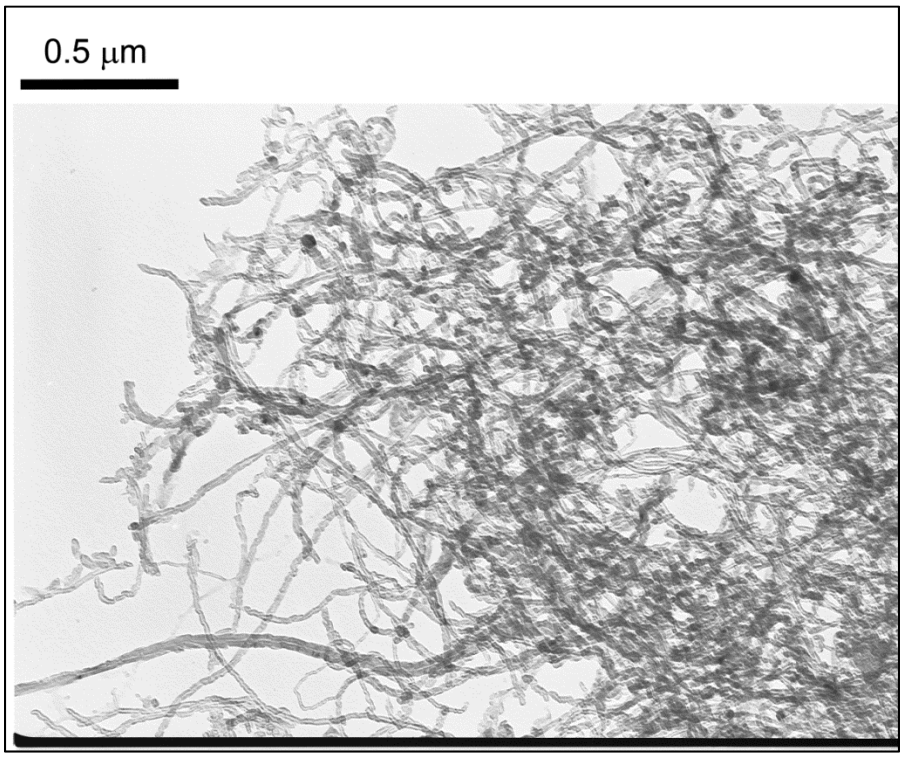

Figure 4-3: TEM image of the as-purchased carbon nanotubes.

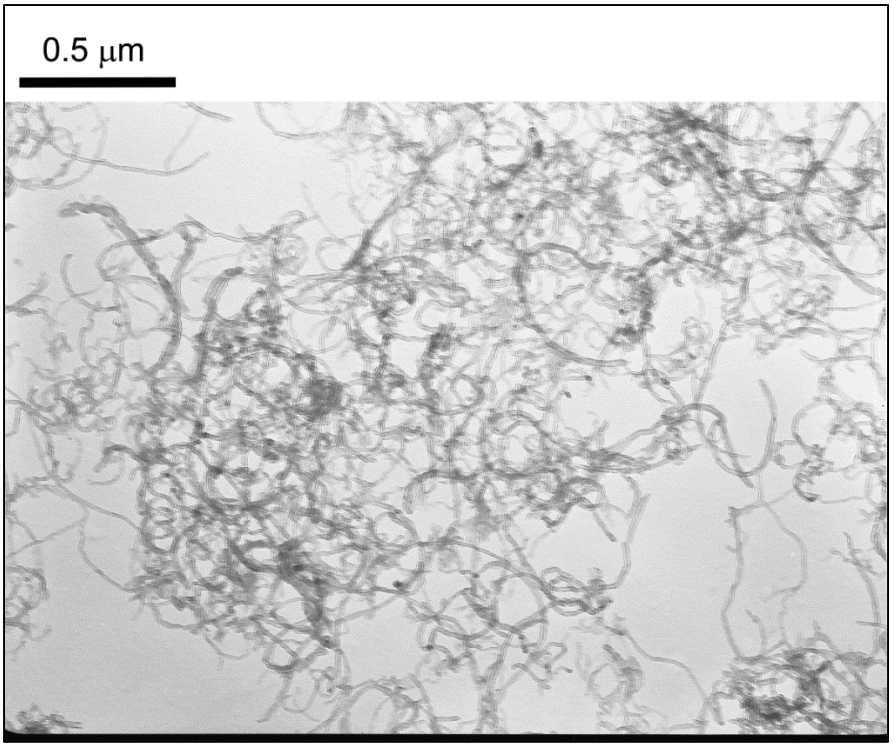

Figure 4-4: TEM image of the acid-treated carbon nanotubes.

The acid treatment of the pristine CNTs contributes enough negative charges on the surface of the nanotubes, resulting in sufficient negative zeta potential in neutral pH solution. The repetitive filtering and washing of the -COOH$^-$ functionalized CNTs in DI water results in reduction of the ionic conductivity of the solution. These two processing steps assist in the preparation of a stable CNT dispersed solution for the EPD experiments after several hours of ultrasonic agitation.

4.3.2: Characterization of the deposited CNT film

The acquired negative zeta potential of the acid-refluxed carbon nanotubes[56] was substantiated by the deposition of CNT film at the anode surface of the EPD cell. One of the interesting results in all the EPD experiments was the selective deposition and strong adhesion of

CNT film only on the aluminum surfaces irrespective of the substrate or insulator films (i.e. SiO_2 and Si_3N_4) underneath the aluminum layer.

Figure **4-5** (a-c) exhibits EPD results (deposition time: 3 minutes, electric field of 10 V/cm) on the samples A, B and C, respectively. The corresponding schematic cross-sectional diagrams of the samples are shown in Figure **4-5** (d-f). As demonstrated by the figure, no deposition was observed on the exposed silicon, silicon dioxide and silicon nitride surfaces whereas profuse deposition was noticed on the aluminum surfaces in all of the samples. Another noteworthy observation was the deposition of CNT film on the aluminum surface even though the metal surface was not directly connected to the DC source in all of the EPD tests. The electrical connection was imparted only on the exposed silicon surface for all samples. It can be, thus, concluded that the silicon substrate acted as an efficient anode for all of the EPD experiments to convey sufficient electrophoretic mobility to the acid-treated CNTs in the EPD suspension. However, it does not behave as a suitable coagulation and deposition surface for the CNTs to adhere and assemble into films. As has been mentioned in the previous sections, in order to obtain continuous deposition, constant flux of CNTs towards the intended electrode is necessary in the migration process; this is only possible when the metal surface, in this case, acquires sufficient positive potential in reference to the cathode. It is interesting to note down that under the mentioned electrical connection scheme in our experiments, the metallic surfaces maintain a substantial positive potential as the silicon substrate which is proved by the migration towards and continuous deposition of CNTs on the metal surfaces. The deposition process exhibits identical results irrespective of the presence of insulator films underneath the metallic surfaces since CNTs were found to adhere only on the metallic surfaces for Sample A also. Similar deposition results of CNT films were also observed when the DC source was directly

connected to the aluminum layer; profuse CNT coating on it and no coating on the silicon and the insulator surfaces. To our best knowledge, this unique conundrum where silicon substrates, without any surface modification or application of binder or adhesion promoter, fail to qualify as suitable deposition sites in EPD of carbon nanotubes has not been reported earlier. The deposition results on different substrates under different experimental conditions are summarized in Table **4-2** below.

Table 4-2: Electrophoretic deposition results on silicon substrates with different surface coatings under different experimental conditions.

Substrate	**Electrophoretic deposition results**
Silicon (resistivity: 0-100 Ω-cm)	No deposition of CNTs on the silicon surfaces after multiple attempts with a range of different deposition time and electric field; only specks of carbonaceous residue observed even after long deposition time (for 30 minutes at an electric field of 15V/cm).
Silicon (resistivity: 0.01-0.02 Ω-cm)	Extremely poor deposition on the surfaces after multiple EPD attempts with a range of different deposition time and electric field; no noticeable changes were observed after long periods of deposition (for 30 minutes at an electric field of 15V/cm).
Silicon (Piranha treated for 30 minutes)	Same observation as above
Silicon (HF treated for native oxide etch)	Same observation as above
Sample A	Profuse CNT coating only at the aluminum surfaces; the exposed silicon showed no deposition results as shown in Figure 4-5.
Sample B	Dense CNT film formation was observed only at the aluminum surfaces; the silicon dioxide and silicon underneath displayed no CNT adhesion as shown in Figure 4-5.
Sample C	Deposition of CNT films was exhibited at the aluminum surfaces; the silicon nitride, silicon dioxide and silicon showed no CNT coating as shown in Figure 4-5.

As has been mentioned in the introduction section of this chapter, no surface functionalization by addition of binder or adhesion promoter or application of SAM molecules was performed on the bare silicon surfaces. Furthermore, for each type of sample (A, B or C) investigated, the EPD experiments were performed under the following EPD conditions:

a. Constant deposition time (3 minutes) with increasing electric field (2.5-15V/cm)
b. Constant electric field (15V/cm) with increasing deposition time (0.5-3 minutes)

For the bare silicon substrates, experiments with long hours of deposition time (e.g. 30 minutes at an electric field of 15V/cm) were also performed to observe CNT film coating. **Figure 4-5** below depicts the deposition results.

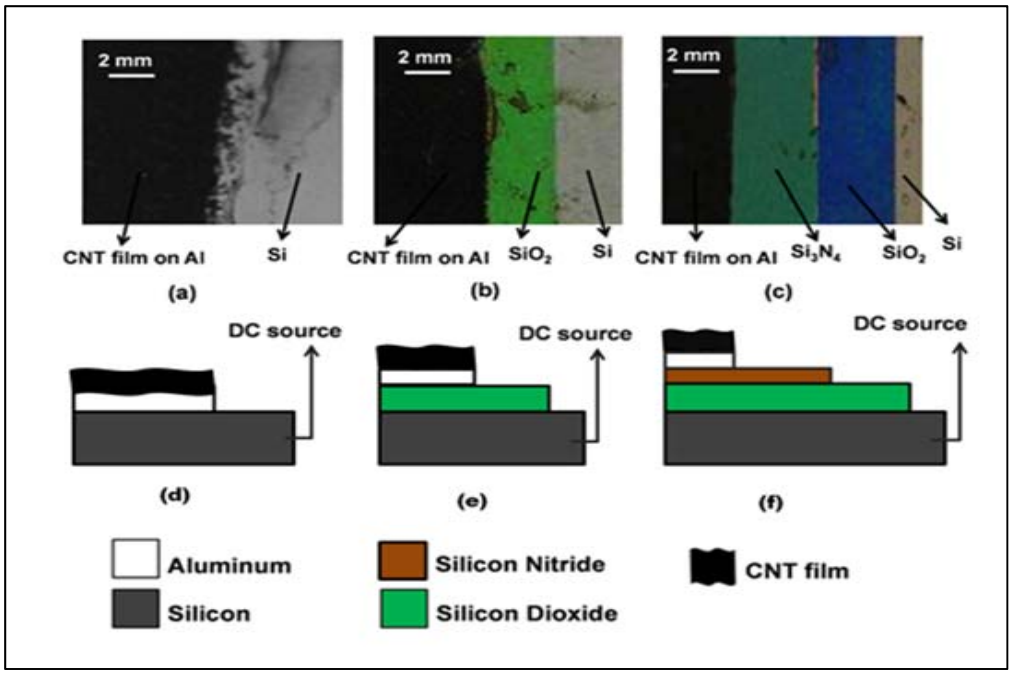

Figure 4-5: Optical images (top view) of deposited CNT film on patterned aluminium on bare silicon or insulators (SiO_2 or Si_3N_4) with electric field of 10 V/cm for 3 minutes: (a) Sample A, (b) sample B and (c) samle C. (d-f) Schematic cross sectional diagram of (d) sample A, (e) sample B and (f) sample C [Reprinted with permission from Springer[102]].

Literature reporting the effect of substrates in the deposition step of the EPD process is extremely scarce. Although electrophoretic deposition on different substrates has been performed extensively, the exact mechanism of deposition has not been universally agreed upon. In this direction, the distortion of electrical double layer (EDL) and thinning mechanism (pioneered by Sarkar and Nicholson[18,82,103]) is the most widely accepted theory which discards the concepts of particle-electrode reaction and particle neutralization at the depositing surface. The theory mainly relies on particle-particle interaction that leads to coagulation and eventual deposition on the target surfaces due to reduction of repulsive forces by the EDL thinning process. Therefore, the preferential adhesion of CNTs on the metallic surfaces over the bare silicon substrates in our experiments is rather intriguing. We have proposed the carbon nanotube-metallic surfaces interactions in the present case based on a theoretical postulate. We believe that the preferential adhesion of the CNT films on the metal surfaces can be explained partly by the hydrophilic interaction between the CNTs (rendered hydrophilic during the acid oxidation step) and the aluminum surface. It is assumed that the hydrophilic nature of both the interacting species in the process favors the adhesion and hence deposition of the CNTs on the metallic surfaces. Similar explanation was provided by Oh *et al.*[41] who performed liquid-phase fabrication of carbon nanotube cathodes for field emission devices. The preferential adhesion of acid treated carbon nanotubes on hydrophilic glass slides is also reported by Shimoda *et al.*[104] in the explanation of the self-assembly process of the nanotubes.

In our experiments, the effect of hydrophilic interaction was further demonstrated by insufficient coating and extremely poor adhesion of the CNTs on bare silicon substrates after numerous EPD attempts with a range of different durations and electric fields. The results were identical even after long deposition time (e.g. 30 minutes at 15V/cm) and silicon substrates with

different resistivity values followed by irreversible agglomeration of the EPD solution as will be discussed in the next section. After the samples were dried, only specks of scattered CNT aggregates were observed on the silicon surfaces. There exists another theory that is well-accepted, explaining the mechanism of electrophoretic deposition, - i.e. the formation of metal hydroxides on the target surface that binds the CNTs with the substrate. However, this theory is based on the role of charger salts which were not used in our experiments and therefore cannot be applied to elucidate our results.

The role of metal (Al) as a preferred deposition surface over the silicon surface was further investigated with EPD experiments on bare silicon substrates which were treated extensively with piranha solution (H_2SO_4:H_2O_2 = 1:1) as well as on native-oxide-etched silicon substrates. Piranha treatment significantly oxidizes the silicon surface, making it hydrophilic. EPD experiments with various conditions of electric field and deposition time resulted in very poor deposition of CNTs on the piranha-treated silicon surfaces. Multiple EPD attempts on the native-oxide-etched substrates resulted in very poor CNT deposition as well.

In order to verify the role of the inter-electrode electric field in the EPD process, a silicon sample coated with aluminum was simply immersed in the CNT suspension for 3 minutes. After the immersion, only a loose, flimsy CNT layer was observed to adhere to the aluminum surface on the sample. The sample, after drying, left minute amounts of carbonaceous residues on the surface. Thus, it can be inferred from this experiment that hydrophilic interaction alone is not sufficient to enable CNT film deposition. The electric field in the EPD process needs to impart sufficient electrophoretic mobility to the nanotubes to overcome the inter-tubular repulsion, to migrate and to adhere on the conducting surfaces.

Therefore, the formation of CNT deposit on the aluminum surfaces can be attributed to both electrophoretic mobility of the charged CNTs in the suspension and adequate hydrophilic interaction on the target surface.

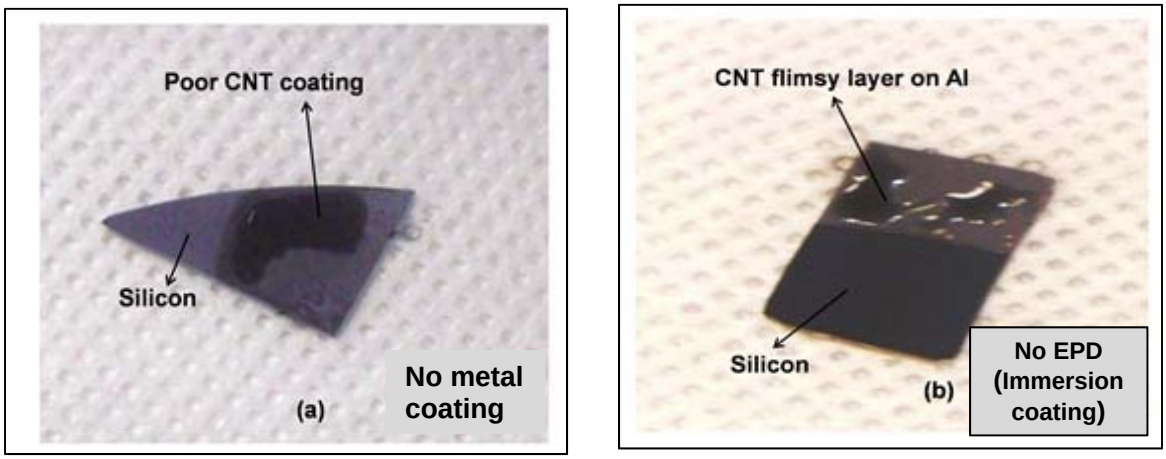

Figure 4-6: (a) Deposition results on silicon substrates without any metal layer (b) Immersion coating results on aluminum surface.

In a separate set of experiments, an appreciable deposition of CNT films was also observed on copper surfaces atop silicon substrates under similar EPD conditions and electrical connections. This result also substantiates the above explanation in regard to efficient CNT film deposition.

i. Microscopic imaging and Raman spectroscopy

Microstructural imaging of the deposited films was performed using an FEI Quanta 3D FEG dual beam SEM (scanning electron microscope) / FIB (focused ion beam) with an acceleration voltage of 20-30 kV. The samples were imaged as produced. **Figure 4-7** shows the scanning electron microscopic images of the CNT film deposited on the aluminum-coated silicon substrates. The images indicate the random nature of the CNT deposition with appreciable homogeneity and excellent packing density without any microscopic voids in the film morphology.

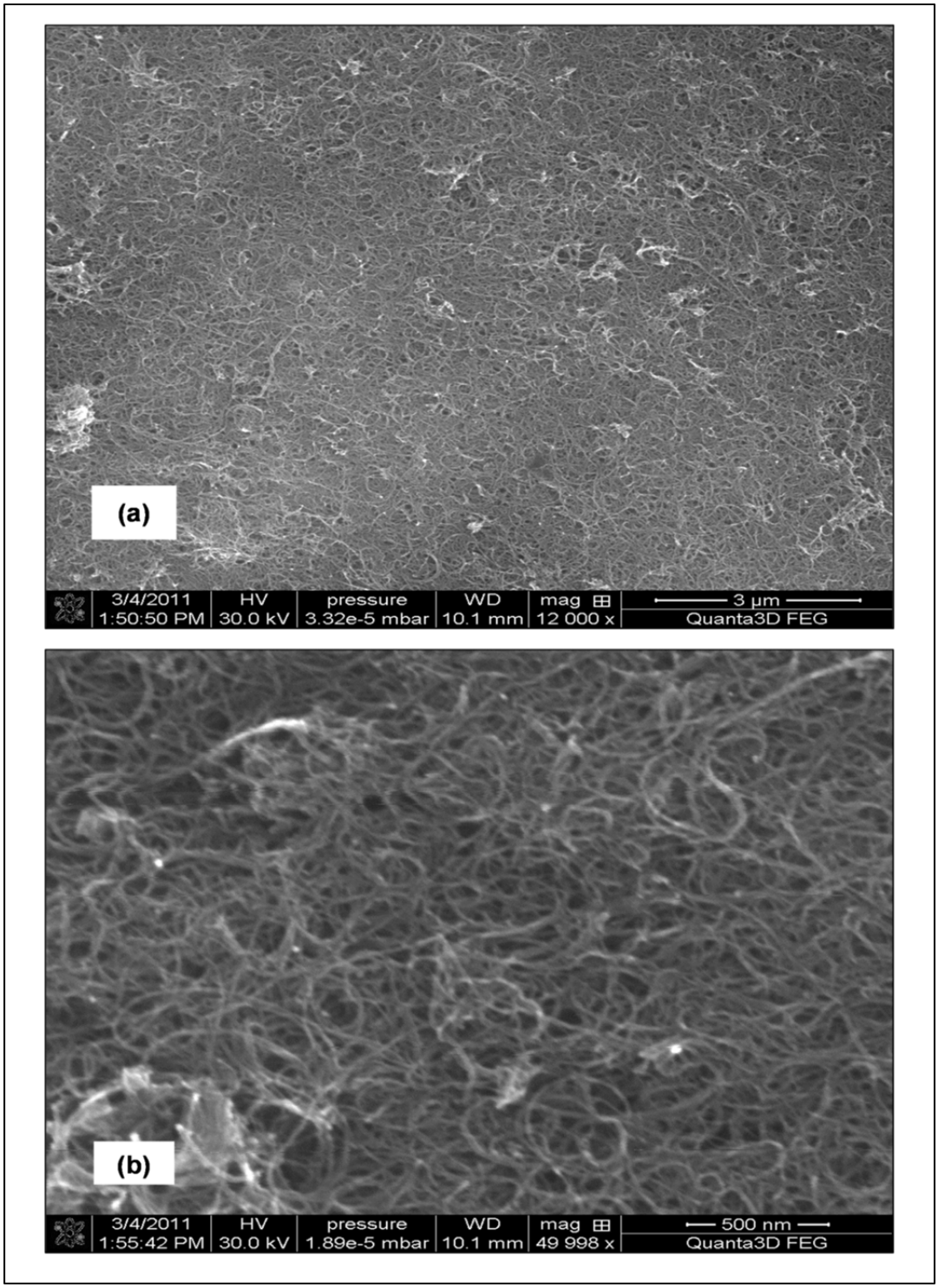

Figure 4-7: Scanning electron microscopic images of deposited CNT film on the sample A. (a) (Top view) CNT film showing appreciable packing density without voids, (b) (top view) magnified image of the CNT film [Reprinted with permission from Springer[102]].

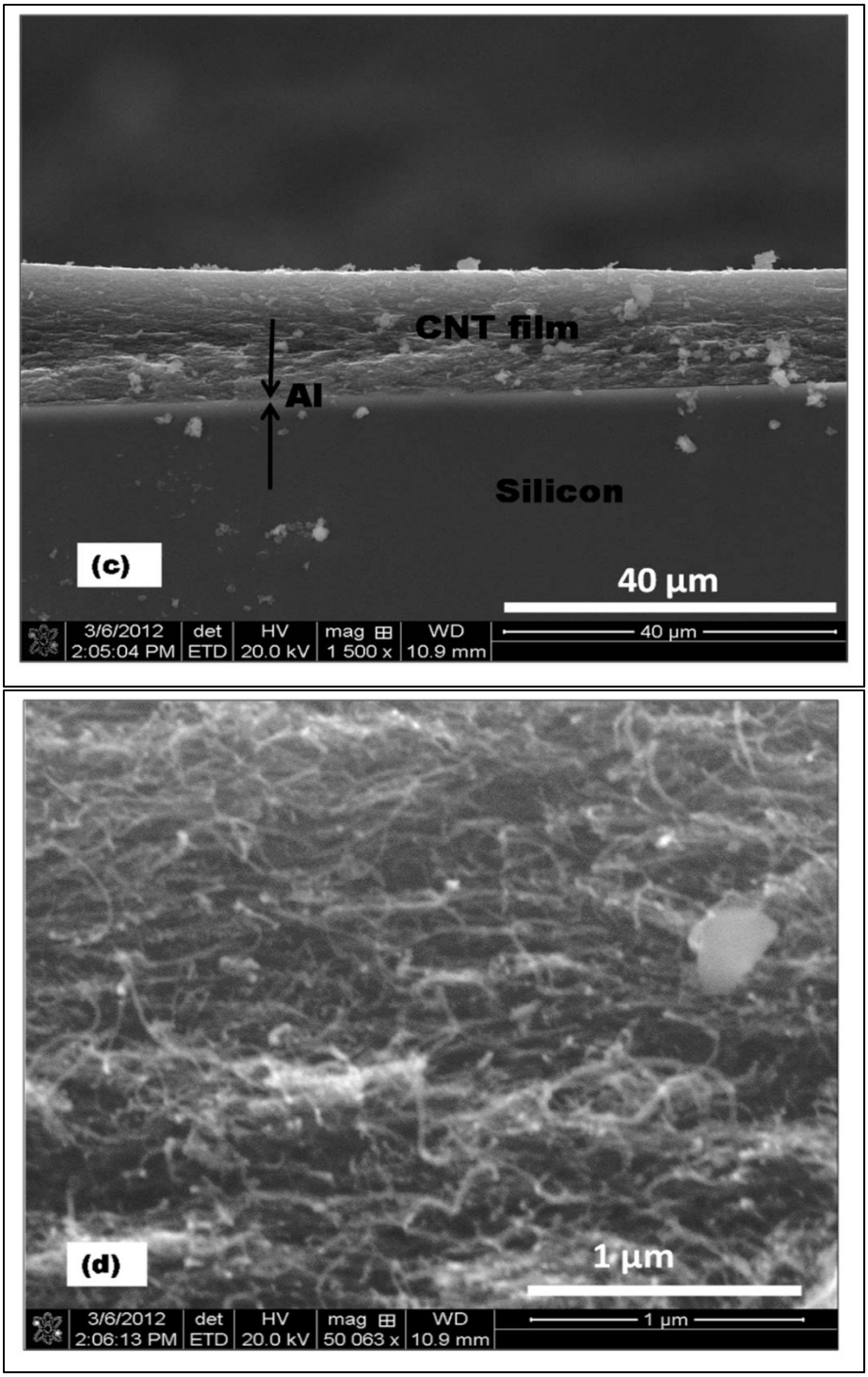

Figure 4-8: Scanning electron microscopic images of deposited CNT film on the sample A. (c) (cross-section) CNT film deposited on Al/Si and (d) (cross-section) magnified image of the CNT film [Reprinted with permission from Springer[102]].

The vibrational attributes of the deposited CNT film was further characterized with Raman spectroscopy[105]. **Figure 4-9** shows the acquired Raman spectra of the CNT film deposited on the sample A for 2 minutes at an applied electric field of 10 V/cm. The peak for the disorder-induced D-band was seen to occur at ~1330 cm^{-1} and those for the tangential G-bands occurred at ~1580 cm^{-1} and ~2700 cm^{-1} for the samples A, B, and C. The absence of prominent radial breathing modes in the Raman spectra was noted for all scans. The Raman spectroscopy results, thus, conclusively prove the presence of multi-walled nanotubes (MWCNTs) in the deposited CNT films.

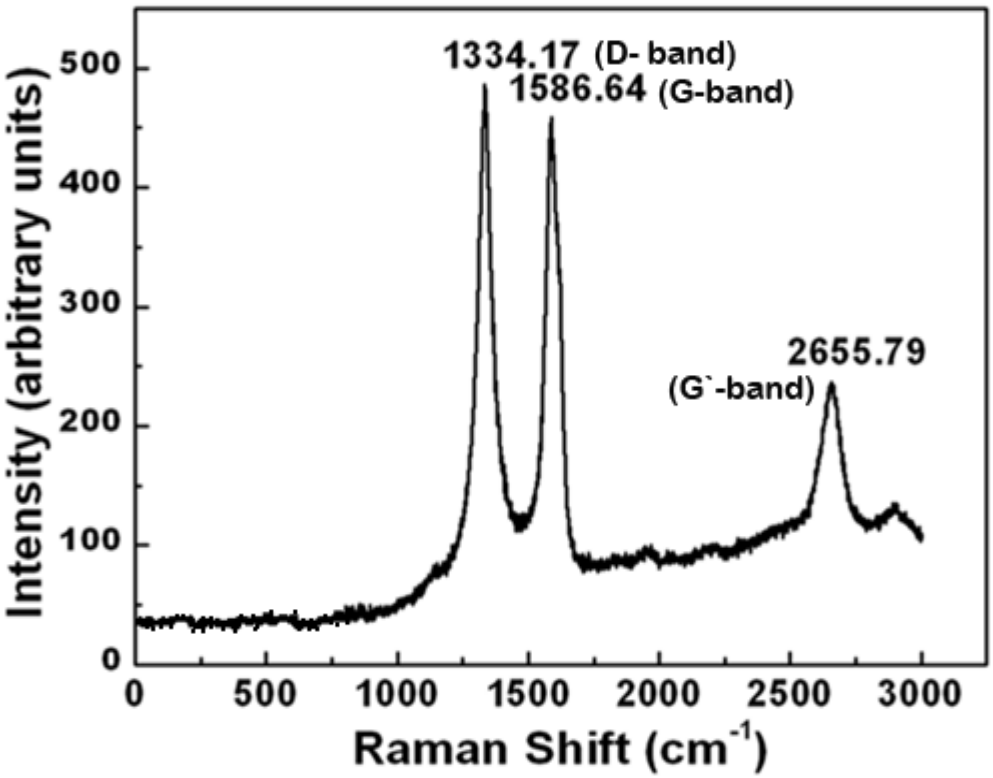

Figure 4-9: Raman spectrum of the carbon nanotube film deposited on sample A for 2 minutes of EPD at an applied electric field: 10 V/cm [Reprinted with permission from Springer[102]].

ii. Thickness and surface roughness

The overall yield and homogeneity of the CNT films are influenced by the electrophoretic deposition control parameters such as inter-electrode electric field and deposition time. For detailed quantitative analysis, film thickness and average surface roughness measurements were performed using a KLA-Tencor P-II surface profiler. For surface roughness measurements, surface profile scanning was performed for 10 times for each sample and the average value was calculated.

It was observed that for the constant deposition time of 3 minutes, the thickness of the CNT film deposited on aluminum-coated samples increased with increasing inter-electrode electric field strength as shown in **Figure 4-10**. For the highest electric fields of 15 V/cm, film thicknesses as high as ~15 μm on samples A and C and ~11 μm on sample B were measured. The results are consistent with conventional EPD characteristics which generally show an increasing trend in deposition yield or thickness in relation to increasing inter-electrode E-field strength. It has also been observed that at low electric field (< 5 V/cm), there is a "no-coating" zone where the deposition is almost negligible or results in non-uniform sparse coating without appreciable adhesion to the substrates.

The thickness of the CNT film deposited on aluminum-coated samples also displays an increasing nature with increasing deposition time (**Figure 4-11**) under constant electric field of 15 V/cm. The mentioned "no-coating" zone is also observed at fairly low deposition time (< 1 minute). The deposited film thickness of the sample B is seen to be somewhat lower than those of the samples A and C over the entire range.

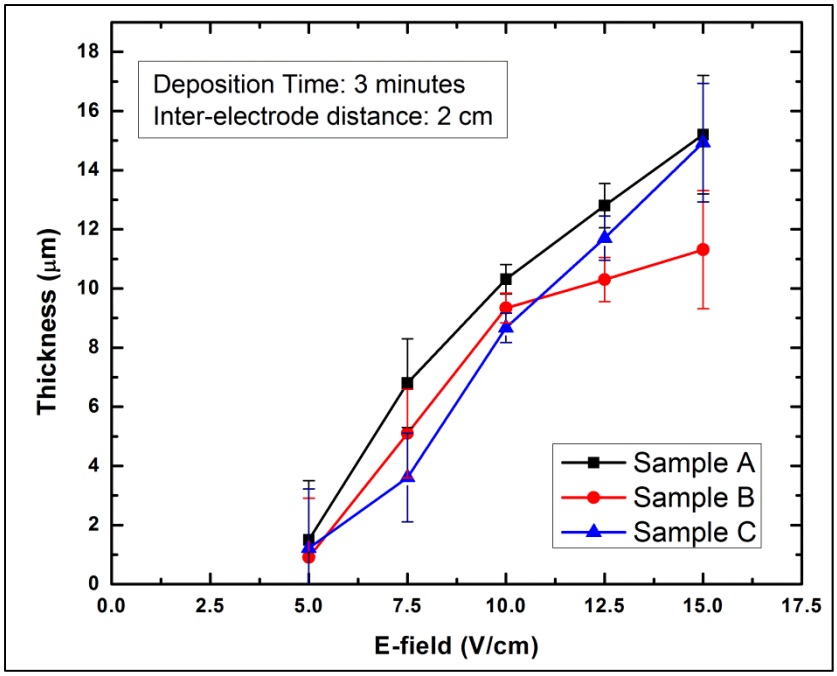

Figure 4-10: Thickness of CNT films on different samples as a function of applied electric field at constant deposition time of 3 minutes.

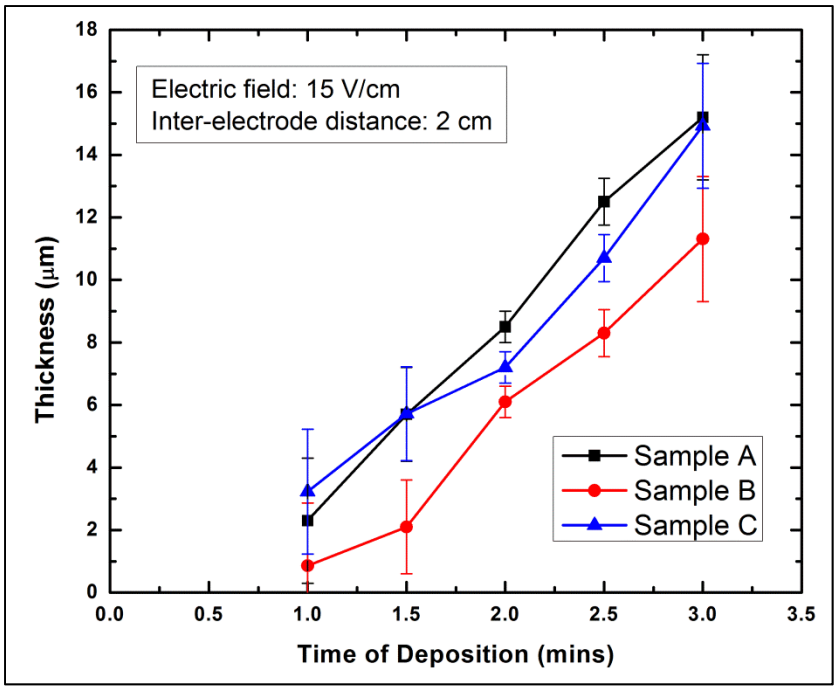

Figure 4-11: Thickness of CNT films on different samples as a function of deposition time at a constant applied electric field of 15 V/cm.

The overall EPD results, thus establish that longer deposition time and higher electric field result in the deposition of a thicker CNT layer. This observation is in accordance with the deposition characteristics reported by Thomas *et al.*[76,106] who performed CNT film deposition by EPD on stainless steel substrates.

Surface roughness measurements of the CNT film coating also indicate the effect of deposition duration and electric field strength in the film quality. **Figure 4-12** shows the surface roughness measurements of the CNT films with varying electric field strength. The surface roughness values are excessively high (~300-350 nm) for low electric field deposition (5 V/cm). This can be attributed to the non-uniform, sparse deposits with poor surface coverage around the "no-coating" zone. Surface roughness values also increase at high electric field (>= 10 V/cm). This might be due to the aggregation of CNTs under high electric field as also reported by Thomas *et al.* **Figure 4-13** exhibits the surface roughness measurement results of the CNT films for varying deposition time. The roughness profile exhibits high values similar to **Figure 4-12** in regard to short and pro-longed deposition time under a constant electric field. As can be seen from the figures, the surface roughness values can be optimized to ~100-150 nm at an electric field of 8-12 V/cm and deposition time of 1.5-2.5 minutes under the reported experimental conditions. Further optimization of the values is necessary for the circuit or device-level performance of the deposited nanotubes, for example, in CNT based thin film transistors (CNT-TFTs) or nanoporous electrodes for surface reaction and detection of different analytes. This can be achieved by precisely controlling the concentration of the EPD solution or by the use of non-aqueous dispersion medium e.g. isopropyl alcohol (IPA) as discussed in the next chapter.

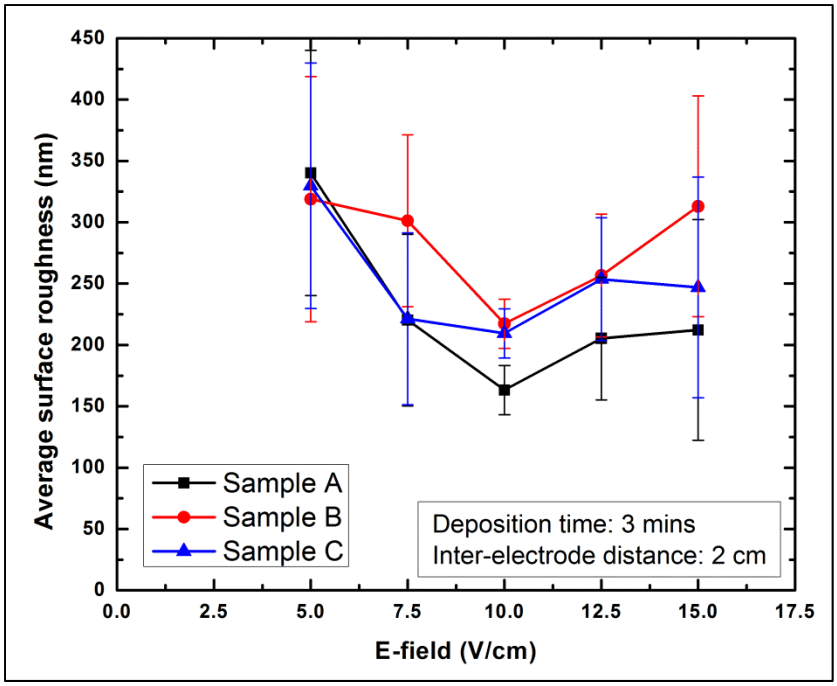

Figure 4-12: Average surface roughness of the CNT films deposited on different samples as a function of applied electric field at constant deposition time of 3 minutes.

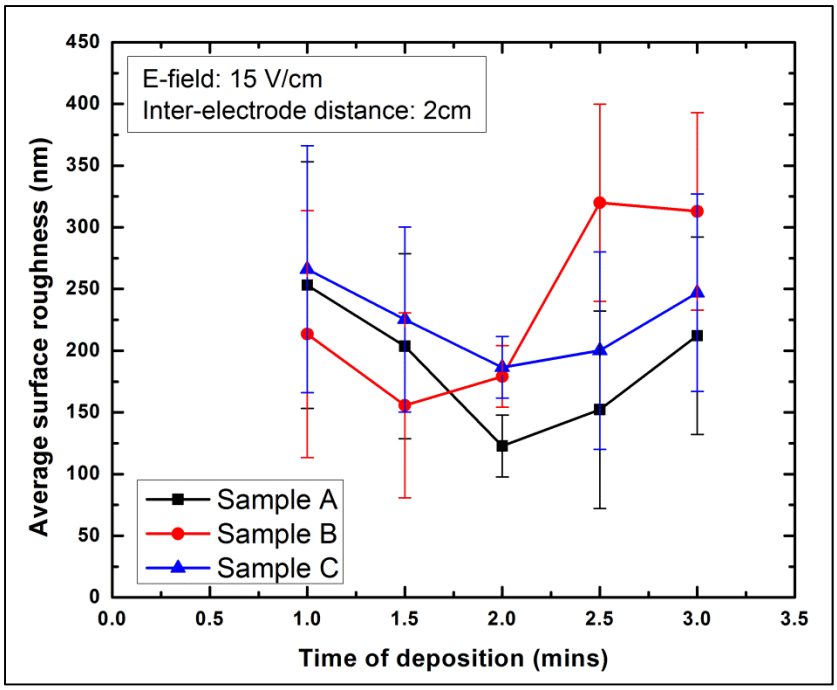

Figure 4-13: Average surface roughness of CNT films deposited on different samples as a function of deposition time at a constant applied electric field of 15 V/cm.

4.3.3: Post-EPD agglomeration of the CNT solution

One of the interesting phenomenon observed throughout the EPD experiments was the agglomeration and subsequent sedimentation of the CNTs resulting into inhomogeneous suspension after the failed EPD attempts. Entangled clusters of CNT flakes were observed to be floating in the solution during the experiments which eventually precipitated as CNT aggregates at the bottom. **Figure 4-14** (b) shows the degraded CNT solution after a failed EPD attempt on a bare silicon sample, which was repetitively observed in the case of bare silicon samples regardless of the EPD conditions. This phenomenon can be explained by the possible attractive interaction between the accumulating CNTs near the anode which failed to adhere to the bare silicon surfaces and the incoming surge of $–COOH^-$ functionalized nanotubes in the solution migrating towards the anode under the applied electric field. The interaction may lead to mutual adhesion of CNTs to form unwanted clusters or aggregated skeins during the electrophoresis process which eventually result into the deterioration of the dispersed solution during and in the post-EPD period. In contrast to this solution behavior with bare silicon substrates, the CNT solution after successful EPD experiments on metal-patterned silicon substrates showed remarkable stability and re-usability for substantial deposition attempts (as shown in **Figure 4-14** (a)).

The post-EPD agglomeration of the dispersion medium after unsuccessful EPD attempts has been a significant observation in this dissertation research. This phenomenon has been consistent for both aqueous and non-aqueous (e.g. IPA) medium which serves as a deciding factor in adjudicating the stability of the EPD suspension during and after the deposition process.

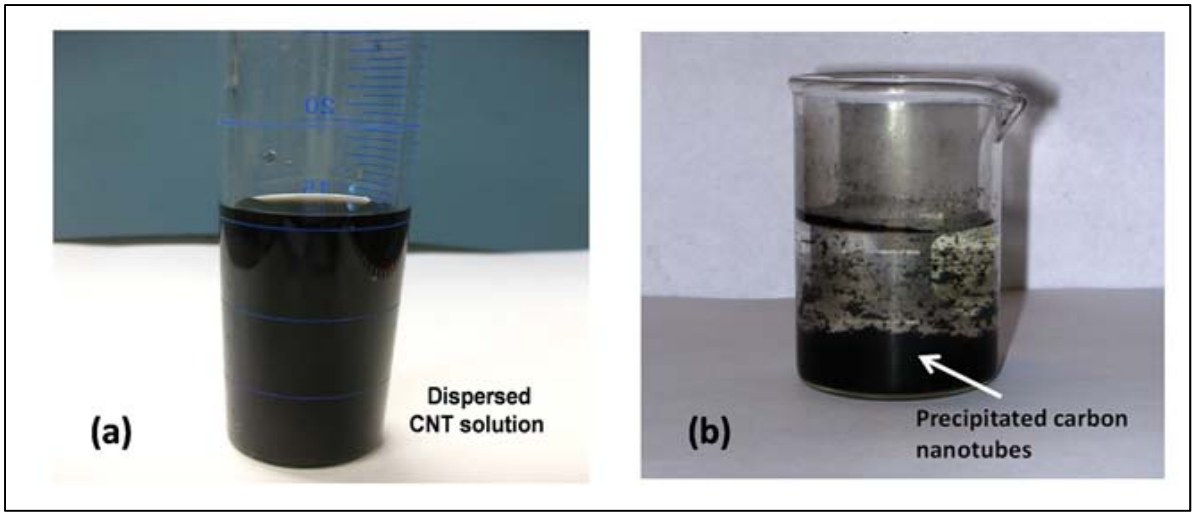

Figure 4-14: Degraded CNT solution with precipitated carbon nanotubes after a failed EPD attempt with bare silicon substrates [Reprinted with permission from Springer[102]].

4.4: Conclusion

Electrophoretic deposition (EPD) of CNTs has been successfully investigated from acid-refluxed, $-COOH^-$ functionalized CNT-dispersed suspension on metal-patterned silicon substrates with or without insulating layers (SiO_2 and Si_3N_4) in between. No surface functionalization was performed on the silicon substrates used in the experiments. The experimental results revealed selective deposition and excellent adhesion of the CNTS only on aluminum surfaces irrespective of the insulator layers underneath and electrical connection to the anode surface. Poor deposition and adhesion results of CNT films on bare and piranha treated/acid etched silicon substrates was also noted in all our EPD experiments. The preferential CNT coating has been attributed to the strong hydrophilic interaction between the metallic surfaces and the oxidized CNTs during the deposition step. The thickness and the surface roughness of the EPD fabricated films have been reported in relation to the EPD process parameters - i.e. the applied inter-electrode electric field and deposition duration. CNT film as thick as ~15 μm was deposited on the silicon substrates at an applied electric field of 15 V/cm

for 3 minutes. Microscopic imaging and Raman spectroscopy confirmed the presence of multi-walled nanotubes (MWCNTs) in the EPD deposits. The morphology of the deposited CNT films exhibited appreciable homogeneity and excellent packing density with continuous surface coverage. Interesting results on the degradation of the CNT solution after failed EPD attempts on bare silicon substrates also reveals the challenge of reusability and preserving desired dispersion during the deposition duration.

CHAPTER 5: ELECTROPHORETIC DEPOSITION OF CARBON NANOTUBES ON SILICON SUBSTRATES WITH SURFACE FUNCTIONALIZATION

5.1: Introduction

The experimental results reported in chapter 4 reflect the challenges in EPD of acid refluxed carbon nanotubes on bare silicon substrates without any surface functionalization. The preferential adhesion of CNTs only on the patterned metal films atop silicon substrates and insulating layers such as silicon dioxide and silicon nitride has been attributed to the hydrophilic surface reaction between the acid-treated CNTs and the interacting metal surfaces. The study was accomplished by the combination of the physical vapor deposition process of metal evaporation on the semiconductor substrates followed by the solution based EPD experiments. This chapter reveals significant progress in the EPD of CNT thin films on Si substrates which were functionalized by polar 3-aminopropyl-triethoxysilane **(**APTES) self-assembling monolayer prior to the deposition step. The organosilane assisted deposition strategy, set forth in our study, has eliminated the need of physical vapor deposition of metal films on the silicon substrates deposition model and has exemplified an entirely solution based, reproducible and relatively quick route of EPD of CNTs on surface functionalized Si substrates. The relevant sections of this report communicate extensive details pertaining to the preparation of aqueous and non-aqueous CNT suspension for the intended EPD process, APTES self-assembly by hydroxylation and silanization technique and different comparative studies on the influence of EPD solution on the deposited film quality and the ingenuity of EPD over dip/immersion coating methods with varying concentration of APTES.

5.2: Experimental procedure

The experimental procedure is divided into 4 sections: (a) preparation of stable CNT suspensions in IPA (CNT-IPA) and water (CNT-water) for the deposition process, (b) preparation of APTES solution with varying concentrations, (c) substrate preparation and (d) EPD process.

5.2.1: Preparation of CNT solution in IPA and water

Multi-walled CNTs (purity: >98%, average wall thickness: 7-13 graphene layers, dimension: 6-13 nm (O.D.) × 2.5-20 μm (length), synthesized by CVD) were purchased from Sigma Aldrich, USA. Approximately 100 mg of the as-purchased CNTs were mixed in 40 ml concentrated sulfuric (H_2SO_4) and nitric (HNO_3) acid (volume ratio = 3:1 respectively). The solution was vigorously stirred for about 15 min with a magnetic spinner and then heated at 120°C for 30 min on a hot plate. The acid-refluxing treatment of the solution produced a black slurry which was cooled for 1 hour (h) in the fume hood. The acid-refluxed solution was then repetitively washed with deionized (D.I.) water (18.2 MΩ-cm) and filtered in medium retentive filter papers (pore size: ~11 μm) until the resulting solution indicated pH 7 (neutral). The final black filtration residue was collected with a laboratory spatula and divided into approximately 2 equal parts. One part of it was mixed with 50 ml of isopropyl alcohol (IPA) and the other one with 50 ml of D.I. water. A second round of repetitive washing and filtering was performed subsequently with IPA and water respectively. Both the solutions were then placed inside an ultrasonicator bath for 2 h to obtain stable CNT suspensions in IPA (referred as CNT-IPA) and water (referred as CNT-Water). The dispersed CNT solutions were then kept inside a chemical hood for 48 hours to examine the solution stability. No visual signs of agglomeration were noticed in both the solutions and therefore were deemed suitable for the subsequent EPD process. **Figure 5-1** shows the CNT dispersed solutions in IPA and water respectively.

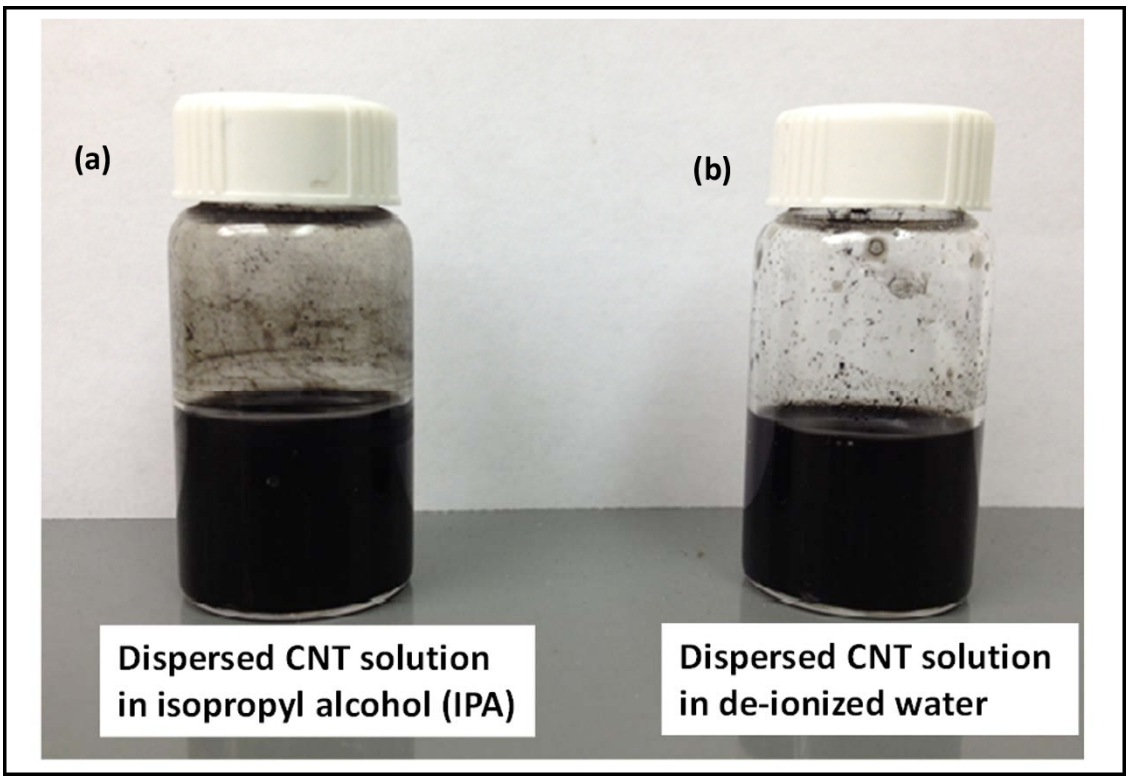

Figure 5-1: Dispersed CNT solution used for EPD experiments (a) stable suspension in isopropyl alcohol (CNT-IPA) and (b) stable suspension in water (CNT-Water).

5.2.2: Preparation of APTES solution with varying concentration

Different APTES solutions with varying concentration - i.e. 5%, 10%, 20% and 50% were prepared by appropriate dilution recipes 95% ethanol and D.I. water. For example, 2 mL of APTES were mixed with 2 mL of DI water and 6 mL of ethanol solution for preparing 20% APTES solution. Similarly 5%, 10% and 50% APTES solution were prepared with proper dilution ratios in water and ethanol. Figure **5-2** depicts the molecular structure of 3-aminopropyl-triethoxysilane **(**APTES) used in the experiments.

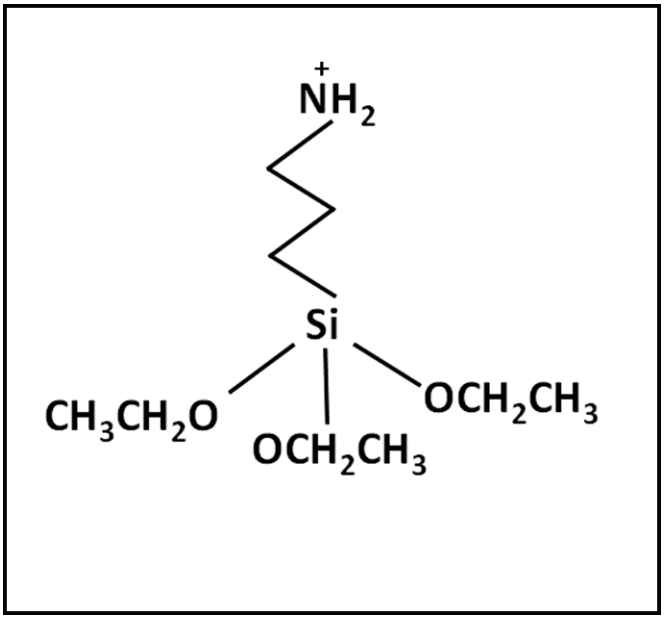

Figure 5-2: Schematic diagram of 3-Aminopropyl-triethoxysilane (APTES).

5.2.3: Substrate preparation

Silicon wafers (resistivity: 0-100 Ω-cm) were used for all of the EPD experiments. The wafers were cleaved into ~1 × 0.5 × 0.055 cm^3 samples and were oxidized in warm piranha solution (H_2SO_4:H_2O_2 = 1:1) for 25 min. The samples were then immersed into approximately 10 ml of different APTES solutions with varying concentrations - i.e. as 5%, 10%, 20% and 50% for 15 minutes. For 100% APTES treatment, the samples were directly immersed into as–purchased 10 mL APTES solution without any dilution for 2 min. After the immersion process, all the samples were rinsed in D.I. water to remove the excess APTES. The rinsed samples were dried in a gentle stream of nitrogen and kept in the oven at 80° C for 1 h.

5.2.4: EPD process

A custom built set-up (as shown in **Figure 5-3**) was used for all the EPD experiments for this study. The organosilane treated silicon samples and a copper plate (dimension: 1.5 × 1 × 0.2 cm^3) were selected as anode (deposition surface) and cathode respectively. The inter-electrode

distance was fixed at 2 cm for all the experiments. Before each set of deposition experiment, both the CNT solutions were subjected to bath sonication for 15 min to minimize the amount of agglomerated CNT in the suspension. Following the deposition process, the samples were carefully taken out of the solution and dried overnight at room temperature. To investigate the effect of APTES concentration on the deposition results, a series of EPD experiments were performed systematically with varying APTES concentration (5%, 10%, 20%, 50% and 100%) with varying deposition voltage of 10-30 V (or varying electric field (E-field) of 5-15 V/cm) for constant deposition time for 3 min.

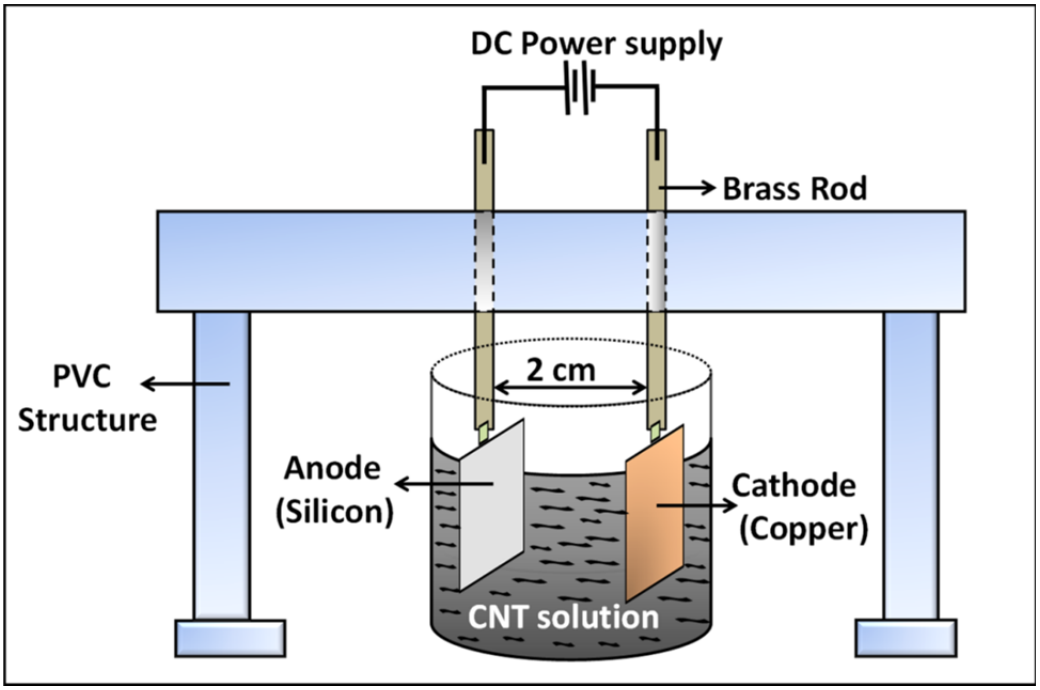

Figure 5-3: Schematic diagram of the electrophoretic deposition set-up.

5.3: Results and discussion

The acid refluxing of the CNTs introduces carboxylic groups (-COOH$^-$) on the sidewalls of the tubes which impart sufficient negative surface charges. The resultant inter-tubular

repulsion between the surface charges ensures appreciable dispersion of the nanotubes in the solution which remains stable all through the deposition experiments. Additionally, dissolution of unwanted residual metal catalysts and entangled carbonaceous skeins in the as-purchased nanotube powder, shortening of the nanotubes and purification are also accomplished by this covalent functionalization of the nanotubes.

The surface functionalization process is achieved by the spontaneous self-assembly of the APTES monolayer on the silicon surfaces. It is triggered by the oxidative piranha treatment which introduces abundant surface hydroxyl groups (-OH) on the silicon samples. This process is known as the "hydroxylation" process. The silanization step proceeds with the hydrolysis of ethoxy (C_2H_5) groups from the APTES molecules which results into the formation of APTES silanols (Si-O-H). The APTES silanols then start to condense with surface silanols on the silicon surfaces, thereby, self-assembling into a monolayer of APTES by a lateral siloxane (Si-O-Si) network as shown in **Figure 5-4**. The self-assembled silioxane networks are oriented in such a way that the positively charged amine groups ($-NH_2^+$) are aligned away from the underlying silicon substrate.

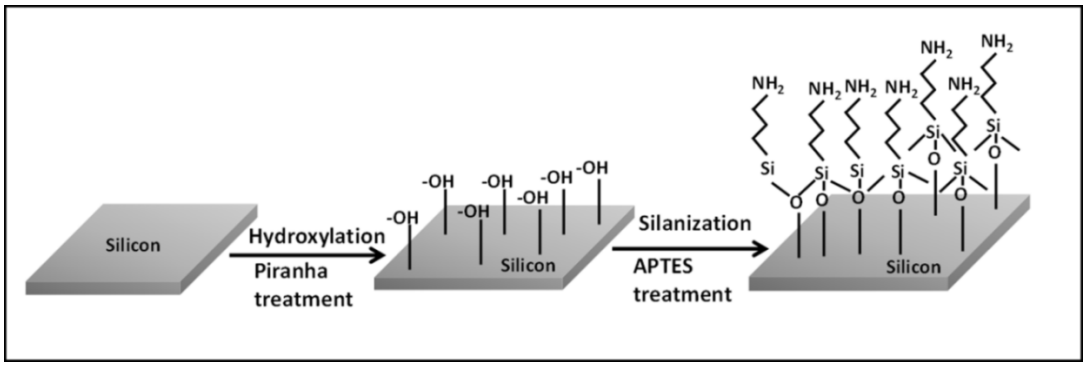

Figure 5-4: Schematic diagram displaying the process of hydroxylation after piranha treatment and silanization by APTES treatment on silicon surface prior to the electrophoretic deposition (EPD) step.

EPD results on the organosilane treated silicon surfaces from CNT-IPA solution with different APTES concentrations (10%, 20%, 50% and 100%) are illustrated in **Figure 5-5**. As can be observed from the figure, the EPD fabricated CNT thin film in conjunction with self-assembled $–NH_2^+$ terminated silane monolayer exhibits remarkable visual homogeneity and packing density in the film quality. Optical microscope observation (100 × magnifications) also revealed continuous surface coverage without any microscopic void or post-drying cracks in the film structure.

The applied electric field (15 V/cm) imparts sufficient electrophoretic mobility to the dispersed CNTs to migrate and arrive near the APTES treated anode surface. The Coulombic force of attraction acting between the positively charged $-NH_2^+$ groups from APTES siloxane structure and the negatively charged $-COOH^-$ functionalized CNTs assist in the gradual coagulation of the nanotubes into a coherent deposit on the anode surface. This is the most significant difference with respect to our findings in the previous chapter[102] where the thermally evaporated metal layer assisted in adhesion of the nanotubes with the underlying silicon surface. It is assumed that the metal layer acts a glue layer by the formation of metallic hydroxides which binds the carbon nanotubes with the silicon surface. In the present case, Coulombic interaction between the self-assembled $–NH_2^+$ moieties on the silicon surfaces and $–COOH^-$ groups on the nanotube surface ensures uniform film formation, thus eliminating the need for physical vapor deposition (e.g. thermal evaporation, sputtering) of a metal layer from the deposition model.

Additionally, the piranha and APTES treatment turns the silicon surfaces sufficiently hydrophilic. The pristine CNTs are also rendered hydrophilic in the acid refluxing step. The remarkable homogeneity and surface coverage by the CNT deposit in all our EPD experiments

can also be attributed to the strong hydrophilic-hydrophilic interaction between the organosilane treated depositing surface and the CNTs arriving near it during the deposition step.

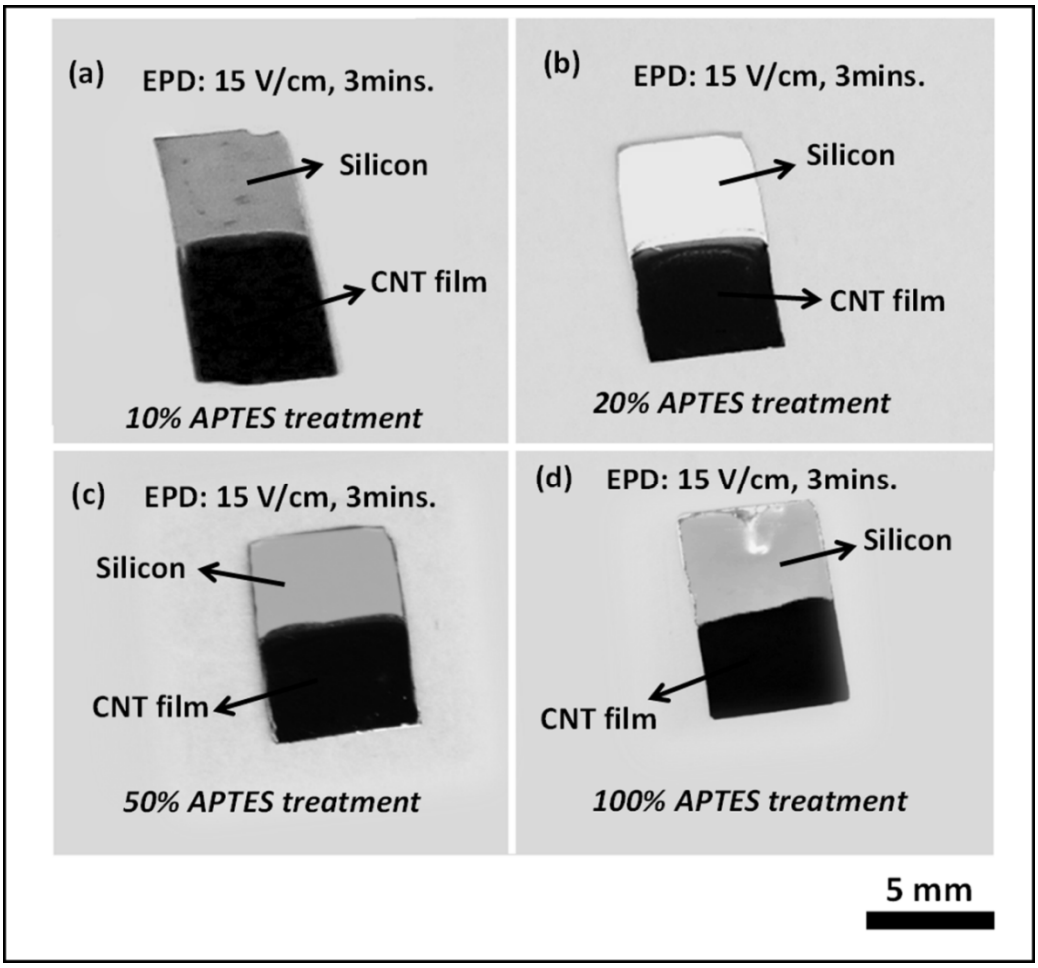

Figure 5-5: Optical images of CNT film deposited on silicon samples by EPD with different APTES concentration at an applied E-field of 15 V/cm for 3 min (a) 10% APTES, (b) 20% APTES, (c) 50% APTES and (d) 100% APTES. All the samples exhibit remarkable film quality.

Additionally, the piranha and APTES treatment turns the silicon surfaces sufficiently hydrophilic. The pristine CNTs are also rendered hydrophilic in the acid refluxing step. The remarkable homogeneity and surface coverage by the CNT deposit in all our EPD experiments

can also be attributed to the strong hydrophilic-hydrophilic interaction between the organosilane treated depositing surface and the CNTs arriving near it during the deposition step.

The beneficial effect of hydrophilic APTES self-assembly process in fabricated film quality is further adjudicated by comparing the coating attributes with methyl ($-CH_3$) terminated hexamethyldisilazane (HMDS) functionalization process. The presence of the non-polar methyl group in the hexamethyldisiloxane ($-O[Si(CH_3)_3]_2$) structure after the HMDS priming treatment renders a surface hydrophobic. The silicon samples were subjected to HMDS vapor coating process at 90° C for 30 min. EPD process was then performed on the HMDS coated samples at an electric field of 15V/cm for 3 min. **Figure 5-6** illustrates the difference in the coating quality between the APTES treated (left) and HMDS treated silicon (right) samples. In contrast to excellent deposition results on the APTES treated sample in (a), the HMDS coated sample in (b) showed discontinuous, inhomogeneous CNT coating with agglomerated and sparse deposits. The results thus conclusively establish the beneficial effect of organosilane surface functionalization with polar $–NH_2$ groups on the silicon samples in the deposition method in the comparison to the non-polar methyl surface treatment which hinders appreciable adhesion and film formation due to its inherent hydrophobicity.

The benefits of APTES assisted EPD of CNTS in comparison with the APTES assisted dip coating of the CNTS were explored in the next set of experiments. The silicon samples were treated with APTES with varying concentration and dipped in CNT-IPA and CNT-water suspension for 3 min. It was observed that EPD fabricated CNT films from the same CNT-IPA suspension in all our experiments show superior film quality in comparison to all the dip coated samples. The samples dip coated in both the CNT-IPA and CNT-water suspension for 3 min with 20% APTES functionalization exhibit poor surface coverage with discontinuous and sparse CNT

deposits. The deposition results on CNT-water dip coated samples for 3 min with 20% APTES treatment show even inferior film quality than the CNT-IPA dip coated samples for the same duration.

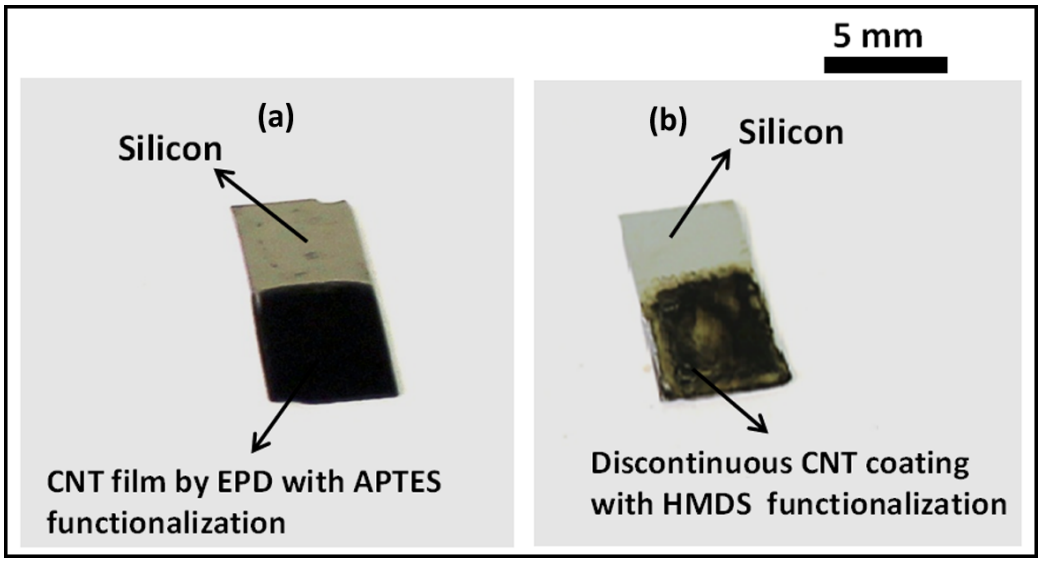

Figure 5-6: Optical images of CNT films deposited by electrophoretic deposition at an applied E-field of 15V/cm for 3 min on (a) 20% APTES treated silicon sample showing superior coating quality in contrast to (b) HMDS treated silicon surfaces.

With a view to improving the deposition results on the dip coated samples, the dip coating duration was increased from 3 min to 6 min for both types of the samples and the APTES treatment of the sample for CNT-water dip coating was increased from 20% to 50%. **Figure 5-7** depicts the experimental results of this comparative study. The results matched with our previous observation in which the CNT-IPA dip coated samples exhibited relatively better film quality in contrast to CNT-water dip coated samples. **Figure 5-7**-c shows extremely inferior coating characteristics on 50% APTES functionalized CNT-water dip coated samples. However the CNT-IPA dipped sample with 20% APTES functionalization still shows inhomogeneous and agglomerated coating features when compared to EPD coated samples (performed at an electric

field of 15V/cm for 3 min with 20% APTES treatment). The results presented above clearly represent APTES assisted EPD technique as a better and reliable deposition technique for CNT thin film compared to the dip coating method, even with longer incubation duration (6 min of dip coating with 20% APTES functionalization vs. 3 min of EPD at 15V/cm from CNT-IPA suspension with 20% APTES functionalization) and surface treatment with increased APTES concentration (6 min of dip coating with 50% APTES from CNT-water vs. 20% APTES assisted EPD from CNT-IPA).

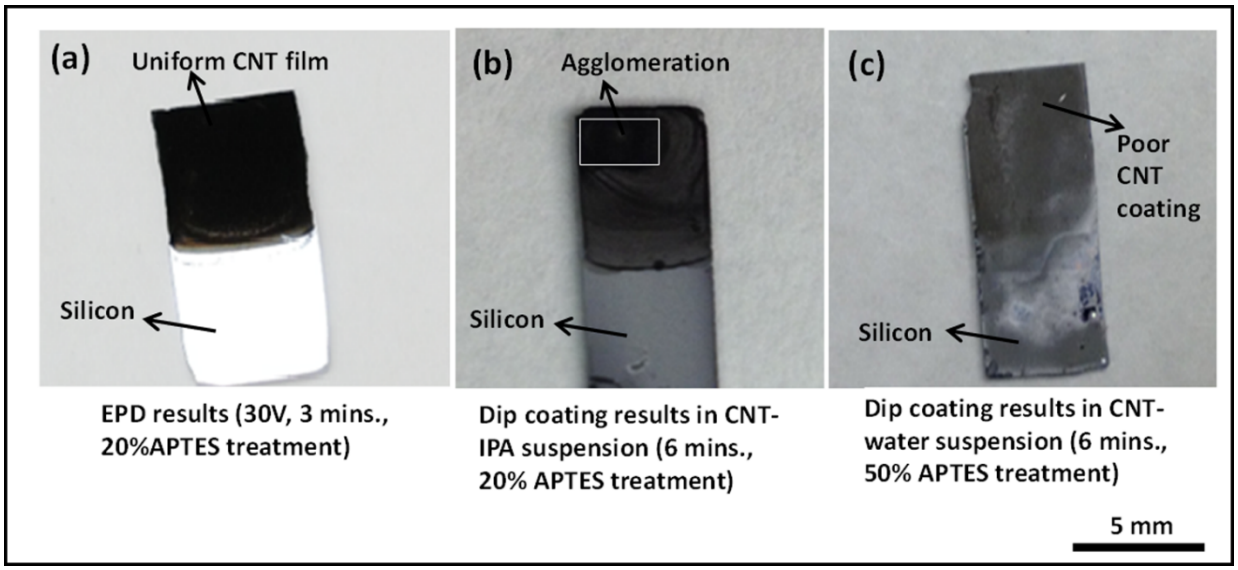

Figure 5-7: Deposition results comparing electrophoretic deposition (EPD) and dip coating on surface functionalized silicon substrates (a) CNT film deposited by EPD at an applied E-field of 15V/cm for 3 min with 20% APTES treatment (b) Dip coated silicon samples in CNT-IPA solution for 6 min with 20% APTES treatment showing agglomerated deposit and (c) Dip coated silicon samples results in CNT-water solution for 6 min with 50% APTES treatment showing poor CNT surface coverage.

Comparative studies on the CNT film quality deposited from CNT-IPA and CNT-water suspension by the proposed electrophoresis method were also conducted in this work. As depicted by **Figure 5-8**, the deposition results from the CNT-IPA suspension for 3 min at 15

V/cm with 20% APTES characterization show superior deposit quality than the CNT-water suspension under identical experimental conditions. The deposit obtained from CNT- water suspension exhibited severe aggregation in the CNT film structure after 2 hours of drying following the deposition step. The results did not improve even though the deposition duration in the CNT-water suspension was increased from 3 min to 6 min at an electric field of 15V/cm. The reason can be primarily attributed to the generation of bubbles in the EPD solution by the electrolysis of water due to the strong electric field across the solution. The evolution of hydrogen and oxygen gases due to the electrolysis process disrupts the flow of the CNT influx and creates voids and discontinuities in the final deposit at the anode. Similar observation was also reported by Du *et al.*[40] and Boccaccini *et al.*[76] in their attempts to study the morphology of the carbon nanotube films by electrophoretic deposition.

The deposition quality also did not improve much when the deposition voltage was reduced to 5 V for longer duration of deposition (30 min) since the resultant electric field (2.5 V/cm) was too weak to offer sufficient electrophoretic mobility to the CNTs to migrate and adhere to the anode surface. Additionally, it was also observed that the EPD attempts with longer deposition duration in CNT-water suspension sometimes resulted in the total degradation of the EPD solution leading to formation of agglomerated CNT flakes and subsequent precipitation of the nanotubes in the solution. This observation is consistent with our findings, as reported in the previous chapter, which reveals sedimentation and eventual agglomeration of the CNTs in the aqueous suspension after failed EPD attempts on bare silicon substrates. On the contrary, similar deposition attempts with CNT-IPA solution rarely showed degradation of the solution although the surface roughness of the final deposit increased due to prolonged deposition on the depositing surface.

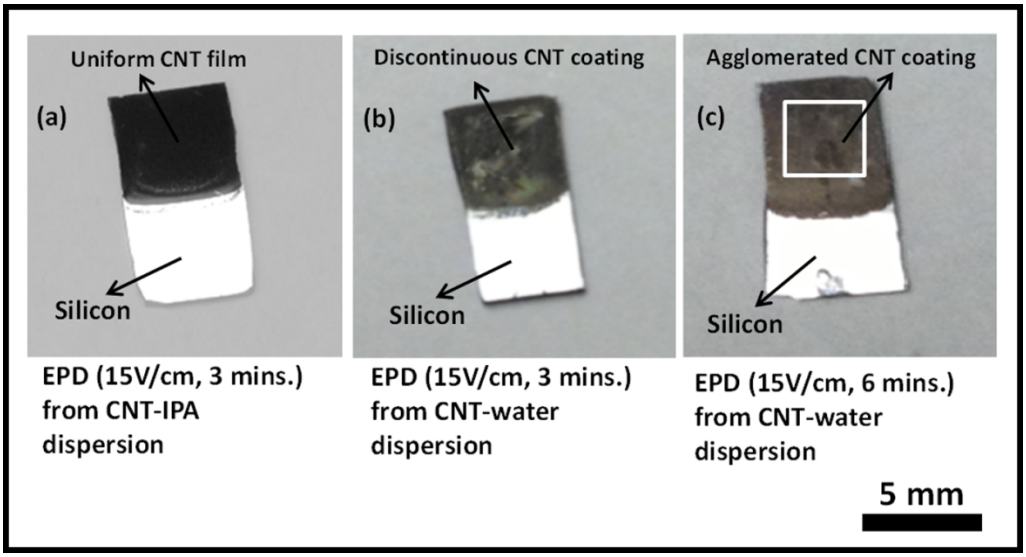

Figure 5-8: Optical images comparing the electrophoretic deposition results at an applied E-field of 15V/cm on 20% APTES treated silicon substrates (a) from CNT-IPA suspension for 3 min, (b) from CNT-water suspension for 3 min and (c) from CNT-water suspension for 6 min.

i. Microscopic imaging and Raman spectroscopy

Microstructural imaging of the deposited films was conducted using a JEOL (Japan Electron Optics Laboratory) JSM 6610 scanning electron microscopy (SEM) with an acceleration voltage of 20-30 kV. The samples were sputter coated with ~10 nm of platinum before the imaging process. The imaging was performed at various points on the substrate surface with different magnification values to investigate the surface coverage of the deposited film. The SEM images of the CNT film deposited on 20% APTES coated silicon substrate are shown in **Figure 5-9**. The acquired high resolution images (Figure **5-9** (a) at × 10k magnification and (b) at × 20k magnification) testify random, horizontal orientation of the carbon nanotubes with excellent homogeneity and packing density without any microscopic cracks or discontinuity in the film structure.

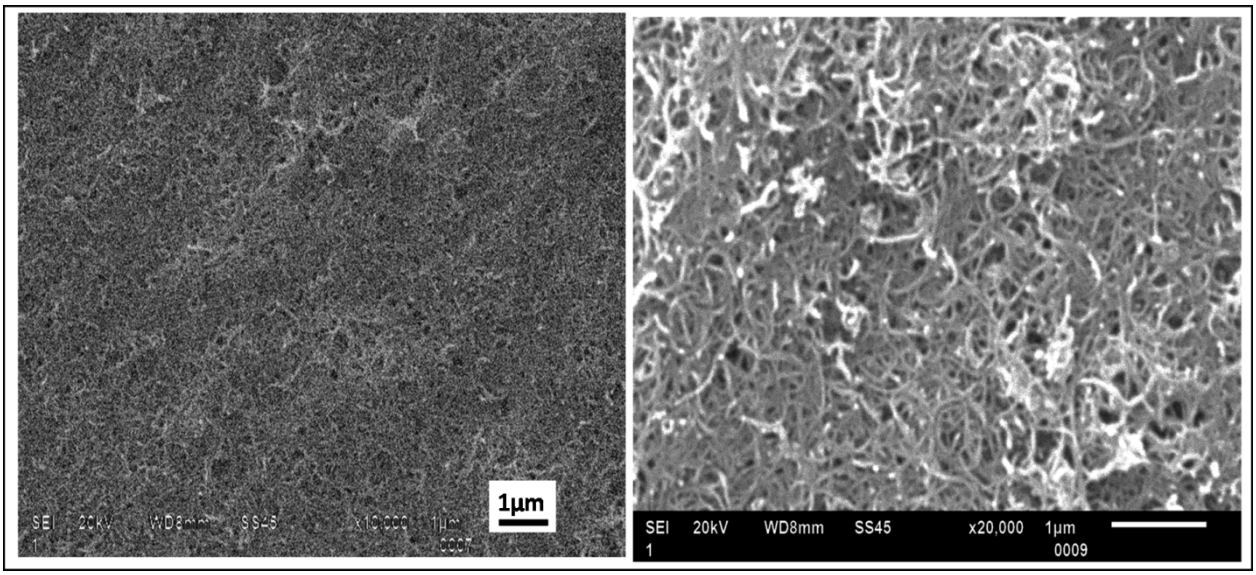

Figure 5-9: Scanning electron microscopic images of CNT film on 20% APTES treated silicon sample deposited at an applied electric field of 15V/cm for 3 min showing appreciable surface coverage and packing density without voids (a) at ×10k magnification and (b) at ×20k magnification.

The spectroscopic behavior of the deposited CNT films was analyzed by Raman spectroscopy. The spectroscopic measurements were performed using a Jobin Yvon Horiba Labram Raman spectrometer. A HeNe laser with wavelength 638 nm and incident power of 17 mW was used for all the spectroscopic analysis. The confocal hole aperture of 200 µm and grating of 1800 lines per mm were selected during the measurement. Extended scans were performed between 500 cm^{-1} and 3000 cm^{-1} for best results. **Figure 5-10** shows the Raman spectra of the carbon nanotube films deposited on the silicon sample with varying APTES concentration (5%, 10%, 20%, 50% and 100%). The peak for the disorder-induced D-band was seen to occur at ~1333 cm^{-1} and those for the tangential G-bands occurred at ~1579 cm^{-1} and ~2645 cm^{-1} for all the samples. The peaks closely matched with the spectroscopic results of dry carbon nanotube powder used in this work. The absence of radial breathing modes (RBM) was also noted for all the samples when scanning was performed from 0 to 400 cm^{-1} (not shown in

the graph). The following conclusions can be drawn from the spectroscopic results: (a) the absence of the prominent radial breathing modes (RBM) for all the acquired Raman spectra between 0 cm^{-1} to 400 cm^{-1} proves the presence of multi-walled nanotubes (MWCNTs) in the EPD deposits and (b) the vibrational attributes of the MWCNTs are not affected by the varying concentration of APTES in the surface functionalization procedure prior to the deposition step.

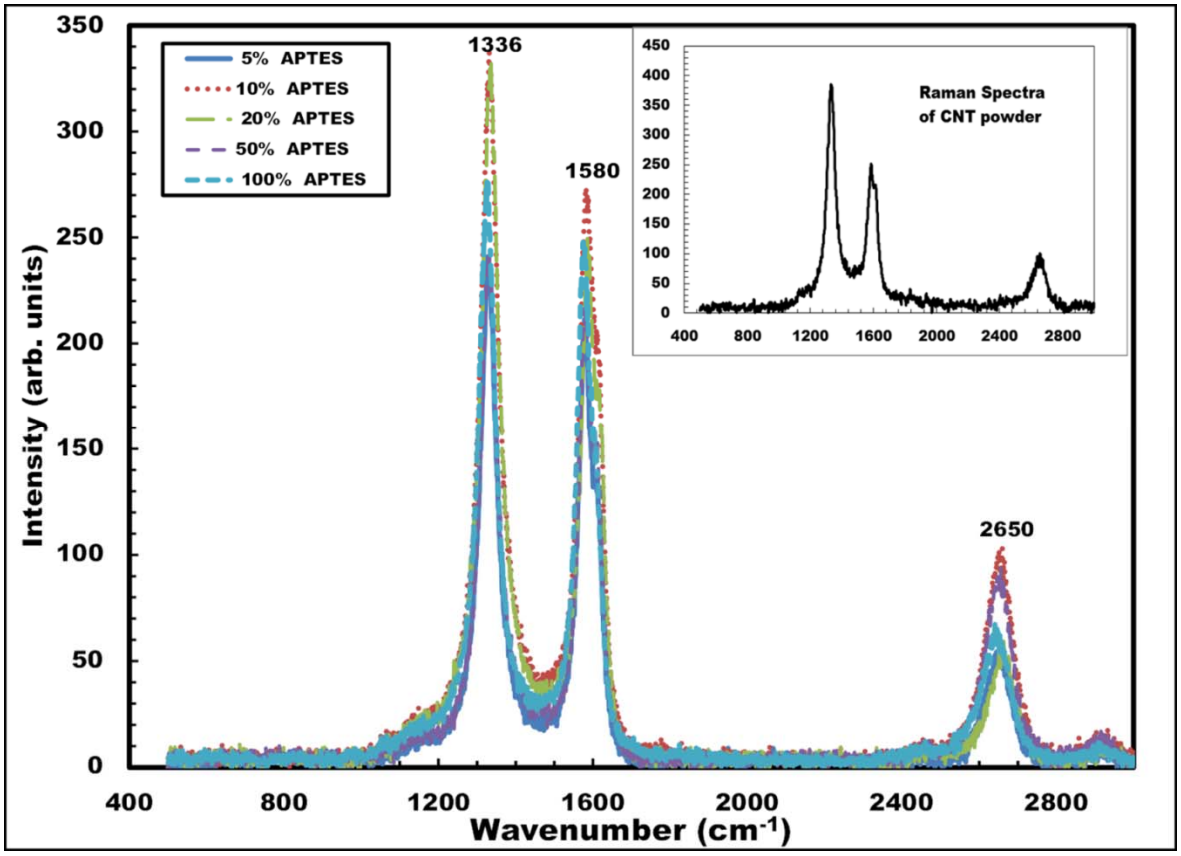

Figure 5-10: Raman spectra of CNT films deposited on silicon samples with varying APTES concentration (5%, 10%, 20%, 50% and 100%). Inset shows Raman spectrum of raw CNT powder used in the work.

ii. Thickness of the deposited films

To explore the effect of varying APTES concentration (5%, 10%, 20%, 50% and 100%) on the thickness of the deposited films, quantitative surface analysis was performed using a

KLA-Tencor D-100 Alpha Step surface profiler. For the thickness profiling, surface scanning was performed for 10 times for each sample and the average value was calculated.

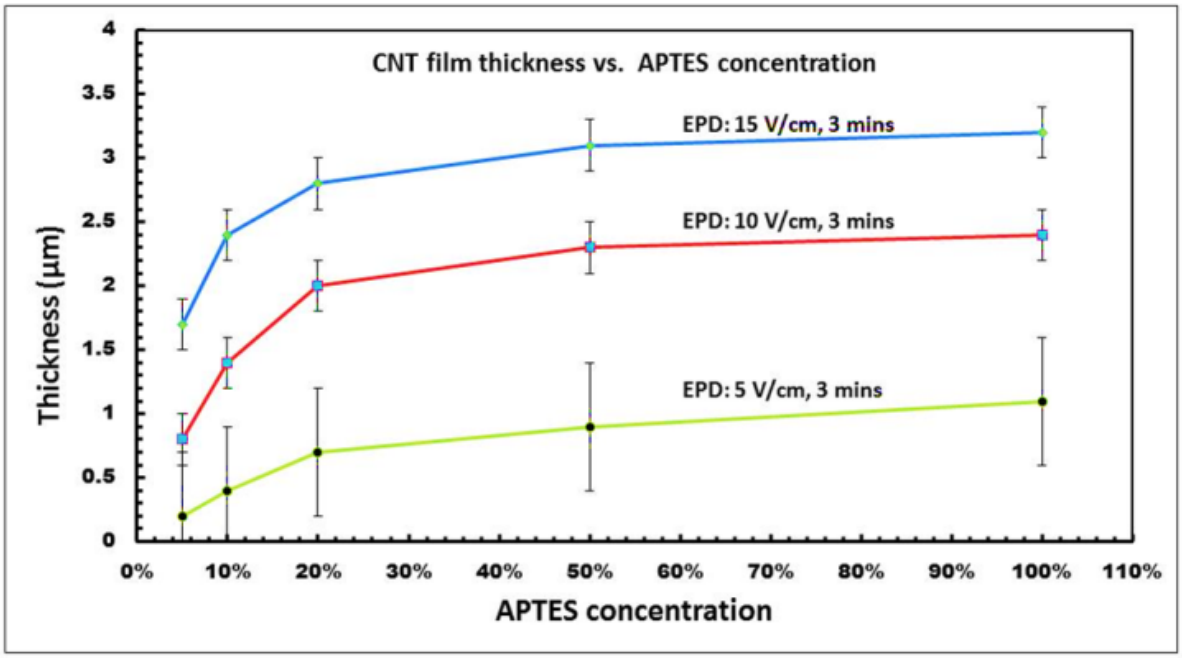

Figure 5-11: Thickness of CNT films deposited on silicon samples with varying APTES concentration at different applied electric field (E-field: 5V/cm, 10V/cm and 15V/cm) for constant deposition duration of 3 min.

It was observed that for constant deposition time and voltage, the thickness of the CNT film deposited on the silicon samples followed an increasing trend with increasing APTES concentration. As shown in **Figure 5-11**, the film thickness of the films increases from 1.4 (±0.2) µm with 5% APTES concentration to 3.3 (±0.2) µm with 100% APTES concentration for highest E-field: 15V/ cm and 3 min of deposition duration. The figure also depicts a distinct increase in the film thickness as the APTES concentration increases from 5% to about 20%. The values tend to reach saturation as the concentration ranges from 50% to 100%. This is prominent for the results obtained with 15V/cm and 10V/cm for 3 min of deposition duration e.g. in **Figure**

5-11 for E-field: 10V/cm and 3 min of deposition duration, the thickness increases by ~2.5 times (from 0.8 μm to 2 μm) when APTES concentration varies from 5% to 20% whereas it barely increases from 2.3 μm with 50% APTES concentration to 2.4 μm with 100% APTES concentration. The saturated values can be attributed to the reduction of inter-electrode electric field strength as the amount of low conducting organosilane increases on the silicon surfaces with 50% to 100% APTES concentration. The reduction in inter-electrode electric field affects the electrophoretic mobility of the CNTs which eventually decreases the influx of the migrating nanotubes towards the deposition surface and thus, slackens down the overall deposition process. Also, for a specific APTES concentration used in the EPD experiments, it can also be noticed that the film thickness increases with the increasing voltage (or electric field) with constant deposition time of 3 min. **Figure 5-11**, thus, conclusively establishes the versatility of the electrophoretic deposition process where the thickness of the deposit on the target surfaces can be precisely controlled in relation to the deposition parameters e.g. inter-electrode electric field, degree of surface functionalization, duration of deposition.

5.4: Conclusion and future work

Electrophoretic deposition (EPD) of –COOH- functionalized carbon nanotubes dispersed in CNT-IPA and CNT-water suspension has been successfully performed on silicon substrates with self -assembled organosilane (APTES) surface functionalization. The deposited film quality and surface properties were reviewed to be dependent on the dispersion medium of CNTs, with the best EPD results obtained from IPA-CNT suspension. EPD results obtained by $–NH_2^+$ terminated APTES surface functionalization display significant difference in terms of improved homogeneity and film quality in contrast to the non-polar $–CH_3$ functionalization by HMDS treatment. The benefits of the EPD technique as a fast, reliable and reproducible room temperature coating process over the dip/immersion coating have also been established in the

chapter. Scanning electron microscopy and Raman spectroscopic results confirmed the presence of MWCNTs in the deposited film. The present work eliminates the need of physical vapor deposition of metal films in the deposition model and ensures deposition of CNTs directly on the semiconducting substrates based on a relatively quick and inexpensive hydrophilic surface functionalization assisted EPD technique. Through a series of systemic studies, we have established a reliable processing recipe of EPD of CNTs on silicon substrates at an applied electric field of 10-15 V/cm for 3 minutes of duration with 20% surface functionalization for excellent and reproducible results.

With regard to potential future work in this direction, we have obtained preliminary results in extending the surface functionalization technique in an attempt to deposit CNTs on glass, insulator substrates (e.g. silicon dioxide and silicon nitrides) by EPD without major variations in the deposition setup. Research endeavors, as revealed in the next chapter, are also directed in the detailed investigation of the surface roughness of the EPD fabricated CNT films and their application as viable substrates for Surface Enhanced Raman Spectroscopy (SERS) of different analytes. Our results in this chapter confirm that the solution based, low cost, electrophoretic deposition technique of carbon nanotubes on semiconductor substrates with $-NH_2$ terminated surface treatment has the immense application potential in CNT based nano-electronics, device integration with existing CMOS technology on different semiconductor substrates and next generation hybrid electronics assisted by organic self-assembly.

(All the figures in the chapter are reprinted with permission from the following publication.)

Publication:

1. Sarkar, A; Daniels-Race, T. Electrophoretic Deposition of Carbon Nanotubes on 3-Amino-Propyl-Triethoxysilane (APTES) Surface Functionalized Silicon Substrates. *Nanomaterials* **2013**, 3, 272-288

CHAPTER 6: SURFACE ENHANCED RAMAN SPECTROSCOPY STUDIES ON SILVER NANOPARTICLE COATED CARBON NANOTUBE NETWORKS FABRICATED BY ELECTROPHORETIC DEPOSITION

6.1: Introduction

The previous chapter of this dissertation exemplifies the versatility of EPD as a fast, reproducible and single-step room temperature coating process of horizontally aligned CNT deposits on APTES treated Si surfaces from organic solvents (e.g. isopropyl alcohol or IPA). The deposition strategy has been further extended in the fabrication of noble metal coated CNT based porous, active substrates for surface enhanced Raman spectroscopic (SERS) applications in this chapter.

Raman spectroscopy, which is based on the inelastic scattering of monochromatic light, has emerged as an extremely versatile spectroscopic tool for the identification and quantitative examination of various compounds in pharmaceuticals, analytical chemistry, bio-medical and polymers science, forensic investigation and art and architecture[107–110]. Although routinely used to analyze the rotational and vibrational levels of target analytes, Raman scattering is limited in its detection sensitivity and weak signature signals. To mitigate this challenge, recently surface-enhanced Raman spectroscopy (SERS) has been rapidly developing into an advanced and powerful analytical tool for ultra-sensitive and selective detection of common and unique molecules adsorbed on noble metal nanostructures[111–113]. The detection limits have been significantly pushed down to the single molecule[114] due to the chemical and electromagnetic enhancement contributions from SERS-active surfaces. It has been reported that SERS relies on surface plasmons, which are induced by the incident electromagnetic (EM) field on highly profiled metallic nanostructures to increase the Raman signal intensity substantially[115]. As an alternative explanation, it has also been proposed that signal enhancement is achieved due to the charge transfer between the chemisorbed species and the metallic surface[116]. Significant

developments in nanofabrication over the past decade have paved the way in understanding the fundamentals and applications of SERS. Innovations in the preparation of SERS active substrates with regard to facile and cost-effective fabrication have been the subject of intensive investigation and study[117,118]. The state-of-art techniques to prepare highly ordered SERS active substrates involve electrochemical roughening of metal surfaces, electro-deposition, self-assembly and Langmuir-Blodgett coating of nanoparticles, nanosphere lithography, nanoimprint, nanolithography and substrate etching[119–123] .

Recently, there has been considerable interest to utilize porous surfaces as viable SERS substrates in tandem with well-researched, nano-structured planar surfaces[124–129]. The motivation for using porous networks is based on the understanding that the large surface area of the porous structure would increase the number of effective "hot spots" (- i.e. sites with enhanced EM field), thereby contributing to surface enhancement of the Raman signals. Due to their large surface area and chemical inertness, recently carbon nanotubes decorated with noble metal nanoparticles (e.g. gold (Au), silver (Ag), platinum (Pt)) offer an interesting option in exploring nanoparticle-nanotube hybrid materials as conducive substrates for routine SERS experiments. He *et al.*[130] have demonstrated the enhancement attributes of Au-coated, horizontally aligned carbon nanotubes (Au-HA-CNTs) as effective SERS substrates for detection of low levels of biological specimens. Maximum enhancement was observed with HA-CNTs when the polarization direction (E-field) of the incident laser beam was parallel to the aligned direction of the HA-CNTs. In their method, horizontally aligned carbon nanotubes (HA-CNTs) were prepared by mechanical pressing technique on the CVD synthesized vertically aligned carbon nanotubes (VA-CNTs). Recent research proceedings in the preparation of CNT based SERS substrates can be found in publications to date[101,131–133] .

In this chapter, the silver nanoparticle (AgNP) coated active substrate, prepared by EPD of horizontally aligned porous CNT networks on amino-silane treated Si surfaces, has been referred to as Ag-CNT-Si SERS substrate. The rhodamine6G (R6G) molecule has been probed as the target analyte. The surface enhanced Raman spectra of the R6G molecule with varying concentrations (from 1 milli-molar-mM - i.e. 1×10^{-3} M to 1 pico-molar-pM - i.e. 1×10^{-12} M) on the Ag-CNT-Si substrates were extensively studied and compared with the results of SERS investigation on Ag coated planar Si substrates (Ag-Si). The subsequent sections of this report reveal pertinent details with regard to electrophoretic deposition of carbon nanotubes on APTES modified Si substrates, synthesis and coating of silver nanoparticles for the fabrication of our final SERS substrate, discussion on detection limits and estimation of enhancement factor from the acquired Raman spectra.

6.2: Experimental procedure

The experimental procedure includes: (a) preparation of stable CNT suspensions in IPA (CNT-IPA) for the EPD process, (b) synthesis of silver nanoparticles (AgNPs), (c) preparation of 20% APTES solution, (d) substrate functionalization by APTES grafting, (e) EPD process, (f) silanization of the electrophoretically deposited CNT samples, and (g) preparation of Ag-CNT-Si SERS substrates

6.2.1: Preparation of CNT solution in IPA (CNT-IPA)

Approximately 100 mg of as-purchased multi-walled CNTs (purity: >98%, average wall thickness: 7-13 graphene layers, dimension: 6-13 nm (O.D.) × 2.5-20 μm (length), CVD, Sigma Aldrich, USA) were acid refluxed in 40 ml concentrated sulfuric (H_2SO_4) and nitric (HNO_3) acid (volume ratio= 3:1 respectively) at 120°C for 30 minutes on a hot plate. The acid-heat treatment of the solution resulted in a black slurry which was cooled for 1 hour in the fume hood. The refluxed solution was then repetitively washed with deionized (D.I.) water (18.2 MΩ-cm) and

filtered in medium retentive filter papers (pore size: ~11 μm) repeatedly until the resulting solution indicated pH 7 (neutral). The black filtration residue was collected with a laboratory spatula and mixed with 50 ml of isopropyl alcohol (IPA). The solution was then placed inside an ultrasonicator bath for 2 hours to obtain stable CNT suspensions in IPA (referred as CNT-IPA). The dispersed CNT solution was then incubated inside a chemical hood for 48 hours for examining the solution stability. No visual sign of agglomeration was noticed in the solution and therefore, was deemed suitable for the subsequent EPD process.

6.2.2: Synthesis of AgNPs

The silver nanoparticles in aqueous medium were synthesized by the chemical reduction of metallic precursors e.g. silver nitrate ($AgNO_3$) using tri-sodium citrate ($Na_3C_6H_50_7$). All the solutions of the reacting chemicals were prepared in D.I. water. To investigate the effect of the stabilizing agent in controlling the nanoparticle aggregation, 3 types of silver nanoparticle (Ag-NP) solutions (A, B and C) were prepared using the following recipe. Solution A was prepared without the addition of any stabilizing agent; for the preparation of samples B and C, poly-vinyl-pyrrolidone powder (PVP, average Mol. weight ~29,000) was added in different proportions as stabilizing agent. For sample A, 0.5 mM of silver nitrate ($AgNO_3$, Mol. weight: 169.87) was prepared by dissolving 21.25 mg in 250 mL of D.I. water. The solution was boiled at 120ºC with constant stirring. In the boiling solution, about 10 mL of 1% $Na_3C_6H_50_7$ solution was added drop wise. Heating was continued until color change was evident (~20-25 minutes). The same recipe was followed for the preparation of solution B and C with the addition of ~1 mg and ~9 mg of PVP respectively as stabilizing agent to the boiling $AgNO_3$ solution.

6.2.3: Preparation of 20% APTES solution

A 20% APTES concentration was deemed suitable for the surface functionalization of silicon substrates prior to the deposition process. A homogenous solution was prepared by

mixing 2 mL of APTES (> 98% as purchased from Sigma Aldrich) with 2 mL of D.I. water and 6 mL of ethanol solution (20% APTES). The prepared solution was incubated in the chemical hood until further application.

6.2.4: Substrate preparation by APTES grafting

Silicon wafers (resistivity: 0-100 Ω-cm) were used for all the experiments. The wafers were cleaved into ~1 × 0.5 × 0.055 cm^3 samples and were treated in warm piranha solution (H_2SO_4:H_2O_2 = 1:1) for 25 minutes. The samples were then rinsed in D.I. water, dried and immersed into 10 ml of as-prepared 20% APTES solution for 30 minutes. After the incubation period, all the samples were rinsed in copious amount of ethanol and water to remove the excess APTES. The rinsed samples were dried in nitrogen and kept in the oven at 80° C for 1 hour.

6.2.5: EPD process

The electrophoretic deposition experiment from CNT-IPA was performed in a custom built set-up (as shown in **Figure 6-1**) with 20% APTES treated silicon sample as the anode and a copper plate (dimension: 1.5 × 1 × 0.2 cm^3) as the cathode. The deposition voltage was set at 30 V (or electric field (E-field) of 15 V/cm) with the constant deposition time for 3 minutes. The inter-electrode distance was fixed at 2 cm for all the EPD experiments. The selected experimental parameters were selected and optimized from our process recipes as reported in chapters 4 and 5. After the deposition process, the samples were dried overnight at room temperature under ambient condition. No significant agglomeration of the nanotubes or discontinuity in the deposited film structure was observed after the drying period. The samples were then prepared for a second round of APTES grafting for CNT sidewall silanization.

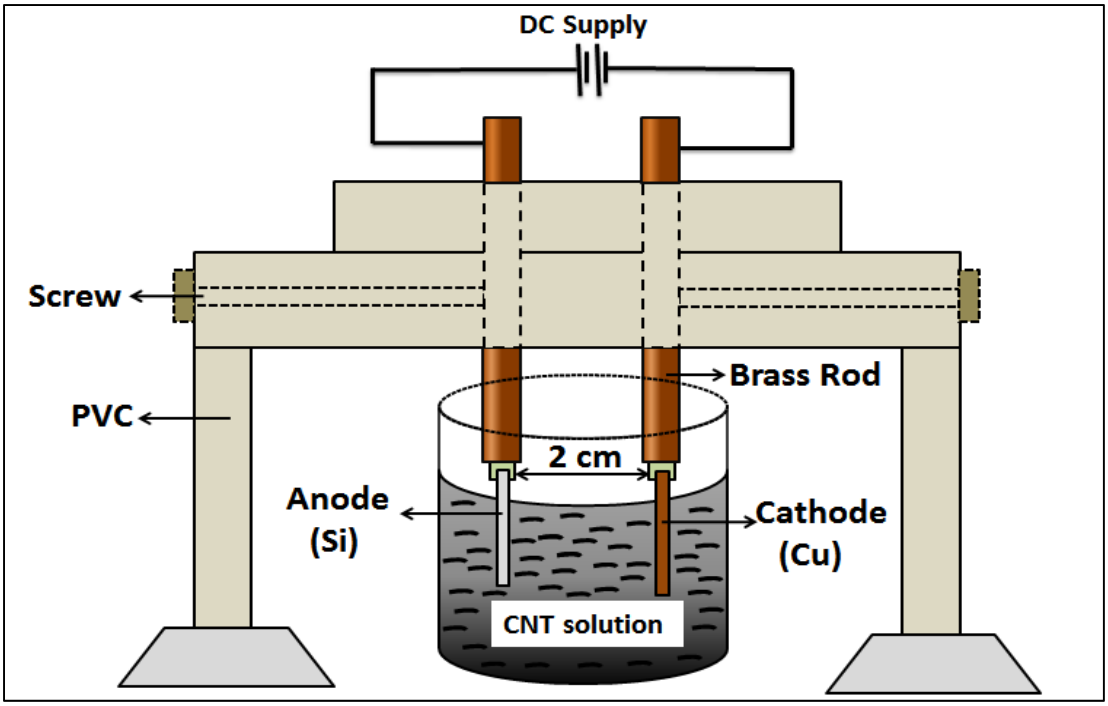

Figure 6-1: Schematic diagram of electrophoretic deposition set-up[102].

6.2.6: Silanization of electrophoretically deposited carbon nanotubes

Silanization of the EPD-fabricated carbon nanotube films was performed by immersing the EPD samples in 20% APTES solution for 1 hour. After the incubation period, the samples were rinsed in D.I. water and carefully dried by blowing a gentle stream of nitrogen to drive away the excess APTES. The samples were then placed inside the oven at 80 ℃ for 1 hour.

6.2.7: Fabrication of SERS substrate

The final SERS substrates with the silanized carbon nanotubes on the silicon samples were fabricated by immersion coating. The substrates were immersed in 10 mL of a suitable AgNP solution for 24 hours. After the deposition process, the substrates were dried in ambient air for 6 hours and finally incubated in different concentrations of R6G solution for at least another 24 hours. Following the incubation period, the samples were dried and prepared for Raman spectroscopy.

6.2.8: Raman Spectroscopy

Raman spectroscopy measurements were conducted using a Jobin Yvon Horiba Labram Raman spectrometer. A HeNe laser with wavelength 638.4 nm and incident power of 17 mW was used for the spectroscopic analysis. The confocal hole aperture of 200 µm and grating of 1800 lines per mm were set during the measurement. Extended scans were performed between 600 cm^{-1} and 1800 cm^{-1} for best results. The exposure time during an extended scanning for each spectral window (acquisition time) was set to be 5 seconds with the accumulation number of 5. A 100X objective from Olympus was used for focusing and during scanning. Each of the acquired Raman spectra was corrected by an 8-order polynomial fitting curve of fluorescence backgrounds using the interfacing LabSpec software.

6.3: Results and discussion

6.3.1: Characterization of synthesized Ag nanoparticles

The silver nanoparticles were synthesized according to the following chemical reaction[134,135]:

$$4Ag^{+} + Na_3C_6H_50_7 + 2H_2O = 4Ag^{0} + C_6H_50_7H_3 + 3Na^{+} + H^{+} + O_2$$

The reduction process outlined in the synthesis procedure, produces negatively charged citrate ion capped AgNPs. **Figure 6-2** shows the optical images of the 3 types of solutions (A, B and C) prepared for the study. As can be noted, from left to right, the color of the solution changes from dark grey (solution A) to reddish grey (solution B) and bright yellow (solution C). In the absence of the stabilizing agent (PVP) in the synthesis step, the AgNPs in solution A started to exhibit signs of agglomeration towards the end of the heating process. The agglomeration became clearly evident when the solution turned dark grey as it was incubated in the chemical hood for 30 minutes.

The addition of PVP in the synthesis process is expected to establish steric stabilization within the nanoparticles, which is rendered by the physical adsorption or grafting of PVP macromolecules on the surfaces of the particles. The stabilizing action of PVP on the synthesized AgNPs was evident from the color of solution B and C. Both the solutions exhibited superior colloidal stability when compared to solution A. The amount of PVP used in the synthesis process also determines the degree of stability in the solutions. For instance, solution B, with the addition of ~0.5 mg of PVP during the synthesis process, showed stable suspension for about 3 weeks before it started to deteriorate while solution C, with ~9 mg of added PVP, exhibited remarkable colloidal stability for months.

The stabilization effect mediated by PVP in the prevention of AgNP clustering and solution degradation was also corroborated by transmission electron microscopy (TEM, JEOL 100CX) images of the solutions (**Figure 6-3**, **Figure 6-4**, **Figure 6-5**). The nanoparticles in solution A exhibited severe agglomeration as shown in **Figure 6-3**. This illustrates the inherent tendency of the nanoparticles to exhibit agglomeration in the absence of sufficient amounts of stabilizing agents. **Figure 6-5** exhibits the presence of unclogged AgNPs in solution C with average diameter of 30-40 nm. In comparison to solution C, the AgNPs in solution B remain more closely packed with the average diameter of 70-80 nm (**Figure 6-4**). The results prove that increasing the amount of stabilizing agent ensures smaller size and improved colloidal stability by minimizing particle aggregation. Solution C, with minimum agglomeration, was selected for the deposition of AgNPs on the CNT-Si samples.

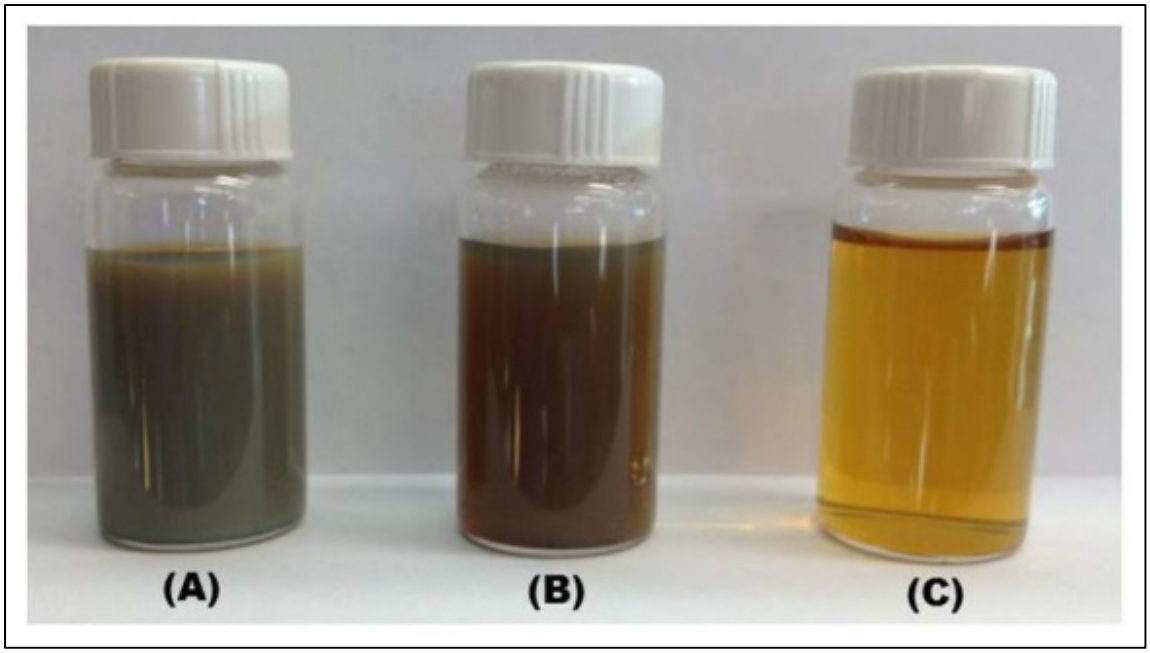

Figure 6-2: Optical images of the synthesized silver nanoparticle solution designated as Solution A, B and C from left to right.

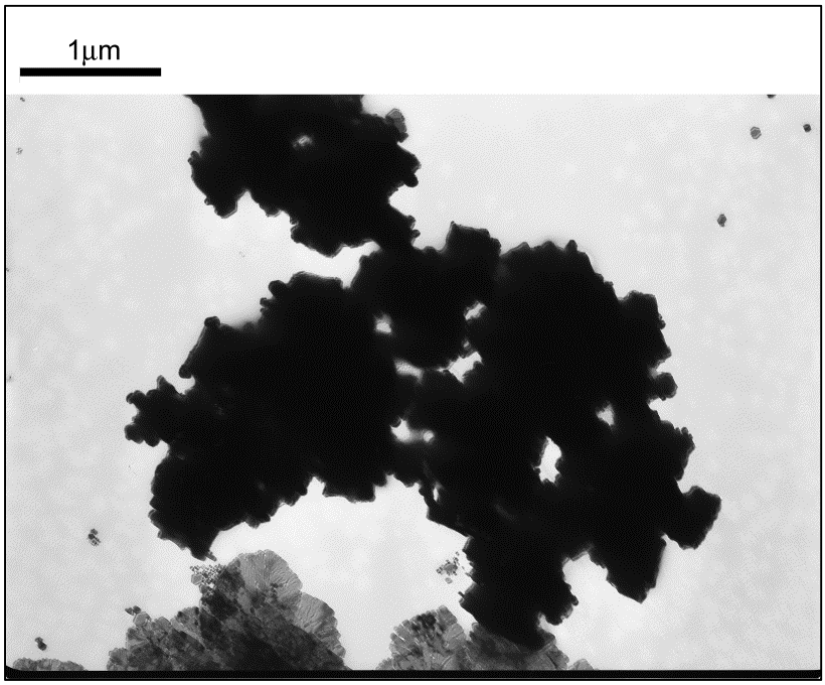

Figure 6-3: TEM image of silver nanoparticles in solution A showing severe aggregation.

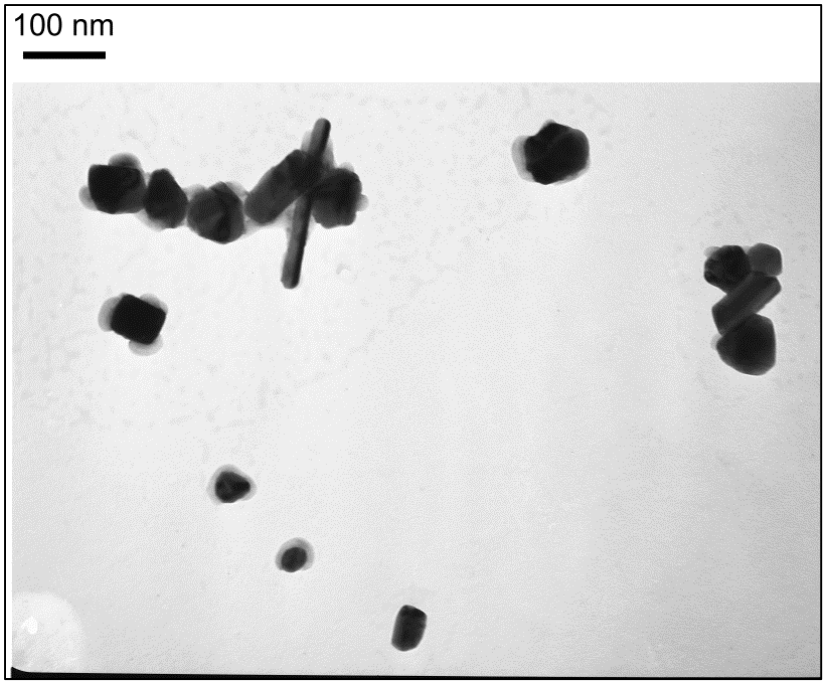

Figure 6-4: TEM image of silver nanoparticles in solution B (Average particle diameter: 70-80 nm).

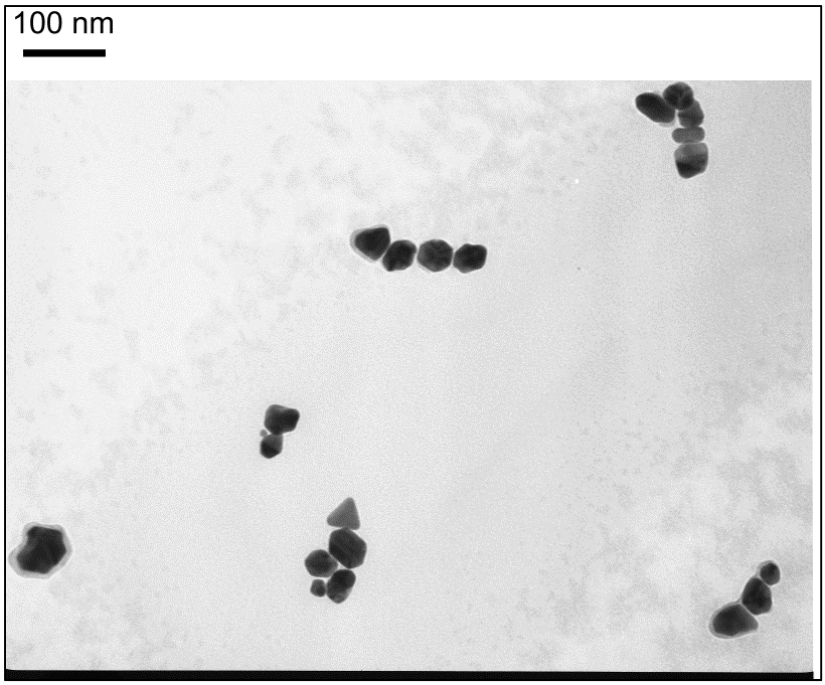

Figure 6-5: TEM image of silver nanoparticles in solution C showing minimum aggregation (Average particle diameter: 30-40 nm).

The acid refluxing of the as-purchased carbon nanotubes prior to the deposition step aids in the dissolution of unwanted residual metal catalysts in the as-purchased nanotube powder, purification and shortening of the nanotubes[56,136,137]. The acid-heat treatment also attaches covalently carboxylic groups (-COOH) on the surface of the nanotubes which impart negative surface charges. This leads to sufficient inter-tubular repulsion, thereby ensuring remarkable stability of the CNT suspension all through the EPD experiments.

The surface functionalization process on the piranha treated Si substrates is accomplished by the self-assembly of APTES monolayer. The piranha treatment induces surface hydroxyl (-OH) on the silicon surface by hydroxylation process. The functional groups generated on the silicon surfaces after this oxidation reaction are referred to as surface silanols (Si-OHs). The next step involves hydrolysis of the ethoxy groups ($-C_2H_5$) from its molecular structure to form APTES silanols. The subsequent condensation reaction between the surface and APTES silanols leads to further dehydration of water molecules and formation of lateral siloxane (Si-O-Si) networks on the silicon surfaces. The siloxane networks are oriented in a way such that the positively charged amine groups ($-NH_2$) are aligned away from the underlying silicon surface. **Figure 6-6** depicts the functionalization process of the hydroxylated Si surface to amine terminated, hydrophilic surface by the organosilane grafting treatment. The gradual film formation by coagulation and deposition of nanotubes from the EPD suspension is ensured by the Coulombic force of attraction acting between the positively charged $-NH_2$ groups from APTES siloxane structure and the negatively charged nanotubes migrating towards the Si surface under the application of the electric field.

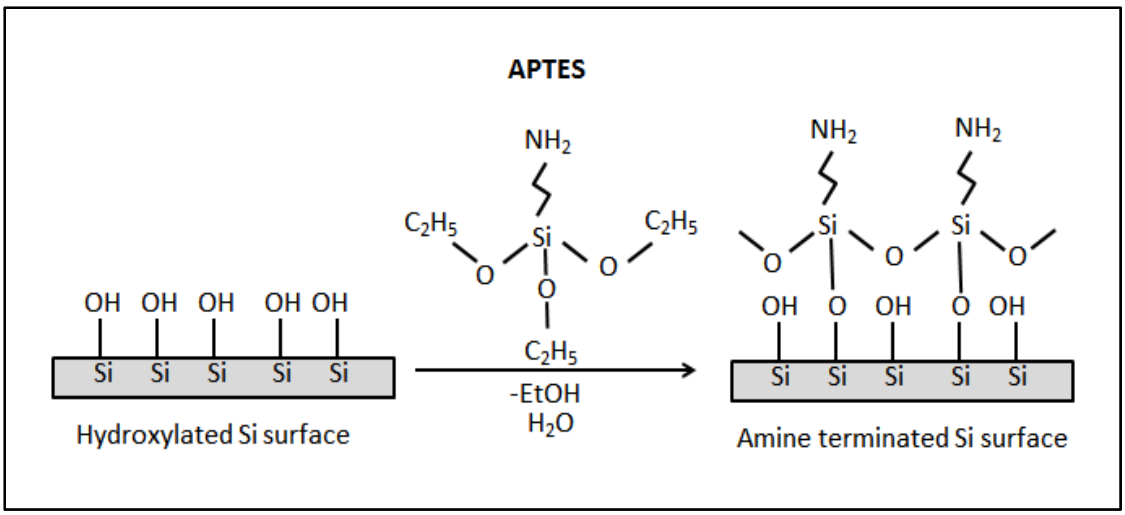

Figure 6-6: Schematic diagram of the surface functionalization of silicon surface by APTES treatment.

Microstructural imaging of the deposited films on 20% APTES treated silicon substrates was performed using a JEOL JSM 6610 scanning electron microscopy (SEM) with an acceleration voltage of 20-30 kV. As revealed in **Figure 6-7**, the deposited CNTs exhibit random, horizontal alignment on the silicon surface with remarkable homogeneity, surface coverage and packing density in the film quality. The deposition results, thus, establish electrophoretic deposition method as a fast, reproducible, room temperature based single-step processing technique in the deposition of horizontally oriented and porous carbon nanotube film on the target surfaces. The proposed deposition model, therefore, eliminates the need of mechanical pressing techniques in the fabrication of SERS substrates with horizontally aligned carbon nanotube coating.

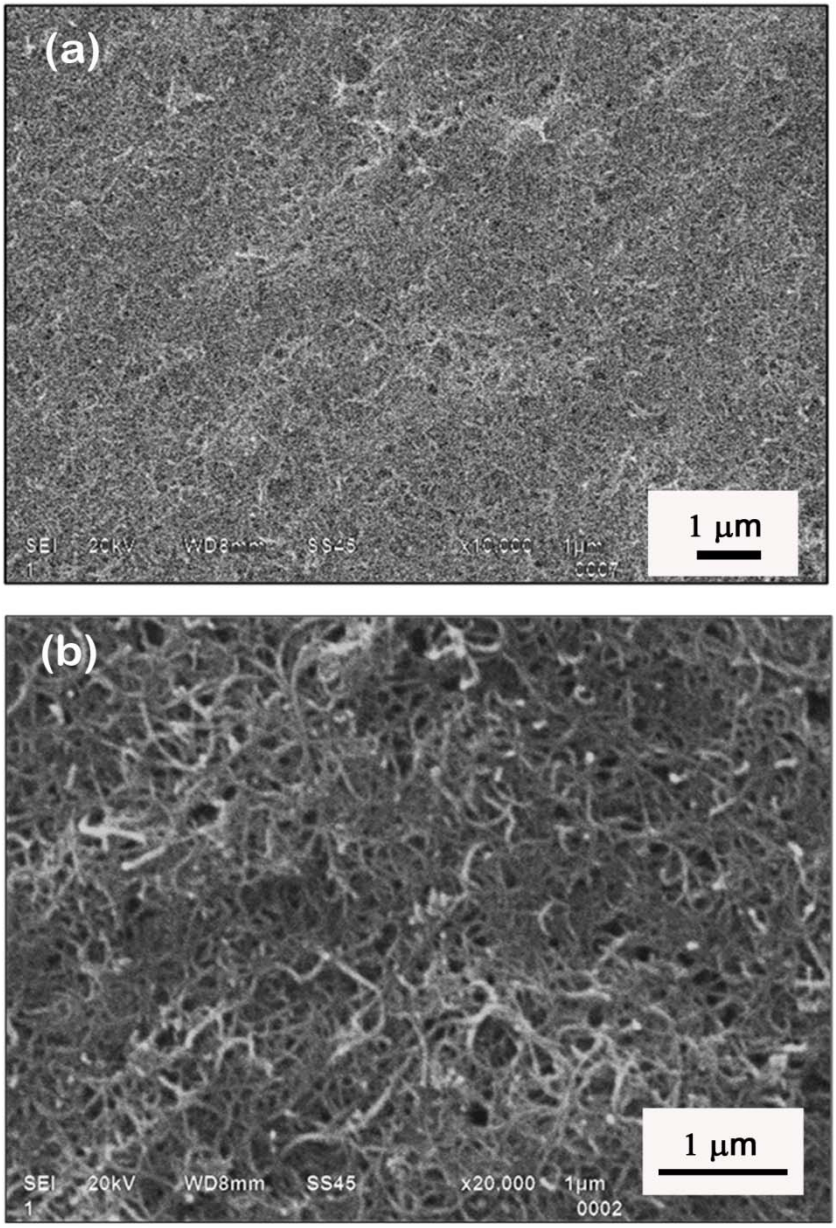

Figure 6-7: Scanning electron microscopic images of CNT film on 20% APTES treated silicon sample deposited at an applied electric field of 15V/cm for 3 mins showing appreciable surface coverage and packing density without voids (a) at ×10k magnification and (b) at ×20k magnification.

6.3.2: Silanization of the deposited CNT films

Different deposition methods e.g. spontaneous deposition, electrochemical deposition, substrate enhanced electrochemical deposition have been explored till date to immobilize metal nanoparticles on the carbon nanotube sidewalls[138–140]. The CNT sidewall silanization technique, based on the reaction of different organosilanes e.g. APTES with the CNT structure has been a popular method in this direction to improve interfacial adhesion between carbon nanotube sidewalls and nanoparticles. A schematic diagram of the CNT silanization process has been depicted in **Figure 6-8**. The acid-purification process introduces abundant hydroxyl groups (-OH) on the carbon nanotube surfaces. The hydrolysis of the ethoxy groups ($-C_2H_5$) in presence of water molecules results in the formation of APTES silanols (Si-OHs). The silanization process is eventually achieved by the dehydration reaction between the CNT hydroxyl groups and APTES silanols leading to the formation of $\sim NH_2$ terminated linker molecules on the CNT sidewalls[57,141]. As mentioned previously, the synthesized silver nanoparticles are capped by negatively charged citrate ions. Therefore, a Coulombic force of attraction exists between the positively charged amine ($\sim NH_2$) groups on the silanized CNT surfaces and negatively charged citrate ions which ensure appreciable immobilization of the silver nanoparticles on the CNT networks.

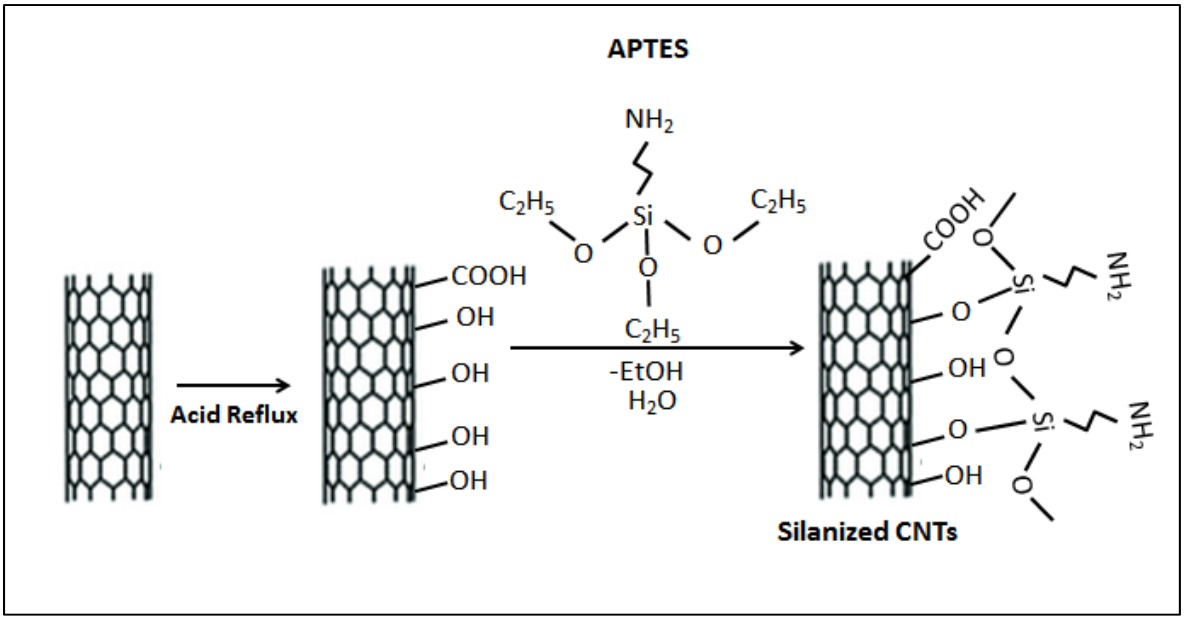

Figure 6-8: Schematic diagram of the surface functionalization of carbon nanotubes by APTES treatment.

6.3.3: Characterization of Ag-CNT-Si SERS substrate

The surface morphology of Ag-CNT nanostructures on the SERS substrates was examined by SEM with an acceleration voltage of 15 kV (**Figure 6-9**). The overall deposition attributes of AgNPs on the horizontally aligned carbon nanotube surfaces indicate discontinuity in surface coverage and stacked nature which are typical characteristic features of immersion coating technique. As can be noted from the figures, the porous nature of the carbon nanotube films serve as a template or "nest" for the attachment of the AgNPs in the form of ensemble of particles. The ensemble of particles or clusters should offer abundant sites for the adsorption of analyte molecules to be probed. It has been pointed out in publications to-date that the SERS effect by the local EM field could be significantly improved when the analyte molecules are localized at the junction of nanoparticle clusters with controlled aggregation[112,142,143]. Therefore, a substantial number of these nanoparticle clusters from these ensembles are also expected to behave as "hot spots" and contribute to the surface enhanced Raman scattering. The efficiency of

Ag-CNT hybrid nanostructures in enhancing the Raman signal of varying concentrations of R6G analyte has been assessed in the following section.

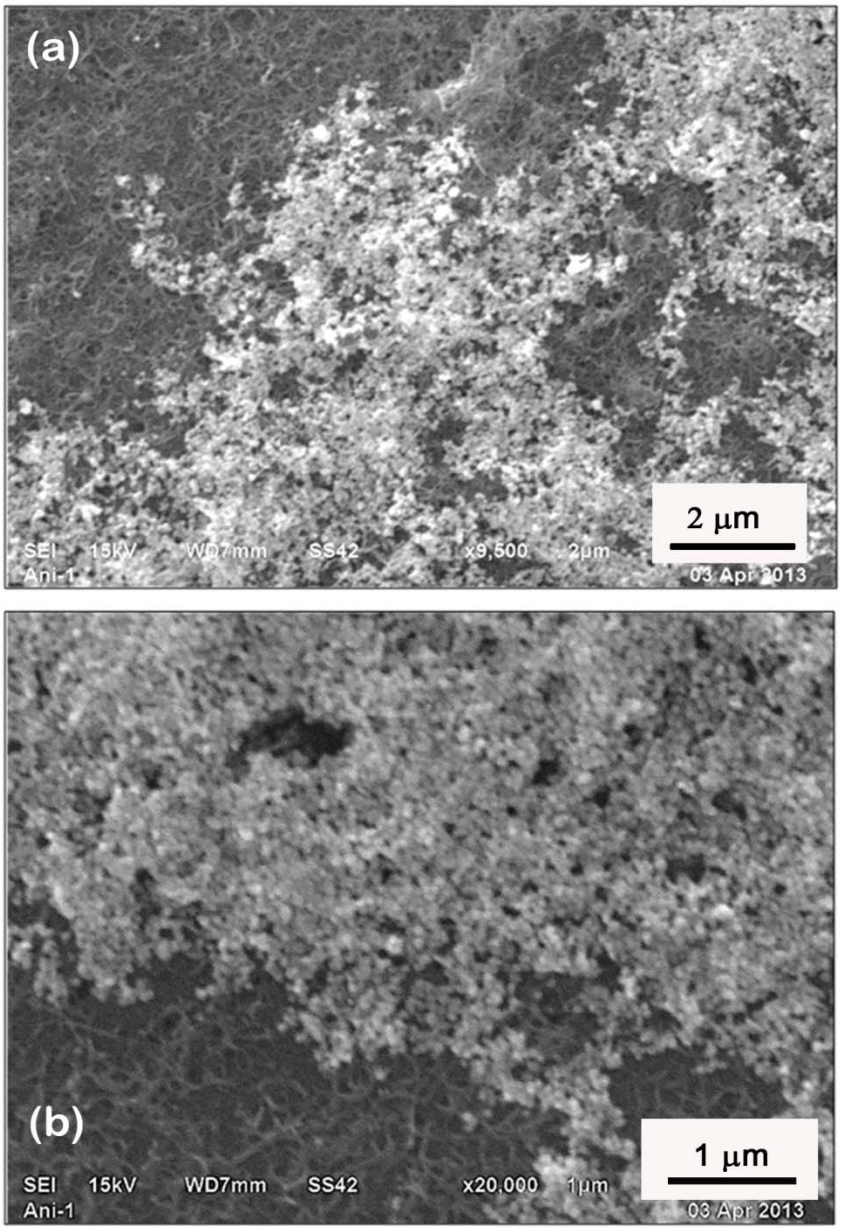

Figure 6-9: Scanning electron microscopic images of silver nanoparticles coated on silanized CNT film deposited on 20% APTES treated silicon sample (a) at ×10k magnification and (b) at ×20k magnification.

6.3.4: Raman spectroscopic results and estimation of SERS enhancement factor

Extensive Raman spectroscopic studies have been conducted using different concentrations of R6G - from 1×10^{-3} to 1×10^{-12} Moles (M) on 3 types of substrates: (a) Si substrates without AgNPs or CNTs (referred as non-SERS substrate) (b) APTES treated Si substrates with immersion coated AgNPs (referred as Ag-Si SERS substrates) and (c) immersion coated AgNPs on electrophoretically deposited CNTs on APTES treated Si substrates (referred as Ag-CNT-Si SERS substrates). The motivation in acquiring the Raman spectra on different substrates with varying analyte concentrations was to compare and assess the efficiency of the fabricated CNT-based SERS substrate in the enhancement of the signal intensity and to explore the detection limit.

The first set of experiments was conducted on non-SERS Si substrates with the R6G concentration of 1 mM. The detection limit was explored by further reducing R6G concentration to 100 μM and 1 μM. The spectrum shows strong peaks at ~ 607, 768, 1176, 1307, 1357, 1506, 1545, 1645 cm^{-1} as reported in Table **6-1**. The Raman peaks displaying the aromatic carbon-carbon stretching vibrational mode between 1300 and 1600 cm^{-1} have been referred to as the significant signature peaks of R6G. Therefore, these peaks have been considered predominantly for the discussion of SERS results in this section. As expected from conventional Raman spectroscopy, the signal intensity values of an analyte should vary with varying analyte concentrations and follow a decreasing trend when the concentration of the analyte is gradually reduced. As can be seen from the Figure **6-10**, the intensity value obtained for 1 mM concentration (2534 arb. units) is slightly higher than the one obtained for 100 μM concentration (2068 arb. units) at 1357 cm^{-1} wavenumber. Similarly, intensity values obtained for 1 μM R6G concentration were generally less than those acquired with 100 μM concentration.

Table 6-1: Assignment of the prominent peaks in Raman spectra of R6G.

Raman Shift (cm^{-1})	Assignment	Raman Shift (cm^{-1})	Assignment
607	C-C-C ring in-plane bending	1357	Aromatic C-C stretching
766	C-H out-of-plane bending	1505	Aromatic C-C stretching
1176	C-H in-plane bending	1564	Aromatic C-C stretching
1307	Aromatic C-C stretching	1645	Aromatic C-C stretching

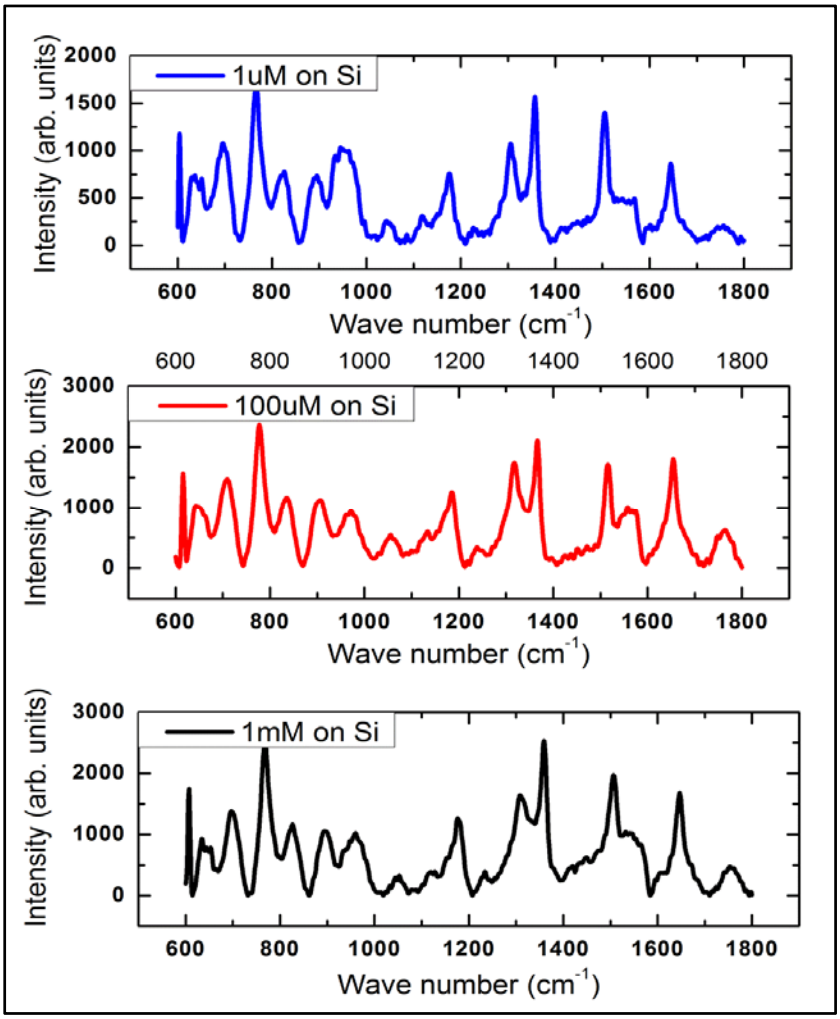

Figure 6-10: Raman spectra of 1 mM, 100 µM and 1 µM R6G concentration on silicon substrates.

Table 6-2 summarizes the intensity values of the Raman peaks obtained at 1307 cm^{-1}, 1357 cm^{-1} and 1506 cm^{-1} for 1 mM, 100 μM and 1 μM R6G concentrations. The acquired signal intensities from 1 mM to 1 μM R6G concentration were generally weak and attain maximum value of ~ 2500 arb. units only. As the R6G concentration was further reduced from 1 μM to lower concentrations (100 nM and 1 nM), the Raman signals became feeble and inconsistent which made it extremely difficult to obtain stable Raman spectra. Therefore, the detection limit with reasonable signal intensity on the non-SERS Si substrates was adjudicated to be 1 μM.

Table 6-2: Raman spectroscopy results on 1 mM, 100 μM and 1 μM R6G concentration on non-SERS Si substrates showing measured intensity values at 1307, 1358 and 1507 cm^{-1}. (Signal intensity is measured in arbitrary units).

R6G concentration on non-SERS Si substrates	**Intensity at 1307 cm^{-1}**	**Intensity at 1358 cm^{-1}**	**Intensity at 1507 cm^{-1}**
1 μM	1040	1558	1453
100 μM	1717	2068	1702
1 mM	1640	2534	1962

The second set of experiments was performed to explore the surface enhanced Raman phenomenon on Ag-Si SERS substrates with the initial R6G concentration of 1 μM. As can be noted in Figure **6-11**, the acquired Raman spectra displayed augmented Raman signals and significant enhancement for all the signature peaks for 1 μM R6G concentration. For example, the intensity value of the Raman peak at 1358 cm^{-1} on Ag-Si SERS substrate has increased by a factor of 11.9 compared to the non-SERS Si substrate. The R6G concentration was then gradually reduced from 1 μM to lower values - i.e. 100 nM and 1 nM to investigate the detection

limit. As can be seen in Figure **6-11**, the acquired spectra for both 100 nM and 1 nM R6G concentration showed prominent and distinct Raman signals for all the signature peaks. The results conclusively indicate the contribution of the AgNPs in augmenting the signal intensity on Ag-Si SERS substrates in comparison to the non-SERS Si substrates. Consistent with our previous observation, the signal intensity displayed a decreasing trend as the concentration of the R6G was reduced. The Raman signals beyond 1 nM were not strong enough to obtain a clear spectrum which thus establishes the detection limit to be 1 nM on Ag-Si SERS substrates.

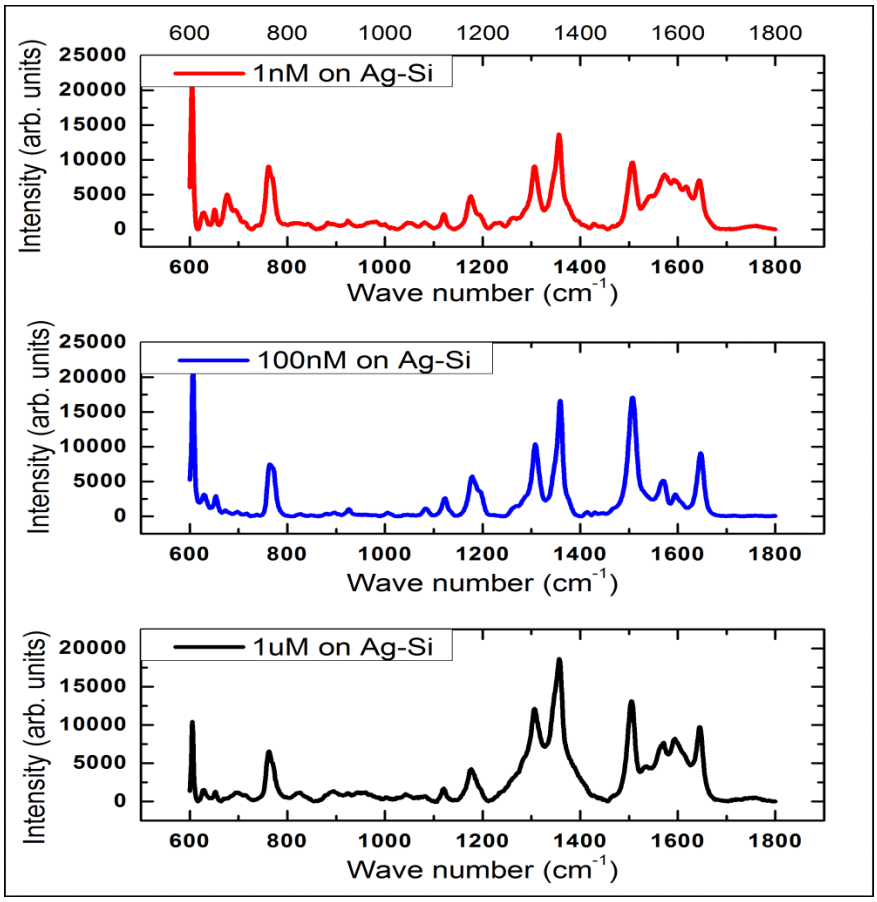

Figure 6-11: Surface enhanced Raman spectra of 1 μM, 100 nM and 1 nM R6G concentration on Ag-Si substrates

Table **6-3** summarizes the intensity values observed at 1305 cm^{-1}, 1358 cm^{-1} and 1507 cm^{-1} in the Raman spectra.

Table 6-3: Surface enhanced Raman spectroscopy (SERS) results on 1 μM, 100 nM and 1 nM R6G concentration on Ag-Si substrates showing measured intensity values at 1305, 1358 and 1505 cm^{-1}. (Signal intensity is measured in arbitrary units).

R6G concentration on Ag- Si SERS substrates	**Intensity at 1305 cm^{-1}**	**Intensity at 1358 cm^{-1}**	**Intensity at 1505 cm^{-1}**
1 nM	8947	13673	9547
100 nM	10264	16255	17060
1 μM	11980	18434	12870

The adeptness of Ag-CNT-Si substrate as a potential SERS substrate was initially adjudicated by probing R6G concentration of 1 μM. The acquired spectra exhibited all the vibrational peaks of R6G with augmented signal intensity. The analyte concentration was then gradually reduced to 100 nM and 1 nM. As illustrated in **Figure 6-12**, the Raman signals exhibited prominent SERS effect for all the peaks with the maximum signal intensity reaching 29587 and 19200 arb. units for 100 nM and 1 nM R6G concentration respectively at 1358 cm^{-1}. The intensity values obtained for different R6G concentration at 1307, 1358 and 1507 cm^{-1} are summarized in **Table 6-4**. The intensity values, when compared with the results on Ag-Si SERS substrate, shows appreciable enhancement in the signal intensity. For example, the signal intensity measured on Ag-CNT-Si substrate is approximately 1.8 times more than the Ag-Si SERS substrates at 1307, 1358 and 1507 cm^{-1} for 100 nM R6G concentration. **Table 6-5** illustrates the comparison results. This improved performance is attributed to the enlarged

specific area for the absorption of analyte molecules offered by the combination of CNT porous network and the ensemble of silver nanoparticles. The limit of detection was studied next by reducing the R6G concentration to 1 pM. **Figure 6-12** depicts the Raman spectroscopic results for 1 pM R6G concentration between 600 and 1800 cm^{-1}. The spectrum shows prominent vibrational peaks of R6G at 1307, 1358 and 1507 cm^{-1}. The intensity values in arb. units of 1 pM concentration are summarized in Table **6-4**. As can be expected, the magnitude of the signal intensity at 1 pM concentration was less compared to 1 nM and 100 nM analyte concentration.

The experimental results, therefore, confirm the effectiveness of AgNPs decorated porous carbon nanotube substrate as an improved SERS substrate. As has been pointed out, the improvement in analyte detection and analysis can be attributed to enhancement of the Raman intensity values of R6G peaks by a factor of 1.8 and superior detection limit of 1 pM analyte concentration. The comparative Raman spectra of 1 μM R6G concentration on all three substrates (**Figure 6-13**) and 1 nM R6G concentration on Ag-Si and Ag-CNT-Si SERS substrates (**Figure 6-14**) also confirm the claim.

The quality of a SERS substrate in spectroscopic examination of an analyte is quantitatively adjudicated by a technology parameter known as enhancement factor (E.F.). Development of ultra-sensitive and optimized substrates with high E.F (of the order of $\sim 10^8$ - 10^{11}) remains an active area of SERS research. The following section represents a comprehensive discussion of the general definition and calculation of E.F. of the AgNP-CNT based SERS substrate presented in this research.

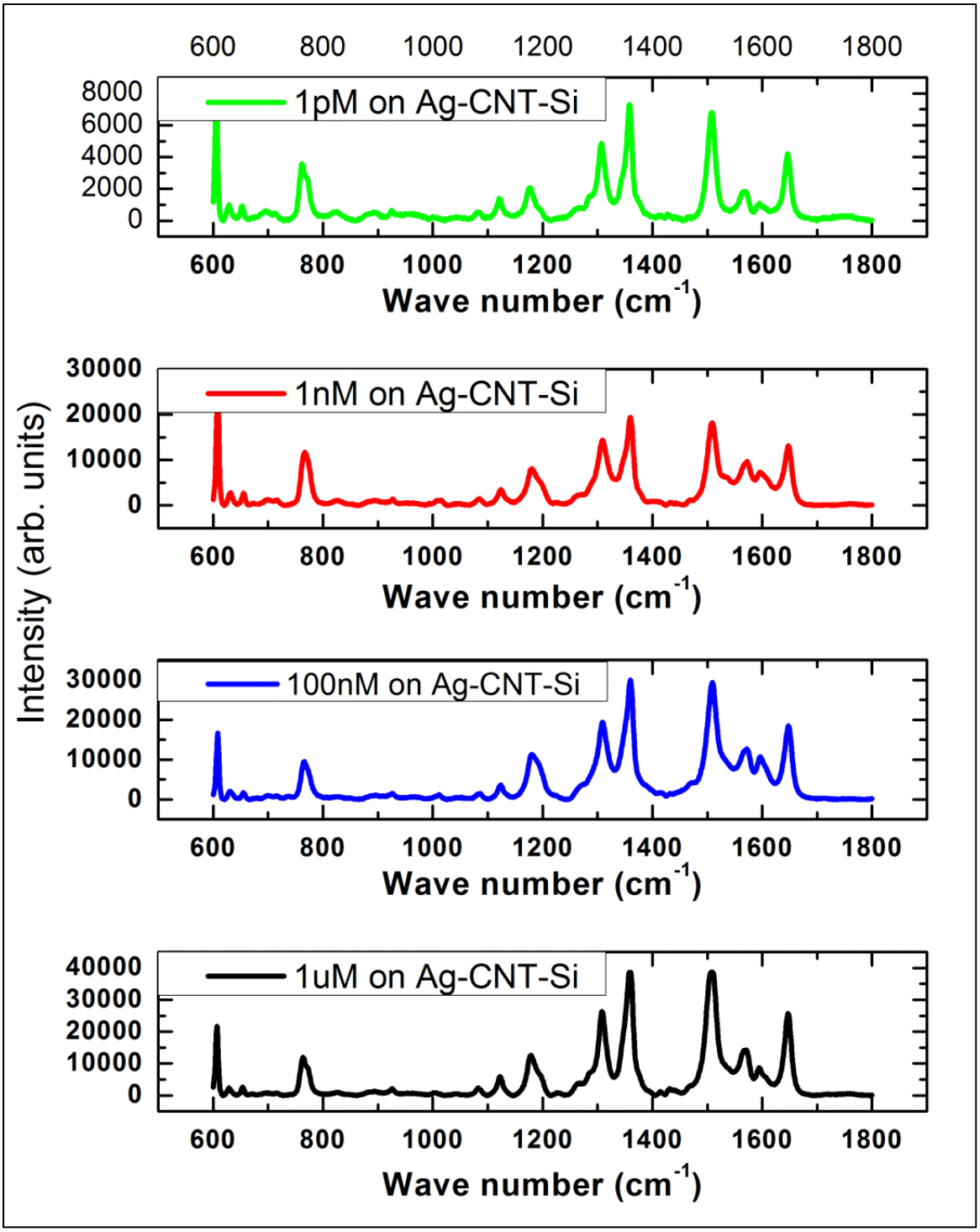

Figure 6-12: Surface enhanced Raman spectra of 1 pM, 1 nM, 100 nM and 1 μM R6G concentration on Ag-CNT-Si substrates.

Table 6-4: Surface enhanced Raman spectroscopy (SERS) results on 1 μM, 100 nM, 1 nM and 1 pM R6G concentration on Ag-CNT-Si substrates showing measured intensity values at 1307, 1358 and 1507 cm^{-1}. (Signal intensity is measured in arbitrary units).

R6G concentration on Ag-CNT- Si SERS substrates	**Intensity at 1307 cm^{-1}**	**Intensity at 1358 cm^{-1}**	**Intensity at 1507 cm^{-1}**
1 pM	4645	7069	6715
1 nM	14200	19200	18033
100 nM	19086	29587	29195
1 μM	26058	38309	38333

Table 6-5: Comparison of surface enhanced Raman spectroscopy (SERS) results on Ag-Si and Ag-CNT-Si substrates with 1 μM, 100 nM and 1 nM R6G concentration at 1307, 1358 and 1507 cm^{-1}. (Signal intensity is measured in arbitrary units and E.F. = Enhancement factor).

	Intensity at 1307 cm^{-1}			**Intensity at 1358 cm^{-1}**			**Intensity at 1507 cm^{-1}**		
R6G conc.	**Ag-Si**	**Ag-CNT-Si**	**E.F.**	**Ag-Si**	**Ag-CNT-Si**	**E.F.**	**Ag-Si**	**Ag-CNT-Si**	**E.F.**
1 μM	11980	26058	**2.17**	18400	38309	**2.08**	12870	38333	**2.97**
100 nM	10264	19086	**1.85**	16255	29587	**1.82**	17060	29195	**1.71**
1 nM	8947	14200	**1.58**	13673	19200	**1.45**	9547	18033	**1.88**

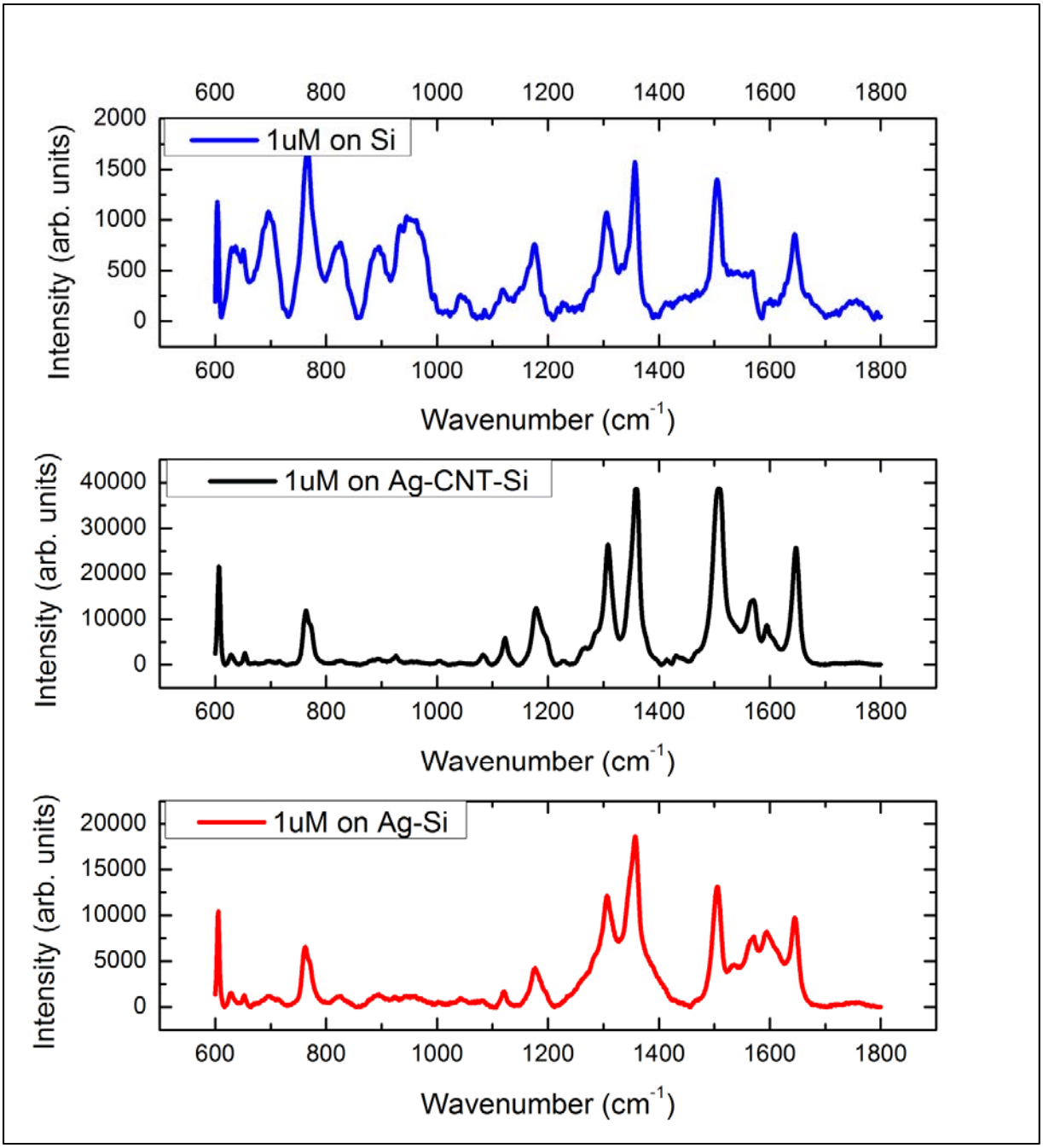

Figure 6-13: Comparison of Raman spectra for 1 μM R6G concentration on silicon, Ag-Si SERS and Ag-CNT-Si SERS substrates.

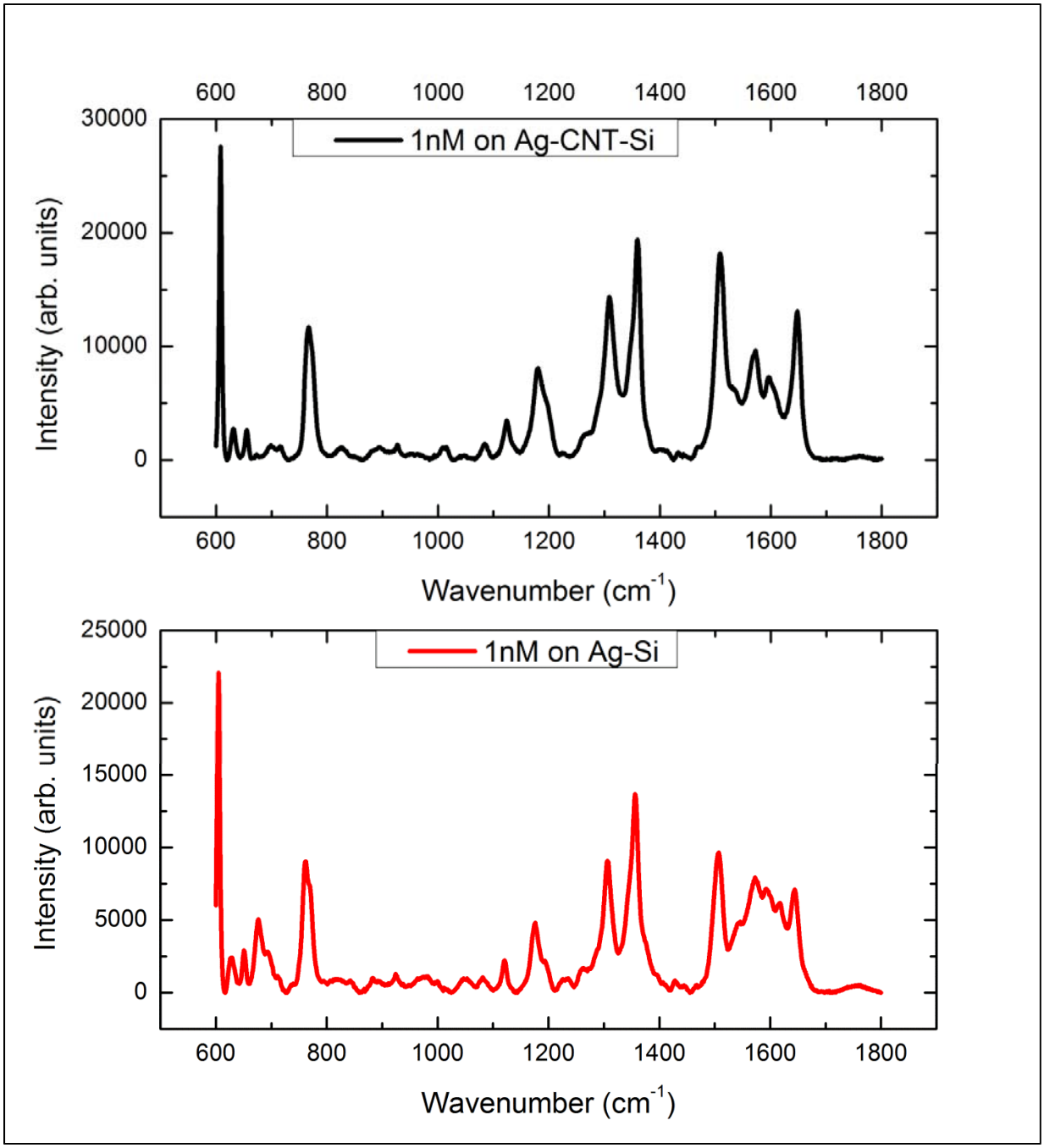

Figure 6-14: Comparison of Raman spectra for 1 nM R6G concentration on Ag-Si SERS and Ag-CNT-Si SERS substrates.

6.3.5: Estimation of the overall enhancement factor (E.F.)

Determination of the overall enhancement factor (E.F.) in SERS applications has been an issue of disagreement in SERS research; various definitions of E.F. and theoretical assumptions have been proposed in calculations which reflect differences in concept and experimental procedure. While the concept of enhancement factor is generally defined as the SERS intensity divided by the intensity from a non-SERS reference sample, additional factors such as concentration of the analyte, probe volume, penetration depth, the diameter of the laser spot are often included in the calculation.

As a result of its debatable definition, the EF value in our research has been estimated using two different approaches[144].

The 1st approach is shown below:

$$E.F. = \frac{I_{SERS}}{I_{Reference}} \times \left(\frac{V_{Reference}}{V_{SERS}} \times \frac{C_{Reference}}{C_{SERS}}\right) \quad (1)$$

where V_{SERS} and $V_{Reference}$ are the probe volumes in μm^3 for the SERS and reference (or, traditional Raman) measurements respectively, C_{SERS} and $C_{Reference}$ are the R6G concentrations in moles which contribute to SERS intensity (I_{SERS}) and traditional Raman intensity ($I_{Reference}$) values. The ratio of the probe volume has been calculated considering probe depth of approximately 1 μm for the reference sample in conventional Raman spectroscopy and generation of the SERS signal from within 10 nm from the SERS surface. The analyte concentration has also been assumed to remain constant within the detection volume which accounts for a fixed number of molecules - i.e. Avogadro's number of molecules (6.023×10^{23}) × the analyte concentration. The diameter of the laser spot has been kept at approximately 20 μm for all the experiments. The Raman spectra of 1 mM R6G concentration on non-SERS Si substrates and 1 pM R6G concentration on Ag-CNT-Si substrate scanned between 600 and 1800

cm^{-1} have been considered as the reference and the SERS sample respectively for our E.F calculation. **Figure 6-15** represents the Raman spectra used for the E.F. calculations. The E.F. at 1358 cm^{-1} has been calculated as follows:

$$E.F. = \frac{7069}{2534} \times \frac{\pi.(10\mu m)^2.1\mu m}{\pi.(10\mu m)^2.10nm} \times \frac{10^{-3}\mathrm{M}}{10^{-12}\mathrm{M}} \times \frac{6.023 \times 10^{23}}{6.023 \times 10^{23}}$$

$$= 2.78 \times 10^{11}$$

The first term above (7069/2534) consists of the ratio of the measured intensity (in arbitrary units) of the Raman peak at 1358 cm^{-1} on the SERS sample (I_{SERS}) for 1 pM R6G as reported in Table **6-4** versus traditional Raman intensity ($I_{Reference}$) for 1 mM R6G as shown as in Table **6-2**. The second term calculates the ratio of probe volumes - i.e. π × area of the laser spot (radius: 10 μm) × probe depth, while the third term ($10^{-3}/10^{-12}$) represents the ratio of concentrations of R6G studied on the reference (1 mM) and SERS sample (1 pM), respectively. Finally, both numerator and denominator terms are multiplied by Avogadro's number as shown to account for the assumed fixed number of molecules in the molar concentrations of the analyte as previously discussed.

The 2nd approach is showed below:

$$\mathrm{E.F.} = \frac{I_{SERS}}{I_{Reference}} \times \frac{C_{Reference}}{C_{SERS}} \quad \text{.....} \quad (2)$$

which assumes linear dependence of intensity values on the concentration and does not consider the complicated assumptions involved with the probe depths.

Using the same parameters defined as above, the E.F has been calculated as follows:

$$E.F. = \frac{7069}{2534} \times \frac{10^{-3}\mathrm{M}}{10^{-12}\mathrm{M}}$$

$$= 2.78 \times 10^{9}$$

The assumptions based on the probe depths of 1 μm for the reference signal and 10 nm for the SERS signal, along with the fixed analyte concentration values at these depths (as indicated in equation (1)) present uncertainties in the calculated value of the E.F.. For instance, the adsorption of the R6G molecules on the Ag-decorated CNT network can display a concentration gradient in the detection volume, as a function of distance within the vertical profile of the SERS surface, which would affect the E.F. value in equation (1).

In our experiment, the immersion coated AgNPs within the EPD-fabricated CNT network show discontinuity in surface coverage which reduces the number of R6G molecules contributing to the SERS process. The molecules which remain adhered to the CNT network directly without AgNPs do not exhibit the SERS effect while the ones attached to the AgNP-CNT network demonstrate enhanced Raman signals. It is also worth mentioning that the effective Raman signals are expected to generate from specific "hot spots" which are located at the interstitial sites between the nanoparticles[145,146]. Therefore, the value of $6.023\times10^{23}\times10^{-12} = 6.023\times10^{11}$ as the maximum number of R6G molecules participating in the SERS process within the probe depth in equation (1) is most likely an overestimate which leads to an underestimated value of E.F. calculated in the present case.

The simplest definition of E.F. can be perceived based on its relevance in studying the limit of detection of a given analyte on a SERS substrate. Therefore, a more practical definition of E.F. can be represented as the ratio of I_{SERS} and $I_{Reference}$ with a linear dependence of intensity on the concentration as in equation (2). It has been reported that such an interpretation of E.F. is more practically feasible in routine SERS experiments even though it results in a smaller value of E.F.[50].

The efficiency of Ag-CNT-Si substrate as viable SERS substrates in comparison to Ag-Si SERS substrates has also been presented with reference to 1 mM R6G concentration on non-SERS Si substrates using equation (2). As has been pointed out, the detection limit for Ag-Si SERS substrate was measured to be 1 nM with reasonable signal intensity. The E.F factor at 1358 cm^{-1} can be now calculated as:

$$E.F. = \frac{13673}{2534} \times \frac{10^{-3}\mathrm{M}}{10^{-9}\mathrm{M}}$$

$$= 5.3 \times 10^{6}$$

The first term in the equation above (13673/2534) represents the ratio of the measured intensity (in arbitrary units) of the Raman peak at 1358 cm^{-1} on the Ag-Si SERS sample (I_{SERS}) for 1 nM R6G as can be noted in Table **6-3** versus traditional Raman intensity ($I_{Reference}$) for 1 mM R6G as shown as in Table **6-2**. The second term ($10^{-3}/10^{-12}$) calculates the ratio of concentrations of R6G studied on the reference (1 mM) and Ag-Si SERS sample (1 nM), respectively.

The overall E.F. as offered by Ag-CNT-Si substrate is about 3 orders of magnitude more as compared to Ag-Si substrates with superior limit of detection - i.e. 1 pM as compared to 1 nM. Considering the debatable parameters concerning E.F., direct comparison of E.F. value with other SERS substrates reported in the literature to-date becomes a complicated issue. The fundamental intent behind this work was to increase the number of effective metal nanoparticle "hot spots" nested in the porous networks of the deposited CNTs in contributing to the surface enhanced phenomenon. The augmented signal intensity of the acquired Raman spectra in presence of the Ag-CNT architecture with respect to the reference sample justifies our research endeavors.

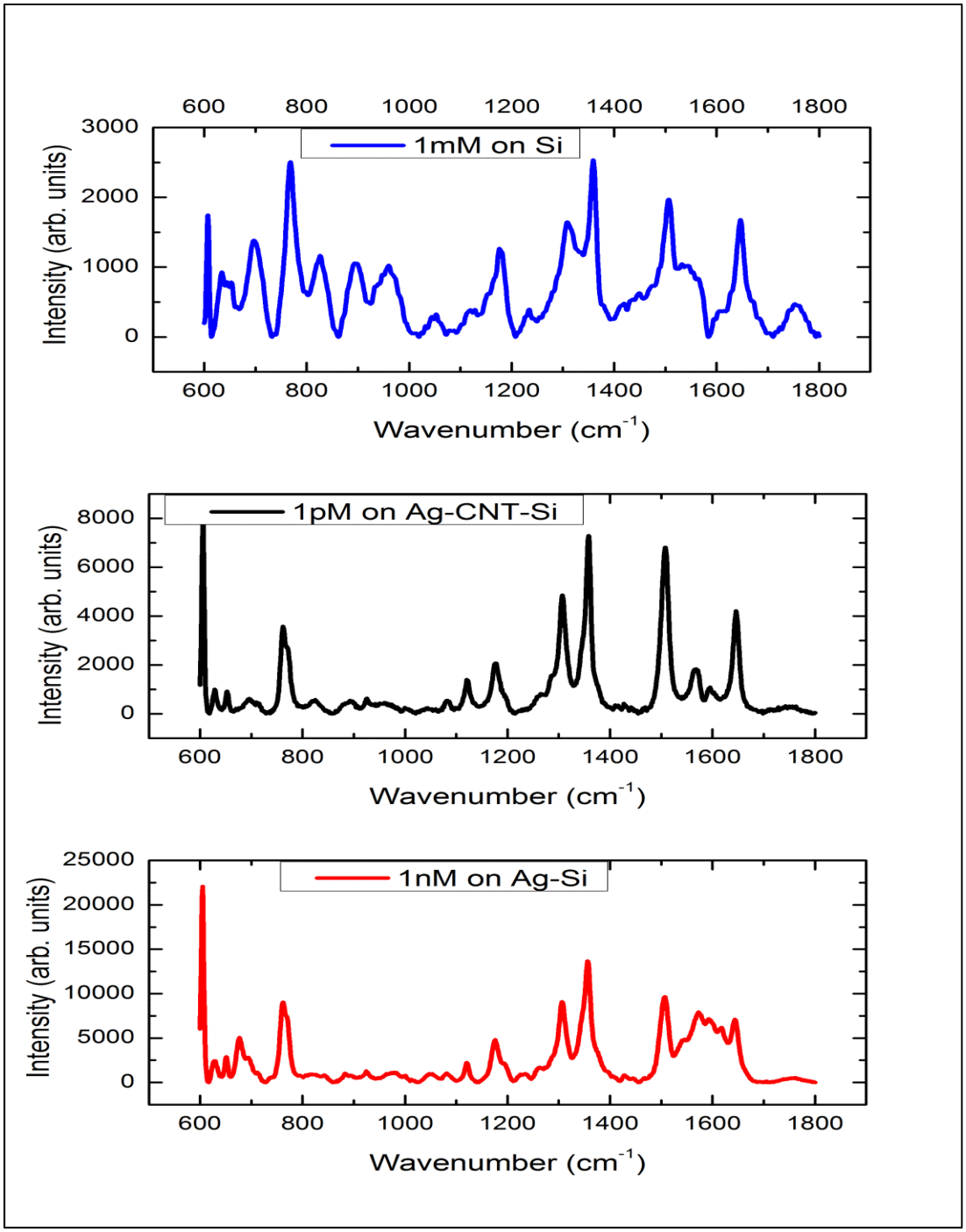

Figure 6-15: Surface enhanced Raman spectra of 1×10^{-12} M R6G concentration on Ag-CNT-Si substrate and 1×10^{-9} M R6G concentration on Ag-Si substrate with respect to reference Raman spectra of 1×10^{-3} M R6G concentration on non-SERS Si substrates. The calculated E.F at 1358 cm^{-1} is 2.78×10^{9} and 5.6×10^{6} respectively.

6.4: Conclusion

In this chapter, fabrication of efficient silver nanoparticles (AgNPs) decorated multi-walled carbon nanotube (MWCNT) based SERS substrates (Ag-CNT-Si) has been reported. The deposition of carbon nanotubes on organosilane (APTES) has been accomplished by the technique of electrophoretic deposition (EPD). EPD presents a facile, cost effective, reproducible, and single-step coating strategy to obtain uniform deposits of horizontally aligned CNT networks on organosilane (APTES) functionalized silicon surfaces. Deposition of AgNPs (average diameter: 30-40 nm) in the form of nano-clusters or ensemble of particles on the silane treated CNT networks has been achieved by immersion coating. The presence of Ag-MWCNT hybrid nanostructures showed enhancement in the Raman intensity of R6G analyte by 9 orders of magnitude with respect to the reference sample (E.F = $\sim 10^9$) and stretched the detection limit to as low as 1×10^{-12} M (or, 1 pM). The Raman spectra of R6G on the Ag-MWCNT nanostructures have been compared with the results obtained on AgNP- planar silicon substrates to corroborate the efficiency of the AgNP decorated porous CNT film in increasing the effective "hot spots" for the enhancement of the Raman signals.

Some of the pressing challenges in this kind of SERS research involve uniform deposition of nanoparticles on the target surfaces, uncertainty in the nature of adsorption of analyte molecules, and the assumptions and practical complications in estimating the enhancement factor (E.F.). There is definitely room for improvement in the deposition attributes of AgNPs on CNT coatings. Electrophoretic deposition of AgNPs can be regarded as a viable option which might be more effective in impregnating the CNT networks. The uncertain nature of adsorption of R6G leads to measurement complications since results would vary depending on their interactions with the metal nano-clusters, individual nanoparticles or the underlying substrate material. A universal consensus in defining and understanding E.F. of the study of

SERS would lead to innovations in the fabrication and performance comparisons of different SERS substrates in future. Our fabrication strategy and analysis bode well with state-of-the-art research in SERS and unveils the potential of this spectroscopic technique in numerous sensor and detection applications.

CHAPTER 7: SUMMARY AND RECOMMENDATION FOR FUTURE WORK

7.1: Summary of results in the pursued research

The growing research interest in the incorporation of carbon nanotubes (CNTs) in present state-of-the-art electronics such as thin film transistors (TFT) technology, field emission devices and nanoporous electrodes for energy applications has triggered widespread CNT thin film research. In recent years, electrophoretic deposition (EPD) has been pursued as an economical and versatile room temperature solution based coating technique for the production of thin and thick films of CNTs on predominantly conductive substrates. The EPD process involves migration of charged particles dispersed in a fluid medium towards an intended electrode (or, the deposition surface) under the application of a direct current (DC) electric field and eventual coagulation as a uniform coating on the electrode. With the prevailing interest in the application of CNTs in IC technology and nanoelectronics, it is extremely interesting to investigate EPD of CNTs on different semiconductor substrates like silicon (Si). To this extent, this dissertation research is predominantly focused on the feasibility and investigation of EPD of CNTs on silicon substrates with and without adequate surface functionalization. The experimental results obtained in this research with regard to the deposition model, conditions and the controlling parameters are summarized below:

i. EPD of CNTs on Si substrates without surface treatment
    a. EPD has been successfully performed from stable, acid-refluxed CNT-dispersed aqueous suspension on metal-patterned (aluminum) silicon substrates with and without insulator layers (SiO_2 and Si_3N_4) in between.
    b. No surface functionalization or treatment was performed on the silicon substrates used in the deposition experiments.

c. The nanotubes exhibited preferential deposition and adhesion exclusively on the metallic surfaces irrespective of the insulator layers underneath, electrical connection to the anode surface and low resistivity of the Si substrates for applied electric field of 2.5-15 V/cm for 0.5-3 minutes.

d. Insufficient deposition and poor adhesion results of the CNT films on bare and piranha treated/acid etched silicon substrates were observed throughout the EPD experiments.

e. Hydrophilic interaction between the metallic surfaces and the oxidized, acid treated nanotubes is assumed to play a crucial factor in the adhesion and eventual formation of CNT thin films.

f. The effects of varying electric field and deposition time on the thickness and surface roughness of the CNT films were studied.

g. Interesting results on the degradation of the CNT solution after the unsuccessful EPD attempts on bare silicon substrates indicate the challenge of reusability and preserving the dispersion desired during the duration of deposition.

ii. Electrophoretic deposition of carbon nanotubes on silicon substrates with organosilane surface treatment

a. Deposition of uniform thin coatings of CNTs carbon nanotubes by EPD has been demonstrated on silicon substrates with 3-aminopropyl-triethoxysilane (APTES) surface functionalization.

b. The gradual coagulation and eventual CNT film formation is profoundly assisted by the Coulombic force of attraction existing between the positively charged $-NH_2$

surface groups of the organosilane molecules and the acid treated, negatively charged nanotubes migrating towards the deposition surfaces.

c. The benefits of EPD technique as a fast, reliable and reproducible room temperature coating process over dip coating have also been demonstrated extensively throughout this study.

d. The effect of varying APTES concentration (5%-100%) on the Raman spectroscopy and thickness of the deposited CNT film has been discussed in details as well.

e. The organosilane assisted EPD approach has eliminated the need of physical vapor deposition of metals on bare silicon substrates and therefore, ensures an economical, fast and entirely solution based room temperature fabrication strategy of CNT thin films for a wide range of next generation electronic applications.

iii. Fabrication of surface enhanced Raman spectroscopy (SERS) substrate based on EPD-fabricated porous CNT networks

a. In this study, fabrication of silver nanoparticles (AgNPs) coated carbon nanotube based porous SERS substrates (referred to as Ag-CNT-Si) has been pursued.

b. Deposition of CNTs on organosilane (APTES) functionalized silicon surfaces at an applied E-field of 15 V/cm for 3 minutes has been accomplished by EPD, as has been discussed in the previous chapter.

c. EPD establishes a facile, cost effective, reproducible and single-step coating strategy to obtain uniform deposits of horizontally aligned porous CNT networks.

d. Deposition of surfactant stabilized AgNPs (average diameter: 30-40 nm) in the form of nano-clusters or ensemble of particles on the silane treated CNT networks has been achieved by immersion coating.

e. The fabrication of Ag-MWCNT hybrid nanostructures displayed enhancement in the Raman intensity of Rhodamine6G (R6G) analyte by ~9 orders of magnitude with respect to the reference sample (E.F = ~10^9) and pushed the detection limit to as low as 1×10^{-12} M or 1 pM.

f. The Raman spectra on the fabricated SERS substrate have been compared with the results obtained on AgNP planar silicon substrates to corroborate the efficiency of the AgNP decorated, horizontally aligned porous CNT films in increasing the effective "hot spots" which contribute to the surface enhancement of the Raman signals.

g. The need for a universal consensus in defining and understanding the concept of Enhancement Factor (E.F.) in SERS research for performance comparison of various innovative SERS substrates has been discussed also.

7.2: Recommendation for future work

7.2.1: Dispersion and electrophoretic deposition of CNTs from ionic liquids

Owing to their chemical inertness, the pristine, as-grown CNTs exhibit a hydrophobic nature and remain as agglomerated skeins which limit their dispersibility in different suspension media. Over the past decade, a variety of non-covalent and covalent surface functionalization strategies have been pursued to improve the degree of dispersion in different solvents. Some of the methods include use of polymer based surfactants to prevent aggregation of the nanomaterials, acid refluxing in strong acid solution or use of volatile, polar solvents as the dispersion media. In recent years, room temperature based ionic liquids (RTILs) have emerged as "green" and better alternatives for the dispersion of CNTs by virtue of their low flammability and volatility, high thermal stability and ionic conductivity, and a broad window of electrochemical stability. Both experimental and simulated results have revealed that ILs interact with the CNTs through strong Van der Waals interaction to form novel CNT-IL hybrid

nanostructures[147,148]. The prospect of dispersion of CNTs in IL-based solvents, the stability performance under moderate to strong electric field and the eventual EPD of IL stabilized carbon nanotube on different substrates can offer an entirely new perspective in thin film coating technique and therefore, should be explored in greater detail.

7.2.2: EPD from aqueous suspension under modulated electric field

The advantages of EPD from aqueous suspension can be realized given its environmental compatibility when compared with the cost, volatility, toxicity and flammability of organic solvent based EPD. As has been pointed out in the previous chapters, the pressing issue in aqueous suspension based EPD is the electrolysis of water at low electric field. The evolution of gas bubbles due to the reduction and oxidation of water frequently leads to coatings of inferior quality. In recent years, there has been active research in the use of modulated electric field, - i.e. pulsed direct current (PDC) and alternating current (AC) in the electrophoretic deposition of nanomaterials[149]. PDC has been shown to produce smooth and uniform coatings by reducing the coalescence between the gas bubbles and minimizing aggregation between the nanoparticles by eliminating the effect of electrosomotic flow in the electrophoretic process. A similar deposition strategy under modulating electric field can be pursued in the EPD of CNTs from aqueous suspension by judicious selection of the on-off cycles of the electric pulses during the deposition duration.

7.2.3: EPD of CNTs on insulator surfaces for plastic electronics

Semiconducting CNT networks deposited through various room temperature based facile coating techniques have been extensively explored as an alternative active layer for thin film transistors (TFTs) on plastic substrates. Towards this research direction, the next primary aim should be to deposit uniform CNT coatings on different insulator substrates such as poly-ethylene terephthalate (PET) polyimide and gate dielectrics - i.e. silicon oxide, hafnium oxide,

aluminum oxide by EPD. Contrary to the common assumption that EPD is only limited to conductive substrates, there have been recent research findings outlining the deposition of novel nanomaterials on porous non-conducting alumina and NiO-YSZ substrates[19,101]. Therefore, the research initiatives to study the feasibility of deposition of CNT networks by EPD on different insulator substrates and detailed investigation of the deposition kinetics should be given pertinent attention.

7.2.4: EPD of silver nanoparticles for better surface coverage and uniform coating

The surface coverage of the immersion coated silver nanoparticles (AgNPs) on the EPD fabricated CNT networks (as depicted in Fig. 9 of Chapter 4) should be improved substantially with respect to the study of SERS. One of the viable options that should be explored in this direction is electrophoretic deposition of AgNPs (or, noble nanoparticles e.g. Au, Pt in general contributing to SERS effect) from suitable suspensions. The deposition strategy should result in uniform and homogenous deposits of nanoparticles on the target surface, which in turn is expected to ensure better penetration of the nanoparticles within the porous CNT network. The number of effective "hot spots" within the porous substrate contributing to the enhanced Raman signals could be thus increased significantly which, would eventually render improved detection sensitivity of different analytes.

7.2.5: SERS study on liquid analyte for bio-medical application

Chapter 4 of this dissertation has focused on the SERS analysis of drop-casted or immersion coated and air-dried R6G analyte with different concentration (from 1 mM to 1 pM). The fabricated SERS substrate should be applied to perform routine SERS experiments on different analytes dissolved or dispersed in a fluid medium as well. A potential application in this context is the implementation of endoscopic SERS for in-situ molecular imaging of human tissue for medical diagnosis and treatment.

REFERENCES

1. Iijima, S. Helical microtubules of graphitic carbon. *Nature* **354,** 56–58 (1991).

2. Iijima, S. & Ichihashi, T. Single-shell carbon nanotubes of 1-nm diameter. *Nature* **363,** 603–605 (1993).

3. Torres, T. *Carbon Nanotubes and Related Structures: Synthesis, Characterization, Functionalization, and Applications*. (2010).

4. Rümmeli, M. H., Ayala, P. & Pichler, T. in *Carbon Nanotubes and Related Structures* (Guldi, D. M. & Nazariortín) 1–21 (Wiley-VCH Verlag GmbH & Co. KGaA, 2010). at <http://onlinelibrary.wiley.com/doi/10.1002/9783527629930.ch1/summary> .

5. Hornyak, G. L. *Introduction to nanoscience*. (CRC Press, 2008).

6. Baker, R. T. K., Barber, M. A., Harris, P. S., Feates, F. S. & Waite, R. J. Nucleation and growth of carbon deposits from the nickel catalyzed decomposition of acetylene. *Journal of Catalysis* **26,** 51–62 (1972).

7. Sinnott, S. B. *et al.* Model of carbon nanotube growth through chemical vapor deposition. *Chemical Physics Letters* **315,** 25–30 (1999).

8. Dai H. *et al.* Single-wall nanotubes produced by metal-catalyzed disproportionation of carbon monoxide. *Chemical Physics Letters* **260,** 471–475 (1996).

9. Prasek Jan, D. J. Methods for carbon nanotubes synthesis—review. *Journal of Materials Chemistry* **21,** 15872–15884 (2011).

10. Grobert, N. Carbon nanotubes – becoming clean. *Materials Today* **10,** 28–35 (2007).

11. Szabó, A. *et al.* Synthesis Methods of Carbon Nanotubes and Related Materials. *Materials* **3,** 3092–3140 (2010).

12. Ebbesen, T. W. & Ajayan, P. M. Large-scale synthesis of carbon nanotubes. *, Published online: 16 July 1992; | doi:10.1038/358220a0* **358,** 220–222 (1992).

13. T. Guo, P. N. Catalytic growth of single-walled manotubes by laser vaporization. *Chemical Physics Letters* 49–54 doi:10.1016/0009-2614(95)00825-O

14. The Wondrous World of Carbon Nanotubes. *Eindhoven University of Technology* 93 (2003).

15. Terranova, M. L., Sessa, V. & Rossi, M. The World of Carbon Nanotubes: An Overview of CVD Growth Methodologies. *Chemical Vapor Deposition* **12,** 315–325 (2006).

16. Zheng, B. & Liu, J. in *The Chemistry Of Nanostructured Materials* 101–125 (WORLD SCIENTIFIC, 2003).

17. Van der Biest, O. O. & Vandeperre, L. J. Electrophoretic Deposition of Materials. *Annual Review of Materials Science* **29,** 327–352 (1999).

18. Besra, L. & Liu, M. A review on fundamentals and applications of electrophoretic deposition (EPD). *Progress in Materials Science* **52,** 1–61 (2007).

19. Besra, L., Compson, C. & Liu, M. Electrophoretic Deposition of YSZ Particles on Non-Conducting Porous NiO–YSZ Substrates for Solid Oxide Fuel Cell Applications. *Journal of the American Ceramic Society* **89,** 3003–3009 (2006).

20. Cao, G. *Nanostructures and Nanomaterials*. (Imperial College Press, 2004).

21. Schramm, L. L. *Emulsions, Foams, and Suspensions*. (John Wiley & Sons, 2006).

22. Napper, D. H. *Polymeric stabilization of colloidal dispersions*. (Academic Press, 1983).

23. Hu, L., Hecht, D. S. & Grüner, G. Carbon Nanotube Thin Films: Fabrication, Properties, and Applications. *Chem. Rev.* **110,** 5790–5844 (2010).

24. Mittal, V. *Surface Modification of Nanotube Fillers*. (John Wiley & Sons, 2011).

25. Vaisman, L., Wagner, H. D. & Marom, G. The role of surfactants in dispersion of carbon nanotubes. *Adv Colloid Interface Sci* **128-130,** 37–46 (2006).

26. Backes, C. *Noncovalent Functionalization of Carbon Nanotubes*. (Springer, 2012).

27. Angelikopoulos, P. & Bock, H. The science of dispersing carbon nanotubes with surfactants. *Phys Chem Chem Phys* **14,** 9546–9557 (2012).

28. Islam, M. F., Rojas, E., Bergey, D. M., Johnson, A. T. & Yodh, A. G. High Weight Fraction Surfactant Solubilization of Single-Wall Carbon Nanotubes in Water. *Nano Letters* **3,** 269–273 (2003).

29. Madni, I., Hwang, C.-Y., Park, S.-D., Choa, Y.-H. & Kim, H.-T. Mixed surfactant system for stable suspension of multiwalled carbon nanotubes. *Colloids and Surfaces A: Physicochemical and Engineering Aspects* **358,** 101–107 (2010).

30. Ryabenko, A. G., Dorofeeva, T. V. & Zvereva, G. I. UV–VIS–NIR spectroscopy study of sensitivity of single-wall carbon nanotubes to chemical processing and Van-der-Waals SWNT/SWNT interaction. Verification of the SWNT content measurements by absorption spectroscopy. *Carbon* **42,** 1523–1535 (2004).

31. Rastogi, R. *et al.* Comparative study of carbon nanotube dispersion using surfactants. *Journal of Colloid and Interface Science* **328,** 421–428 (2008).

32. Yu, J., Grossiord, N., Koning, C. E. & Loos, J. Controlling the dispersion of multi-wall carbon nanotubes in aqueous surfactant solution. *Carbon* **45,** 618–623 (2007).

33. Didenko, V. V., Moore, V. C., Baskin, D. S. & Smalley, R. E. Visualization of Individual Single-Walled Carbon Nanotubes by Fluorescent Polymer Wrapping. *Nano Lett* **5,** 1563–1567 (2005).

34. O'Connell M.J. *et al.* Reversible water-solubilization of single-walled carbon nanotubes by polymer wrapping. *Chemical Physics Letters* **342,** 265–271 (2001).

35. Zhao, J., Lu, J. P., Han, J. & Yang, C.-K. Noncovalent functionalization of carbon nanotubes by aromatic organic molecules. *Applied Physics Letters* **82,** 3746–3748 (2003).

36. Hu, C. *et al.* Water-soluble single-walled carbon nanotubes via noncovalent functionalization by a rigid, planar and conjugated diazo dye. *Carbon* **44,** 428–434 (2006).

37. Liu, C.-H., Li, J.-J., Zhang, H.-L., Li, B.-R. & Guo, Y. Structure dependent interaction between organic dyes and carbon nanotubes. *Colloids and Surfaces A: Physicochemical and Engineering Aspects* **313–314,** 9–12 (2008).

38. Dumonteil, S. *et al.* Dispersion of Carbon Nanotubes Using Organic Solvents. *Journal of Nanoscience and Nanotechnology* **6,** 1315–1318

39. Choi, W. B. *et al.* Electrophoresis deposition of carbon nanotubes for triode-type field emission display. *Applied Physics Letters* **78,** 1547–1549 (2001).

40. Du C., Heldbrant D. & Pan N. Preparation and preliminary property study of carbon nanotubes films by electrophoretic deposition. *Materials Letters* **57,** 434–438 (2002).

41. Oh, S. J., Zhang, J., Cheng, Y., Shimoda, H. & Zhou, O. Liquid-phase fabrication of patterned carbon nanotube field emission cathodes. *Applied Physics Letters* **84,** 3738 –3740 (2004).

42. Bae J.C., Yoon Y.J., Lee S.-J. & Baik H.K. Field emission properties of carbon nanotubes deposited by electrophoresis. *Physica B* **323,** 168–170 (2002).

43. Yoshikazu Nakayama, S. A. Field-emission device with carbon nanotubes for a flat panel display. *Synthetic Metals* 207–210 doi:10.1016/S0379-6779(00)00365-9

44. Yu, K., Zhu, Z., Li, Q. & Lu, W. Electronic properties and field emission of carbon nanotube films treated by hydrogen plasma. *Applied Physics A: Materials Science & Processing* **77,** 811–817 (2003).

45. Girishkumar, G., Vinodgopal, K. & Kamat, P. V. Carbon Nanostructures in Portable Fuel Cells: Single-Walled Carbon Nanotube Electrodes for Methanol Oxidation and Oxygen Reduction. *J. Phys. Chem. B* **108,** 19960–19966 (2004).

46. Nguyen, T. T., Nguyen, S. U., Phuong, D. T., Nguyen, D. C. & Mai, A. T. Dispersion of denatured carbon nanotubes by using a dimethylformamide solution. *Advances in Natural Sciences: Nanoscience and Nanotechnology* **2,** 035015 (2011).

47. Bahr, J. L., Mickelson, E. T., Bronikowski, M. J., Smalley, R. E. & Tour, J. M. Dissolution of small diameter single-wall carbon nanotubes in organic solvents? *Chem. Commun.* 193–194 (2001). doi:10.1039/B008042J

48. Zhong, J. *et al.* Bio–nano interaction of proteins adsorbed on single-walled carbon nanotubes. *Carbon* **47,** 967–973 (2009).

49. Zheng, M. *et al.* DNA-assisted dispersion and separation of carbon nanotubes. *Nat Mater* **2,** 338–342 (2003).

50. Daniel, S. *et al.* A review of DNA functionalized/grafted carbon nanotubes and their characterization. *Sensors and Actuators B: Chemical* **122,** 672–682 (2007).

51. Wei, G., Pan, C., Reichert, J. & Jandt, K. D. Controlled assembly of protein-protected gold nanoparticles on noncovalent functionalized carbon nanotubes. *Carbon* **48,** 645–653 (2010).

52. Chen, R. J., Zhang, Y., Wang, D. & Dai, H. Noncovalent Sidewall Functionalization of Single-Walled Carbon Nanotubes for Protein Immobilization. *J. Am. Chem. Soc.* **123,** 3838–3839 (2001).

53. Chen, R. J. *et al.* Noncovalent functionalization of carbon nanotubes for highly specific electronic biosensors. *PNAS* **100,** 4984–4989 (2003).

54. Dyke, C. A. & Tour, J. M. Covalent Functionalization of Single-Walled Carbon Nanotubes for Materials Applications. *J. Phys. Chem. A* **108,** 11151–11159 (2004).

55. Lee, J., Kim, M., Hong, C. K. & Eun Shim, S. Measurement of the dispersion stability of pristine and surface-modified multiwalled carbon nanotubes in various nonpolar and polar solvents. *Measurement Science and Technology* **18,** 3707–3712 (2007).

56. Esumi, K., Ishigami, M., Nakajima, A., Sawada, K. & Honda, H. Chemical treatment of carbon nanotubes. *Carbon* **34,** 279–281 (1996).

57. Martinez-Hernandez, A. L., Velasco-Santos, C. & Castano, V. M. Carbon Nanotubes Composites: Processing, Grafting and Mechanical and Thermal Properties. *Current Nanoscience* **6,** 12–39 (2010).

58. Xu, P. *et al.* A facile strategy for covalent binding of nanoparticles onto carbon nanotubes. *Applied Surface Science* **254,** 5236–5240 (2008).

59. Huang, W. *et al.* Attaching Proteins to Carbon Nanotubes via Diimide-Activated Amidation. *Nano Lett.* **2,** 311–314 (2002).

60. Jiang, K. *et al.* Protein immobilization on carbon nanotubes via a two-step process of diimide-activated amidation. *J. Mater. Chem.* **14,** 37–39 (2004).

61. Yang, P. Nanotechnology: Wires on water. *Nature* **425,** 243–244 (2003).

62. Madou, M. J. *Fundamentals of Microfabrication: The Science of Miniaturization*. (CRC Press, 2002).

63. Armitage, N. P., Gabriel, J.-C. P. & Grüner, G. Quasi-Langmuir–Blodgett thin film deposition of carbon nanotubes. *Journal of Applied Physics* **95,** 3228–3230 (2004).

64. Lay, M. D., Novak, J. P. & Snow, E. S. Simple Route to Large-Scale Ordered Arrays of Liquid-Deposited Carbon Nanotubes. *Nano Letters* **4,** 603–606 (2004).

65. Lin, J.-H., Chen, C.-S., Rümmeli, M. H. & Zeng, Z.-Y. Self-assembly formation of multi-walled carbon nanotubes on gold surfaces. *Nanoscale* **2,** 2835–2840 (2010).

66. Maune, H. T. *et al.* Self-assembly of carbon nanotubes into two-dimensional geometries using DNA origami templates. *Nature Nanotechnology* **5,** 61–66 (2010).

67. Zhang, F. *et al.* Layer-By-Layer Self-Assembly of Sulphydryl-Functionalized Multiwalled Carbon Nanotubes and Phosphate-Functionalized Gold Nanoparticles: Detection of Hydrazine. *ChemPlusChem* **77,** 914–922 (2012).

68. Seemann, L., Stemmer, A. & Naujoks, N. Local Surface Charges Direct the Deposition of Carbon Nanotubes and Fullerenes into Nanoscale Patterns. *Nano Lett.* **7,** 3007–3012 (2007).

69. Kim, S. *et al.* Spin- and Spray-Deposited Single-Walled Carbon-Nanotube Electrodes for Organic Solar Cells. *Advanced Functional Materials* **20,** 2310–2316 (2010).

70. Kim, J. H., Nam, K.-W., Ma, S. B. & Kim, K. B. Fabrication and electrochemical properties of carbon nanotube film electrodes. *Carbon* **44,** 1963–1968 (2006).

71. Jo, J. W., Jung, J. W., Lee, J. U. & Jo, W. H. Fabrication of highly conductive and transparent thin films from single-walled carbon nanotubes using a new non-ionic surfactant via spin coating. *ACS Nano* **4,** 5382–5388 (2010).

72. Song, J.-W. *et al.* Inkjet printing of single-walled carbon nanotubes and electrical characterization of the line pattern. *Nanotechnology* **19,** 095702 (2008).

73. Lee, C. W. *et al.* High-Performance Inkjet Printed Carbon Nanotube Thin Film Transistors with High-k HfO2 Dielectric on Plastic Substrate. *Small* **8,** 2941–2947 (2012).

74. Denneulin, A. *et al.* The influence of carbon nanotubes in inkjet printing of conductive polymer suspensions. *Nanotechnology* **20,** 385701 (2009).

75. Dan, B., Irvin, G. C. & Pasquali, M. Continuous and scalable fabrication of transparent conducting carbon nanotube films. *ACS Nano* **3,** 835–843 (2009).

76. Thomas, B. J. C., Boccaccini, A. R. & Shaffer, M. S. P. Multi-Walled Carbon Nanotube Coatings Using Electrophoretic Deposition (EPD). *Journal of the American Ceramic Society* **88,** 980–982 (2005).

77. Boccaccini, A. R. *et al.* Electrophoretic deposition of carbon nanotubes. *Carbon* **44,** 3149–3160 (2006).

78. Corni, I., Ryan, M. & Boccaccini, A. Electrophoretic deposition: From traditional ceramics to nanotechnology. *Journal of the European Ceramic Society* **28,** 1353–1367 (2008).

79. Van Tassel, J. J. & Randall, C. A. Mechanisms of Electrophoretic Deposition. *Key Engineering Materials* **314,** 167–174 (2006).

80. Zhitomirsky, I. Cathodic electrodeposition of ceramic and organoceramic materials. Fundamental aspects. *Advances in Colloid and Interface Science* **97,** 279–317 (2002).

81. Bansal, N. P. & Boccaccini, A. R. *Ceramics and Composites Processing Methods*. (John Wiley & Sons, 2012).

82. Sarkar, P. & Nicholson, P. S. Electrophoretic Deposition (EPD): Mechanisms, Kinetics, and Application to Ceramics. *Journal of the American Ceramic Society* **79,** 1987–2002 (1996).

83. Y. Fukada, N. N. Electrophoretic deposition—mechanisms, myths and materials. **39,** 787–801 (2004).

84. Hamaker, H. C. Formation of a deposit by electrophoresis. *Trans. Faraday Soc.* **35,** 279–287 (1940).

85. Hamaker, H. C. & Verwey, E. J. W. Part II.—(C) Colloid stability. The role of the forces between the particles in electrodeposition and other phenomena. *Trans. Faraday Soc.* **35,** 180–185 (1940).

86. Grillon, F., Fayeulle, D. & Jeandin, M. Quantitative image analysis of electrophoretic coatings. *J Mater Sci Lett* **11,** 272–275 (1992).

87. Klumpp, C., Kostarelos, K., Prato, M. & Bianco, A. Functionalized carbon nanotubes as emerging nanovectors for the delivery of therapeutics. *Biochim. Biophys. Acta* **1758,** 404–412 (2006).

88. Cho, J. *et al.* Characterisation of carbon nanotube films deposited by electrophoretic deposition. *Carbon* **47,** 58–67 (2009).

89. Jung, S. M., Hahn, J., Jung, H. Y. & Suh, J. S. Clean carbon nanotube field emitters aligned horizontally. *Nano Lett.* **6,** 1569–1573 (2006).

90. Wang, L., Chen, Y., Chen, T., Que, W. & Sun, Z. Optimization of field emission properties of carbon nanotubes cathodes by electrophoretic deposition. *Materials Letters* **61,** 1265–1269 (2007).

91. Lima, M. D., Andrade, M. J. de, Bergmann, C. P. & Roth, S. Thin, conductive, carbon nanotube networks over transparent substrates by electrophoretic deposition. *J. Mater. Chem.* **18,** 776–779 (2008).

92. Wei Li *et al.* Electrochemical Characterization of Multi-walled Carbon Nanotubes/ Polyvinyl Alcohol Coated Electrodes for Biological Applications. *Int. J. Electrochem. Sci.* **8,** 5738–5734 (2013).

93. Singh, I., Kaya, C., Shaffer, M. S. P., Thomas, B. C. & Boccaccini, A. R. Bioactive ceramic coatings containing carbon nanotubes on metallic substrates by electrophoretic deposition. *J Mater Sci* **41,** 8144–8151 (2006).

94. Boccaccini, A. R. *et al.* Carbon Nanotube Coatings on Bioglass-Based Tissue Engineering Scaffolds. *Advanced Functional Materials* **17,** 2815–2822 (2007).

95. Chicatún, F. *et al.* Carbon nanotube deposits and CNT/SiO2 composite coatings by electrophoretic deposition. *Advances in Applied Ceramics* **106,** 186–195 (2007).

96. Cho, J., Schaab, S., Roether, J. A. & Boccaccini, A. R. Nanostructured carbon nanotube/TiO2 composite coatings using electrophoretic deposition (EPD). *J Nanopart Res* **10,** 99–105 (2008).

97. Du, C., Heldebrant, D. & Pan, N. Preparation of carbon nanotubes composite sheet using electrophoretic deposition process. *Journal of Materials Science Letters* **21,** 565–568 (2002).

98. Pei, S., Du, J., Zeng, Y., Liu, C. & Cheng, H.-M. The fabrication of a carbon nanotube transparent conductive film by electrophoretic deposition and hot-pressing transfer. *Nanotechnology* **20,** 235707 (2009).

99. Du, C. & Pan, N. High power density supercapacitor electrodes of carbon nanotube films by electrophoretic deposition. *Nanotechnology* **17,** 5314 (2006).

100. Talebi, T., Haji, M., Raissi, B. & Maghsoudipour, A. YSZ electrolyte coating on NiO–YSZ composite by electrophoretic deposition for solid oxide fuel cells (SOFCs). *International Journal of Hydrogen Energy* **35,** 9455–9459 (2010).

101. Hideyuki, N. *et al.* Preparation of Thin and Dense Lanthanum Cobaltite Coating on Porous Tubular Alumina Supports by Electrophoretic Deposition. *Journal of the Ceramic Society of Japan* **114,** 36–41 (2006).

102. Sarkar, A. & Hah, D. Electrophoretic Deposition of Carbon Nanotubes on Silicon Substrates. *Journal of Electron Mater* **41,** 3130–3138 (2012).

103. Sarkar, P., Datta, S. & Nicholson, P. S. Functionally graded ceramic/ceramic and metal/ceramic composites by electrophoretic deposition. *Composites Part B: Engineering* **28,** 49–56 (1997).

104. Shimoda, H. *et al.* Self-Assembly of Carbon Nanotubes. *Advanced Materials* **14,** 899–901 (2002).

105. Dresselhaus, M. S., Jorio, A. & Saito, R. Characterizing Graphene, Graphite, and Carbon Nanotubes by Raman Spectroscopy. *Annual Review of Condensed Matter Physics* **1,** 89–108 (2010).

106. Thomas, B. J. C. *et al.* Electrophoretic Deposition of Carbon Nanotubes on Metallic Surfaces. *Key Engineering Materials* **314,** 141–146 (2006).

107. Lewis, I. R. & Edwards, H. G. M. *Handbook of Raman Spectroscopy: From the Research Laboratory to the Process Line*. (CRC Press, 2001).

108. Kudelski, A. Analytical applications of Raman spectroscopy. *Talanta* **76,** 1–8 (2008).

109. Movasaghi, Z., Rehman, S. & Rehman, I. U. Raman Spectroscopy of Biological Tissues. *Applied Spectroscopy Reviews* **42,** 493–541 (2007).

110. Peticolas, W. L. Applications of Raman spectroscopy to biological macromolecules. *Biochimie* **57,** 417–428 (1975).

111. Stiles, P. L., Dieringer, J. A., Shah, N. C. & Van Duyne, R. P. Surface-Enhanced Raman Spectroscopy. *Annual Review of Analytical Chemistry* **1,** 601–626 (2008).

112. Kneipp, K., Moskovits, M. & Kneipp, H. *Surface-enhanced Raman Scattering: Physics and Applications*. (Springer, 2006).

113. Moskovits, M. Surface-enhanced Raman spectroscopy: a brief retrospective. *Journal of Raman Spectroscopy* **36,** 485–496 (2005).

114. Lu, L.-Q., Zheng, Y., Qu, W.-G., Yu, H.-Q. & Xu, A.-W. Hydrophobic Teflon films as concentrators for single-molecule SERS detection. *J. Mater. Chem.* **22,** 20986–20990 (2012).

115. Lee, S. J., Guan, Z., Xu, H. & Moskovits, M. Surface-Enhanced Raman Spectroscopy and Nanogeometry: The Plasmonic Origin of SERS. *J. Phys. Chem. C* **111,** 17985–17988 (2007).

116. Weaver, M. J., Zou, S. & Chan, H. Y. The new interfacial ubiquity of surface-enhanced Raman spectroscopy. *Anal. Chem.* **72,** 38A–47A (2000).

117. Ko, H., Singamaneni, S. & Tsukruk, V. V. Nanostructured surfaces and assemblies as SERS media. *Small* **4,** 1576–1599 (2008).

118. Lin, X.-M., Cui, Y., Xu, Y.-H., Ren, B. & Tian, Z.-Q. Surface-enhanced Raman spectroscopy: substrate-related issues. *Anal Bioanal Chem* **394,** 1729–1745 (2009).

119. Zhang, X., Yonzon, C. R., Young, M. A., Stuart, D. A. & Van Duyne, R. P. Surface-enhanced Raman spectroscopy biosensors: excitation spectroscopy for optimisation of substrates fabricated by nanosphere lithography. *IEE Proc Nanobiotechnol* **152,** 195–206 (2005).

120. Liu, Y.-C., Wang, C.-C. & Tsai, J.-F. Improved surface-enhanced Raman scattering on electrochemically roughened silver substrates prepared in bielectrolyte solutions. *Anal. Chim. Acta* **584,** 433–438 (2007).

121. Bian, J.-C. *et al.* Electrodeposition of silver nanoparticle arrays on ITO coated glass and their application as reproducible surface-enhanced Raman scattering substrate. *Applied Surface Science* **258,** 1831–1835 (2011).

122. Lu, Y., Xue, G. & Dong, J. HNO3 etched silver foil as an effective substrate for surface-enhanced Raman scattering (SERS) analysis. *Applied Surface Science* **68,** 485–489 (1993).

123. Talian, I., Mogensen, K. B., Oriňák, A., Kaniansky, D. & Hübner, J. Surface-enhanced Raman spectroscopy on novel black silicon-based nanostructured surfaces. *Journal of Raman Spectroscopy* **40,** 982–986 (2009).

124. Pan, Z. *et al.* Surface-enhanced Raman spectroscopy using silver-coated porous glass-ceramic substrates. *Appl Spectrosc* **59,** 782–786 (2005).

125. Figueroa, M., Pourrezaei, K. & Tyagi, S. Fabrication of flexible and porous surface enhanced raman scattering (SERS) substrates using nanoparticle inks. *AIP Conference Proceedings* **1461,** 47–53 (2012).

126. Kuncicky, D. M., Prevo, B. G. & Velev, O. D. Controlled assembly of SERS substrates templated by colloidal crystal films. *J. Mater. Chem.* **16,** 1207–1211 (2006).

127. Ko, H., Chang, S. & Tsukruk, V. V. Porous substrates for label-free molecular level detection of nonresonant organic molecules. *ACS Nano* **3,** 181–188 (2009).

128. Panarin, A. Y., Terekhov, S. N., Kholostov, K. I. & Bondarenko, V. P. SERS-active substrates based on n-type porous silicon. *Applied Surface Science* **256,** 6969–6976 (2010).

129. Zeiri, L., Rechav, K., Porat, Z. & Zeiri, Y. Silver nanoparticles deposited on porous silicon as a surface-enhanced Raman scattering (SERS) active substrate. *Appl Spectrosc* **66,** 294–299 (2012).

130. He, X. N. *et al.* Surface-enhanced Raman spectroscopy using gold-coated horizontally aligned carbon nanotubes. *Nanotechnology* **23,** 205702 (2012).

131. Beqa, L., Singh, A. K., Fan, Z., Senapati, D. & Ray, P. C. Chemically attached gold nanoparticle–carbon nanotube hybrids for highly sensitive SERS substrate. *Chemical Physics Letters* **512,** 237–242 (2011).

132. Jiang, W. F., Zhang, Y. F., Wang, Y. S., Xu, L. & Li, X. J. SERS activity of Au nanoparticles coated on an array of carbon nanotube nested into silicon nanoporous pillar. *Applied Surface Science* **258,** 1662–1665 (2011).

133. Zhao, H., Fu, H., Tian, C., Ren, Z. & Tian, G. Fabrication of silver nanoparticles/single-walled carbon nanotubes composite for surface-enhanced Raman scattering. *J Colloid Interface Sci* **351,** 343–347 (2010).

134. García-Barrasa, J., López-de-Luzuriaga, J. M. & Monge, M. Silver nanoparticles: synthesis through chemical methods in solution and biomedical applications. *cent.eur.j.chem.* **9,** 7–19 (2011).

135. Lee, P. C. & Meisel, D. Adsorption and surface-enhanced Raman of dyes on silver and gold sols. *J. Phys. Chem.* **86,** 3391–3395 (1982).

136. Datsyuk, V. *et al.* Chemical oxidation of multiwalled carbon nanotubes. *Carbon* **46,** 833–840 (2008).

137. Saito, T., Matsushige, K. & Tanaka, K. Chemical treatment and modification of multi-walled carbon nanotubes. *Physica B: Condensed Matter* **323,** 280–283 (2002).

138. Tsai, Y.-C., Hsu, P.-C., Lin, Y.-W. & Wu, T.-M. Electrochemical deposition of silver nanoparticles in multiwalled carbon nanotube-alumina-coated silica for surface-enhanced Raman scattering-active substrates. *Electrochemistry Communications* **11,** 542–545 (2009).

139. Zeng, Z. *et al.* Electrochemical deposition of Pt nanoparticles on carbon nanotube patterns for glucose detection. *Analyst* **135,** 1726–1730 (2010).

140. Qu, L. & Dai, L. Substrate-enhanced electroless deposition of metal nanoparticles on carbon nanotubes. *J. Am. Chem. Soc.* **127,** 10806–10807 (2005).

141. Kathi, J., Rhee, K.-Y. & Lee, J. H. Effect of chemical functionalization of multi-walled carbon nanotubes with 3-aminopropyltriethoxysilane on mechanical and morphological properties of epoxy nanocomposites. *Composites Part A: Applied Science and Manufacturing* **40,** 800–809 (2009).

142. Sztainbuch, I. W. The effects of Au aggregate morphology on surface-enhanced Raman scattering enhancement. *J Chem Phys* **125,** 124707 (2006).

143. Schwartzberg, A. M. *et al.* Unique Gold Nanoparticle Aggregates as a Highly Active Surface-Enhanced Raman Scattering Substrate. *J. Phys. Chem. B* **108,** 19191–19197 (2004).

144. Chen, Y.-C., Young, R. J., Macpherson, J. V. & Wilson, N. R. Silver-decorated carbon nanotube networks as SERS substrates. *Journal of Raman Spectroscopy* **42,** 1255–1262 (2011).

145. Wang, H.-H. *et al.* Highly Raman-Enhancing Substrates Based on Silver Nanoparticle Arrays with Tunable Sub-10 nm Gaps. *Advanced Materials* **18,** 491–495 (2006).

146. Camargo, P. H. C., Au, L., Rycenga, M., Li, W. & Xia, Y. Measuring the SERS enhancement factors of dimers with different structures constructed from silver nanocubes. *Chemical Physics Letters* **484,** 304–308 (2010).

147. Wang, J., Chu, H. & Li, Y. Why Single-Walled Carbon Nanotubes Can Be Dispersed in Imidazolium-Based Ionic Liquids. *ACS Nano* **2,** 2540–2546 (2008).

148. Crescenzo, A. D. *et al.* Disaggregation of single-walled carbon nanotubes (SWNTs) promoted by the ionic liquid-based surfactant 1-hexadecyl-3-vinyl-imidazolium bromide in aqueous solution. *Soft Matter* **5,** 62–66 (2008).

149. Ammam, M. Electrophoretic deposition under modulated electric fields: a review. *RSC Advances* **2,** 7633 (2012).

APPENDIX A: PERMISSION TO REPRINT FROM JOHN WILEY AND SONS

1. Permission to use Figure 2-1 in the dissertation

Confirmation Number: 11095334
Order Date: 05/28/2013
Order Details
Carbon nanotubes and related structures: synthesis, characterization, functionalization, and applications
Order detail ID: 63704794
Order License Id: 3157800760854
Chapter Title: Carbon Nanotubes and Related Structures: Production and Formation
Author(s): Rmmeli, Mark H. ; Ayala, Paola ; Pichler, Thomas
DOI: 10.1002/9783527629930.CH1
Date: Feb 17, 2010
ISBN: 978-3-527-32406-4
Publication Type: Book
Publisher: Wiley-VCH
Author/Editor: Guldi, D. M.; Martin, Nazario
Permission Status: Granted
Permission type: Republish or display content
Type of use: reuse in a dissertation/thesis
Book title: Carbon Nanotubes and Related Structures: Synthesis, Characterization, Functionalization, and Applications
Licensed copyright line: Copyright © 2010, John Wiley and Sons
Start page 1
End page 21
Requestor type University/Academic
Format Print and electronic
Portion Figure/table
Number of figures/tables 2
Original Wiley figure/table number(s) Figure 1.7 and Figure 1.9
Will you be translating? No
Order reference number: 0012

2. Permission to use Figure 2-20 in the dissertation

This is a License Agreement between ANIRBAN SARKAR ("You") and John Wiley and Sons ("John Wiley and Sons") provided by Copyright Clearance Center ("CCC"). The license consists of your order details, the terms and conditions provided by John Wiley and Sons, and the payment terms and conditions.
All payments must be made in full to CCC. For payment instructions, please see information listed at the bottom of this form.
License Number 3157910195051
License date May 28, 2013
Licensed content publisher John Wiley and Sons

Licensed content publication	Journal of the American Ceramic Society
Licensed content title	Electrophoretic Deposition (EPD): Mechanisms, Kinetics, and Application to Ceramics
Licensed copyright line	Copyright © 2005, John Wiley and Sons
Licensed content author	Partho Sarkar,Patrick S. Nicholson
Licensed content date	Sep 28, 2005
Start page	1987
End page	2002
Type of use	Dissertation/Thesis
Requestor type	University/Academic
Format	Print and electronic
Portion	Figure/table
Number of figures/tables	4
Original Wiley figure/table number(s)	Figure 2, Figure 4, Figure 10, Figure 1
Will you be translating?	No
Total	0.00 USD

APPENDIX B: PERMISSION TO REPRINT FROM SPRINGER

1. Permission to use Figure 4-2, Figure 4-5, Figure 4-7, Figure 4-8, Figure 4-9, Figure 4-14 in the dissertation

This is a License Agreement between ANIRBAN SARKAR ("You") and Springer ("Springer") provided by Copyright Clearance Center ("CCC"). The license consists of your order details, the terms and conditions provided by Springer, and the payment terms and conditions.
All payments must be made in full to CCC. For payment instructions, please see information listed at the bottom of this form.

License Number	3157090923805
License date	May 27, 2013
Licensed content publisher	Springer
Licensed content publication	Journal of Electronic Materials
Licensed content title	Electrophoretic Deposition of Carbon Nanotubes on Silicon Substrates
Licensed content author	Anirban Sarkar
Licensed content date	Jan 1, 2012
Volume number	41
Issue number	11
Type of Use	Thesis/Dissertation
Portion	Figures
Author of this Springer article	Yes and you are a contributor of the new work
Order reference number	009
Title of your thesis / dissertation	Electrophoretic deposition of carbon nanotubes on silicon sustrates
Expected completion date	Jan 2014
Estimated size(pages)	175
Total	0.00 USD

APPENDIX C: PERMISSION TO REPRINT FROM ELSEVIER

1. Permission to use Figure 2-7, Figure 2-9 in the dissertation

This is a License Agreement between ANIRBAN SARKAR ("You") and Elsevier ("Elsevier") provided by Copyright Clearance Center ("CCC"). The license consists of your order details, the terms and conditions provided by Elsevier, and the payment terms and conditions.

All payments must be made in full to CCC. For payment instructions, please see information listed at the bottom of this form.

Supplier	Elsevier Limited The Boulevard,Langford LaneKidlington, Oxford, OX5 1GB,UK
Registered Company Number	1982084
Customer name	ANIRBAN SARKAR
Customer address	3101 P F Taylor Hall BATON ROUGE, LA 70803
License number	3157820372636
License date	May 28, 2013
Licensed content publisher	Elsevier
Licensed content publication	Progress in Materials Science
Licensed content title	A review on fundamentals and applications of electrophoretic deposition (EPD)
Licensed content author	Laxmidhar Besra, Meilin Liu
Licensed content date	January 2007
Licensed content volume number	52
Licensed content issue number	1
Number of pages	61
Start Page	1
End Page	61
Type of Use	reuse in a thesis/dissertation
Intended publisher of new work	other
Portion	figures/tables/illustrations
Number of figures/tables/illustrations	6
Format	both print and electronic
Are you the author of this Elsevier article?	No
Will you be translating?	No
Order reference number	0015
Title of your thesis/dissertation	Electrophoretic deposition of carbon nanotubes on silicon substrates
Expected completion date	Jan 2014
Estimated size (number of pages)	175
Elsevier VAT number	GB 494 6272 12
Permissions price	0.00 USD
VAT/Local Sales Tax	0.0 USD / 0.0 GBP
Total	0.00 USD

2. Permission to use Figure 2-13 in the dissertation

This is a License Agreement between ANIRBAN SARKAR ("You") and Elsevier ("Elsevier") provided by Copyright Clearance Center ("CCC"). The license consists of your order details, the terms and conditions provided by Elsevier, and the payment terms and conditions.
All payments must be made in full to CCC. For payment instructions, please see information listed at the bottom of this form.

Supplier	Elsevier Limited The Boulevard,Langford Lane Kidlington, Oxford, OX5 1GB,UK
Registered Company Number	1982084
Customer name	ANIRBAN SARKAR
Customer address	3101 P F Taylor Hall BATON ROUGE, LA 70803
License number	3157500564399
License date	May 28, 2013
Licensed content publisher	Elsevier
Licensed content publication	Carbon
Licensed content title	Controlled assembly of protein-protected gold nanoparticles on noncovalent functionalized carbon nanotubes
Licensed content author	Gang Wei,Changjiang Pan,Jörg Reichert,Klaus D. Jandt
Licensed content date	March 2010
Licensed content volume number	48
Licensed content issue number	3
Number of pages	9
Start Page	645
End Page	653
Type of Use	reuse in a thesis/dissertation
Portion	figures/tables/illustrations
Number of figures/tables/illustrations	2
Format	both print and electronic
Are you the author of this Elsevier article?	No
Will you be translating?	No
Order reference number	0011
Title of your thesis/dissertation	Electrophoretic deposition of carbon nanotubes on silicon substrates
Expected completion date	Jan 2014
Estimated size (number of pages)	175
Elsevier VAT number	GB 494 6272 12
Permissions price	0.00 USD
VAT/Local Sales Tax	0.0 USD / 0.0 GBP
Total	0.00 USD

3. Permission to use Figure 2-15 in the dissertation

This is a License Agreement between ANIRBAN SARKAR ("You") and Elsevier ("Elsevier") provided by Copyright Clearance Center ("CCC"). The license consists of your order details, the terms and conditions provided by Elsevier, and the payment terms and conditions.
All payments must be made in full to CCC. For payment instructions, please see information listed at the bottom of this form.

Supplier	Elsevier Limited The Boulevard,Langford Lane Kidlington,Oxford,OX5 1GB,UK
Registered Company Number	1982084
Customer name	ANIRBAN SARKAR
Customer address	3101 P F Taylor Hall BATON ROUGE, LA 70803
License number	3154601453503
License date	May 23, 2013
Licensed content publisher	Elsevier
Licensed content publication	Applied Surface Science
Licensed content title	A facile strategy for covalent binding of nanoparticles onto carbon nanotubes
Licensed content author	Ping Xu,Daxiang Cui,Bifeng Pan,Feng Gao,Rong He,Qing Li,Tuo Huang,Chenchen Bao,Hao Yang
Licensed content date	15 June 2008
Licensed content volume number	254
Licensed content issue number	16
Number of pages	5
Start Page	5236
End Page	5240
Type of Use	reuse in a thesis/dissertation
Intended publisher of new work	other
Portion	figures/tables/illustrations
Number of figures/tables/illustrations	1
Format	both print and electronic
Are you the author of this Elsevier article?	No
Will you be translating?	No
Order reference number	002
Title of your thesis/dissertation	Electrophoretic deposition of carbon nanotubes on silicon sustrates
Expected completion date	Jan 2014
Estimated size (number of pages)	175
Elsevier VAT number	GB 494 6272 12
Permissions price	0.00 USD
VAT/Local Sales Tax	0.0 USD / 0.0 GBP
Total	0.00 USD

4. Permission to use Figure 2-12 in the dissertation

This is a License Agreement between ANIRBAN SARKAR ("You") and Elsevier ("Elsevier") provided by Copyright Clearance Center ("CCC"). The license consists of your order details, the terms and conditions provided by Elsevier, and the payment terms and conditions.
All payments must be made in full to CCC. For payment instructions, please see information listed at the bottom of this form.

Supplier	Elsevier Limited The Boulevard,Langford Lane Kidlington,Oxford,OX5 1GB,UK
Registered Company Number	1982084
Customer name	ANIRBAN SARKAR
Customer address	3101 P F Taylor Hall BATON ROUGE, LA 70803
License number	3154610139170
License date	May 23, 2013
Licensed content publisher	Elsevier
Licensed content publication	Advances in Colloid and Interface Science
Licensed content title	The role of surfactants in dispersion of carbon nanotubes
Licensed content author	Linda Vaisman,H. Daniel Wagner,Gad Marom
Licensed content date	21 December 2006
Licensed content volume number	128–130
Licensed content issue number	None
Number of pages	10
Start Page	37
End Page	46
Type of Use	reuse in a thesis/dissertation
Intended publisher of new work	other
Portion	figures/tables/illustrations
Number of figures/tables/illustrations	2
Format	both print and electronic
Are you the author of this Elsevier article?	No
Will you be translating?	No
Order reference number	003
Title of your thesis/dissertation	Electrophoretic deposition of carbon nanotubes on silicon sustrates
Expected completion date	Jan 2014
Estimated size (number of pages)	175
Elsevier VAT number	GB 494 6272 12
Permissions price	0.00 USD
VAT/Local Sales Tax	0.0 USD / 0.0 GBP
Total	0.00 USD

5. Permission to use Figure 2-2 in the dissertation

This is a License Agreement between ANIRBAN SARKAR ("You") and Elsevier ("Elsevier") provided by Copyright Clearance Center ("CCC"). The license consists of your order details, the terms and conditions provided by Elsevier, and the payment terms and conditions.
All payments must be made in full to CCC. For payment instructions, please see information listed at the bottom of this form.

Supplier	Elsevier Limited The Boulevard,Langford Lane Kidlington,Oxford,OX5 1GB,UK
Registered Company Number	1982084
Customer name	ANIRBAN SARKAR
Customer address	3101 P F Taylor Hall BATON ROUGE, LA 70803
License number	3154621402973
License date	May 23, 2013
Licensed content publisher	Elsevier
Licensed content publication	Chemical Physics Letters
Licensed content title	Model of carbon nanotube growth through chemical vapor deposition
Licensed content author	S.B. Sinnott,R. Andrews,D. Qian,A.M. Rao,Z. Mao,E.C. Dickey,F. Derbyshire
Licensed content date	17 December 1999
Licensed content volume number	315
Licensed content issue number	1-2
Number of pages	6
Start Page	25
End Page	30
Type of Use	reuse in a thesis/dissertation
Intended publisher of new work	other
Portion	figures/tables/illustrations
Number of figures/tables/illustrations	2
Format	both print and electronic
Are you the author of this Elsevier article?	No
Will you be translating?	No
Title of your thesis/dissertation	Electrophoretic deposition of carbon nanotubes on silicon substrates
Expected completion date	Jan 2014
Estimated size (number of pages)	175
Elsevier VAT number	GB 494 6272 12
Permissions price	0.00 USD
VAT/Local Sales Tax	0.0 USD / 0.0 GBP
Total	0.00 USD

6. Permission to use Figure 2-21 in the dissertation

This is a License Agreement between ANIRBAN SARKAR ("You") and Elsevier ("Elsevier") provided by Copyright Clearance Center ("CCC"). The license consists of your order details, the terms and conditions provided by Elsevier, and the payment terms and conditions.
All payments must be made in full to CCC. For payment instructions, please see information listed at the bottom of this form.

Supplier	Elsevier Limited The Boulevard,Langford Lane Kidlington,Oxford,OX5 1GB,UK
Registered Company Number	1982084
Customer name	ANIRBAN SARKAR
Customer address	3101 P F Taylor Hall BATON ROUGE, LA 70803
License number	3154601147433
License date	May 23, 2013
Licensed content publisher	Elsevier
Licensed content publication	Biochimica et Biophysica Acta (BBA) – Biomembranes
Licensed content title	Functionalized carbon nanotubes as emerging nanovectors for the delivery of therapeutics
Licensed content author	Cédric Klumpp,Kostas Kostarelos,Maurizio Prato,Alberto Bianco
Licensed content date	March 2006
Licensed content volume number	1758
Licensed content issue number	3
Number of pages	9
Start Page	404
End Page	412
Type of Use	reuse in a thesis/dissertation
Portion	figures/tables/illustrations
Number of figures/tables/illustrations	1
Format	both print and electronic
Are you the author of this Elsevier article?	No
Will you be translating?	No
Order reference number	001
Title of your thesis/dissertation	Electrophoretic deposition of carbon nanotubes on silicon sustrates
Expected completion date	Jan 2014
Estimated size (number of pages)	175
Elsevier VAT number	GB 494 6272 12
Permissions price	0.00 USD
VAT/Local Sales Tax	0.0 USD / 0.0 GBP
Total	0.00 USD

APPENDIX D: PERMISSION TO REPRINT FROM ACS PUBLICATIONS

1. Permission to use Figure 2-18 in the dissertation

Title: Continuous and Scalable Fabrication of Transparent Conducting Carbon Nanotube Films
Author: Budhadipta Dan, Glen C. Irvin, and Matteo Pasquali
Publication: ACS Nano
Publisher: American Chemical Society
Date: Apr 1, 2009
PERMISSION/LICENSE IS GRANTED FOR YOUR ORDER AT NO CHARGE
This type of permission/license, instead of the standard Terms & Conditions, is sent to you because no fee is being charged for your order. Please note the following:

- Permission is granted for your request in both print and electronic formats, and translations.
- If figures and/or tables were requested, they may be adapted or used in part.
- Please print this page for your records and send a copy of it to your publisher/graduate school.
- Appropriate credit for the requested material should be given as follows: "Reprinted (adapted) with permission from (COMPLETE REFERENCE CITATION). Copyright (YEAR) American Chemical Society." Insert appropriate information in place of the capitalized words.
- One-time permission is granted only for the use specified in your request. No additional uses are granted (such as derivative works or other editions). For any other uses, please submit a new request.

If credit is given to another source for the material you requested, permission must be obtained from that source.

APPENDIX E: PERMISSION TO REPRINT FROM TAYLOR & FRANCIS

1. Permission to use Figure 2-3 in the dissertation

Confirmation Number: 11097034
Order Date: 06/04/2013
Order Details
Order detail Id: 63744376
Order license Id: 3162061059400
Permission type: Republish or display content
Type of use: Republish in a thesis/dissertation
Requestor type: Academic institution
Format Print, Electronic
Portion chart/graph/table/figure
Number of charts/graphs/tables/figures 1
Title or numeric reference of the portion(s) Carbon based Nanomaterials Figure 9.20
Title of the article or chapter the portion is from Carbon-Based Nanomaterials
Editor of portion(s) N/A
Author of portion(s) N/A
Volume of serial or monograph N/A
Page range of portion 460-475
Publication date of portion 2008
Rights for Main product Duration of use Life of current edition
Creation of copies for the disabled no
With minor editing privileges no
For distribution to Worldwide
In the following language(s) Original language of publication
With incidental promotional use no
Lifetime unit quantity of new product 0 to 499
Made available in the following markets education and research
The requesting person/organization Anirban Sarkar/Louisiana State University
Author/Editor Anirban Sarkar
Title Electrophoretic deposition of carbon nanotubes on silicon substrates
Publisher Louisiana State University
Expected publication date Jan 2014
Estimated size (pages) 175

VITA

Anirban Sarkar was born in 1984 at Kolkata in West Bengal, an eastern state of India. He finished his Bachelor of Technology (B.Tech) in Electronics and Communication engineering at the College of Engineering and Management, Kolaghat (C.E.M.K) affiliated to West Bengal University of Technology (W.B.U.T), India, in May 2007. He has been enrolled as a doctoral candidate in the Division of Electrical and Computer Engineering of the School of Electrical Engineering and Computer Science at Louisiana State University, Baton Rouge, Louisiana since Fall 2007. His research interests lie in the development of carbon nanotube based transistors and hybrid electronics for the next generation consumer electronics.